THE NATURE OF OLIVINE-RICH CUMULATE ROCKS OF THE LOWER CRITICAL AND LOWER ZONES OF THE NORTHWESTERN BUSHVELD COMPLEX

by

SUSAN ANN HAIKNEY
BSc. Hons. (Rhodes University)

Thesis submitted in fulfilment
of the requirements for the
Degree of

Master of Science

in the Department of Geology,
Rhodes University,
Grahamstown.

- 1992 -

DECLARATION

All work in this thesis is the original work of the author, except where specific acknowledgement is made of the work of others.

SIGNED: 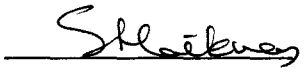

S.A. HAIKNEY

1992

CONTENTS

LIST OF FIGURES

LIST OF TABLES

ACKNOWLEDGEMENTS

I should like to thank the CSIR for sponsoring this project through the FRD National Geodynamics Program, and the Geological Survey for drilling the boreholes. Gencor/Genmin is thanked for providing me with a bursary for the first eighteen months of this study, and for giving me access to facilities for the writing-up and final stages of this thesis. My thanks too, to Prof. Eales for all his help and patience for what has turned out to be a drawn out process of getting this thesis to this stage. Roger Scoon was a co-supervisor for the first few months of the project, and he is thanked for his advice and help in getting me going on the right foot. My co-workers at Rhodes, Billy de Klerk, Bernd Teigler and Wolfgang Maier are all thanked for their help, discussions and encouragement. Bernd Teigler is thanked for his permission to use some of his data and diagrams from his PhD thesis. Dr. Chris Lee from JCI is thanked for giving me access to unpublished data.

Maureen Kempen is thanked for draughting the diagrams and Brenda Thompson is thanked for her assistance with some of the typing.

Finally, my thanks to family and friends, in particular my husband, Ian de Klerk, for their constant encouragement.

ABSTRACT

Boreholes NG1 and NG2 were drilled on the farm Nooitgedacht 406 KQ to intersect the lower Critical and Lower Zones of the western Bushveld Complex. The aim of this study is to describe the textural features and chemical characteristics of the olivine-bearing rocks in the intersections, as determined by petrographic studies, XRF analysis and microprobe analysis.

The olivine-bearing rocks are dunites, harzburgites and olivine pyroxenites. They comprise olivine and orthopyroxene, with minor chromite, clinopyroxene and plagioclase, and their textures vary between adcumulate, mesocumulate and poikilitic. The sequence intersected can be broadly correlated with that in the eastern Bushveld Complex.

Of the whole-rock inter-element ratios, the MMF (MgO/[MgO+FeO]) ratio is the clearest indicator of cyclicity. The olivine-rich rocks are more primitive than the associated rocks, and seem to become more primitive with height in most intervals. The plagioclase in the olivine-bearing rocks is unusually sodic in composition, having a maximum Na_2O content of 8.12%. A comparison of olivine and plagioclase compositions with those in other intrusions has revealed that the only other major intrusion with sodic plagioclase is the Kiglapait intrusion of Canada. In the Kiglapait intrusion the sodic plagioclase occurs in conjunction with fayalitic olivine as opposed to the forsteritic variety of this study.

Chemical variations in the rocks sampled indicate that periodic replenishment of the magma from which the rocks crystallised must have occurred. In some of the olivine-bearing intervals where little fractionation is evident, replenishment seems to have been continuous. In other intervals fractionation appears to have continued uninterrupted for significant periods, prior to rejuvenation by fresh influxes of magma.

1. INTRODUCTION

Over the past few years staff and students at Rhodes University have been involved in research on the Bushveld Igneous Complex, as part of the National Geoscience Program of the CSIR. A substantial proportion of the research has been concentrated on the western part of the complex. Most of the work has been done in areas which are of economic importance, or overlie such intervals i.e. the upper Critical and Main Zones (Kruger, 1983, de Klerk, 1982, Field, 1987, Mitchell, 1986, and Botha, 1987) The work offered here deals with the olivine-bearing rocks in the lower Critical Zone and upper part of the Lower Zone, intersected in the boreholes NG1 and NG2, drilled on the farms Nooitgedacht KQ 406 and Zwartklip KQ 405 at the Union Section of Rustenburg Platinum Mines, northwest of the Pilanesberg (Figure 1.1).

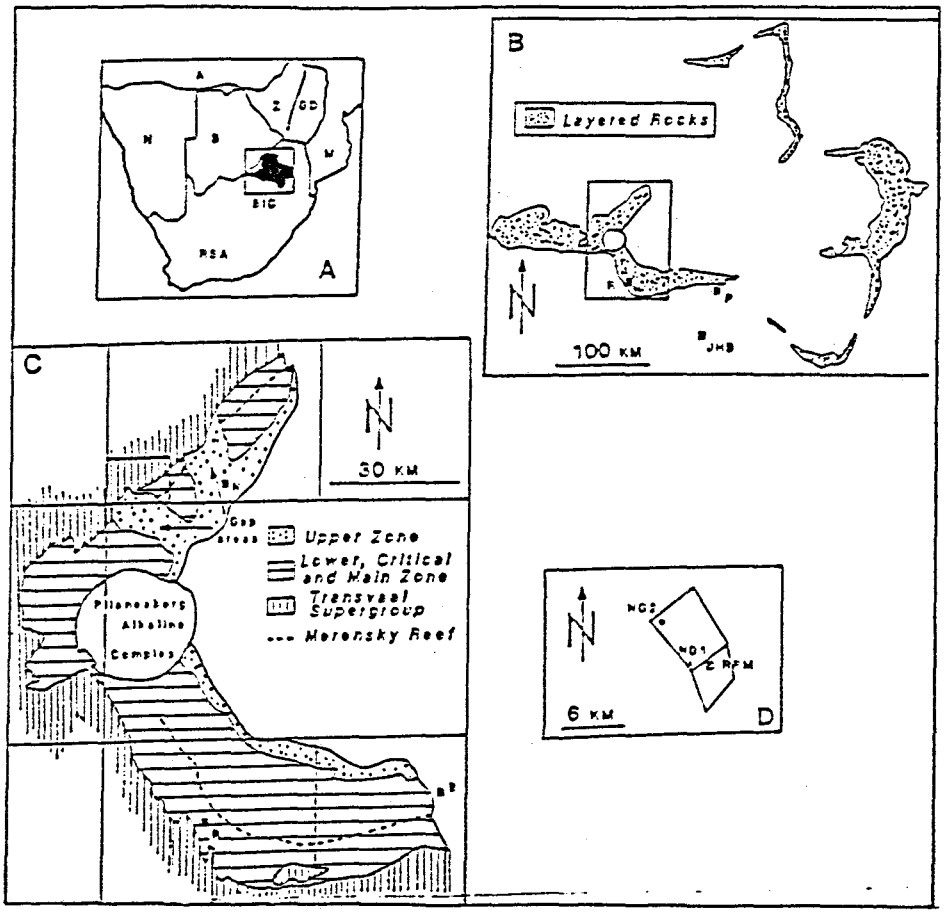

Figure 1.1: Locality map of the Bushveld Complex (A), the extent of the layered rocks (B), the geology of the western limb of the Bushveld Complex (C) and the NG drilling sites (D). P: Pretoria; JHB: Johannesburg; R: Rustenburg; B: Brits; N: Northam (after Teigler, 1990).

It was hoped that core from the whole of the Lower Zone would be available, but this, unfortunately was not the case during the author's period of study at Rhodes University. Core from NG2 to a depth of about 327 m was available for study, with more core, to a depth of 530 m becoming available at the last moment, so whole rock and mineralogical data are complete to 327 m, but only olivine data from the remaining core. The hole was eventually stopped at 774.70 m (Teigler, 1991).

Little detailed study has been done on the lower Critical and Lower Zones in the western part of the Bushveld, so one of the main purposes of this research is to provide a clear description of the properties of these rocks in order that they may be compared with their correlatives in other parts of the Complex. The olivine-bearing rocks were chosen for particular attention, because olivine is one of the first minerals to crystallise from a cooling mafic magma, and therefore its chemistry and petrography could be indicative of the crystallisation history of the suite of rocks. The pyroxenites, chromitites and norites of the NG intersections were the subject of detailed research by B. Teigler (1991).

2. SCOPE OF FIELD INVESTIGATION

In collecting data and gaining some background information for this investigation, two visits were made to the Bushveld Complex in 1987. During the first visit three mines were visited, namely Rooiberg Tin, Zaaiplaats Tin and Impala Platinum Mines. Time was spent in both the eastern and western parts of the Complex, with more emphasis on the eastern part, due to good exposure of the rocks there. In the western part of the complex the drilling sites of NG1 and NG2 were visited. In Pretoria, core from NG1 and NG2 was logged and sampled and brought back to Grahamstown for analytical work. The second visit coincided with the NGP Conference on the Bushveld, held near Rustenburg in 1987. As part of the conference proceedings, visits were paid to Millsell Chrome Mine and Impala Platinum Mine where the Critical Zone lithologies were examined.

3. RESEARCH METHODS

In this chapter details of sample preparation and data collection are presented.

3.1 LOGGING AND SAMPLING

The first ca. 700 m of core from NG1 was logged and sampled at the Geological Survey in Pretoria by Professor H.V. Eales, W.J. de Klerk and F.C. Walraven. The remaining 130 m of NG1 and 360 m of NG2 was logged and sampled by W.J. de Klerk, Dr. R.N. Scoon, B.E. Teigler and S.A. Haikney, and the final 400 m by B.E. Teigler and W.D. Maier. Samples of half core were taken wherever the lithology changed, and where there were thick homogeneous sequences, samples were taken at 5 m intervals.

3.2 NUMBERING SYSTEM

The system used for numbering the samples was to assign the borehole name, followed by the depth of the middle point of the sample below the borehole collar, e.g. NG1 324.75. This scheme was chosen, primarily, to facilitate the interpolation of further samples between samples previously taken, and to provide a simple method for locating samples on profiles.

3.3 PETROGRAPHIC ANALYSIS

80 thin sections from NG1 and 68 from NG2 were cut from the dunites and harzburgites. Modal analyses were carried out on 66 samples from NG1 and 56 samples from NG2, using an integrating stage. A spacing of 1 mm was used between points along a row, and 1 mm between rows. Grain-size measurements were made wherever there was an obvious change in grain-size. This was done by measuring the longest and shortest diameters of the 50 largest grains in the slide (to avoid sectioning effects). Using the method of Friedman (1958) cumulative frequency curves were drawn, and the average grain-size for the slide was taken to be the fiftieth percentile (median). The thin sections were also examined for texture and phase relations.

3.4 MICROPROBE ANALYSIS

Microprobe analyses of olivine orthopyroxene, clinopyroxene, plagioclase and chromite were carried out using the Jeol 733 Superprobe at Rhodes University. The samples were prepared and run in the standard manner employed at the University (see Appendix III in Teigler, 1991)

3.5 CHEMICAL ANALYSES

Whole rock analyses were carried out by XRF methods. Fused discs and pressed pellets were made and run following standard procedures used at the University (see Appendix III in Teigler, 1991).

4. OVERVIEW OF THE BUSHVELD IGNEOUS COMPLEX

4.1 INTRODUCTION

The Bushveld Igneous Complex is unique: it is the largest known layered mafic intrusion, underlying an area of 65 000 square kilometres (Tankard et al., 1982). It has persistent igneous layering, and extremely large reserves of economically important minerals, such as the platinum group minerals and nickel, chromium, vanadium, titanium, iron and tin ore minerals.

Hall (1932) drew together all the previous work done on the Bushveld Complex to that date, and produced a comprehensive review of the contemporary understanding of the Complex. He proposed that the Complex is composed of six major components:

- a First Volcanic Phase of basaltic or andesitic amygdaloidal lavas interstratified with the Pretoria Group;
- a Second Volcanic Phase of acid lavas, tuffs and other pyroclastic rocks, occurring both interstratified with and independently of the sediments (the Rooiberg Series);
- a Granophyre or Minor Plutonic Phase, closely associated with the previous volcanic phase;
- a Sill Phase of basic intrusions where thick sheets of gabbro and dolerite penetrated the floor of the Complex;
- an Earlier Main Plutonic Phase (or Norite Zone); an extremely large lopolithic sill emplaced between the Pretoria Series below and the Rooiberg Series above (now the Rustenburg Layered Suite);
- a Later Main Plutonic or Red Granite Phase, emplaced as sheets and as dykes roofed by sediments of the Rooiberg Series or the Felsite group (now the Lebowa Granite Suite).

For the purposes of this thesis, the Bushveld Complex will be taken to comprise layered mafic and ultramafic sequences, granites, granophyres and felsites (after Tankard et al., 1982); the various peripheral satellites will be ignored. The Complex has five lobes, comprising western, far western, eastern, southeastern and northern lobes arranged about two axes; one trending east-northeast follows

the line of the eastern, western and far western lobes, and another trending north-northwest follows a line joining the northern and southeastern lobes. The peripheries of the lobes are mafic and ultramafic, but the cores of the lobes are not exposed. There does not seem to be continuity between the lobes in the east and the west, but on the basis of geophysical data there is some continuity between the eastern lobes (Tankard et al., 1982).

4.2 STRATIGRAPHY

4.2.1 Rustenburg Layered Suite

The best field exposures of the Rustenburg Layered Suite occur in the eastern Bushveld, where the full succession is exposed. In the western lobe exposure is poor and information on the details of stratigraphy has been gathered largely from borehole core and underground mapping. There are five zones. From the bottom upwards they are: the Marginal Zone, Lower Zone, Critical Zone, Main Zone and Upper Zone. There is no general consensus as to where the boundaries of the zones should be, because different workers base their sub-divisions on different kinds of data: petrographic, geochemical, field relations, etc.

4.2.1.1 Marginal Zone

The Marginal Zone is also known as the Chill Zone, Hendriksplaats Norite and Maruleng Norite. A thin chill facies where the rocks of the Critical Zone or Main Zone are in contact with the Pretoria Group sediments was first described by Daly (1928), and was reinvestigated by Nel (1940). Willemse (1959) did not find a chilled margin between his Basal Zone (Lower Zone) and the sediments of the Pretoria Group, but Frick (1973) found an area where the chilled margin has a cross-cutting relationship with the country rocks. He found it to vary in width from 1.5 to 7.0 metres, dipping at 60 degrees to the west in the area north of Dullstroom, the dip of the Bushveld Complex layering in the same area being 10 degrees in the same direction.

Two types of magmas (Davies and Tredoux, 1985) are believed to have been involved in the crystallisation of the Rustenburg Layered Suite; the one is a magnesian basalt (MgO approximately 12%) and the other a tholeiitic basalt (MgO approximately 7%). The different chemistry of the two magmas is reflected in the Marginal Zone rocks in the eastern Bushveld, which can be divided into a pyroxenitic group and a gabbroic group, using the terminology of Harmer and Sharpe (1985). The pyroxenitic group (B_1) which comprises pyroxenites, peridotites and norites borders the Lower and lower Critical Zones; the gabbroic group (B_2 and B_3) borders the upper Critical and Main Zones.

In the pyroxenite group the most common rocks are orthopyroxenites; they are generally medium- to coarse-grained. Rare olivine may occur within sheets with a basal layer rich in xenoliths. In the norites, biotite and quartz attain the status of essential constituents, while clinopyroxene, chromite, magnetite and ilmenite are accessory. Ultramafic rocks occur as sills and as discontinuous pods in the eastern Bushveld. The majority of the peridotites contain subhedral to anhedral olivine (Fo_{83} - Fo_{90}), enclosed in orthopyroxene oikocrysts, with accessory intercumulus plagioclase (An_{59} - An_{76}) and clinopyroxene, orthopyroxene (cumulus), biotite, chromite and sulphides (Harmer and Sharpe, 1985). The gabbroic (B_2) rocks bordering the Critical Zone comprise plagioclase (An_{52} - An_{58}), orthopyroxene, clinopyroxene, quartz, ilmenite, magnetite and rare biotite.

The stratigraphically higher marginal (B_3) gabbros of Harmer and Sharpe (1985) bordering the Main Zone are coarser (0.2 - 0.7 mm) than those below, and they often contain inclusions of floor rocks. They are generally composed of plagioclase (An_{54} - An_{65}), clinopyroxene, orthopyroxene, pigeonite and abundant magnetite, with biotite, K-feldspar, quartz and sphene as accessory minerals (Harmer and Sharpe, 1985). It is thought that the chill facies represents the composition of contemporary magmas which were modified by earlier fractional crystallisation.

4.2.1.2 Lower Zone

The Lower Zone rocks in the eastern lobe are divided (SACS, 1980) into four units:

- Serokolo Bronzitite
- Rostock Bronzitite
- Jagdlust Harzburgite
- Clapham Bronzitite

The Clapham Bronzitite consists mainly of feldspathic bronzitite with a harzburgite layer at the base, and two thin noritic layers. The overlying Rostock and Serokolo Bronzitites are nearly monomineralic rocks, containing 95 - 99.8 volume percent bronzite, with minor amounts of plagioclase and clinopyroxene (Tankard et al., 1982). In the Jagdlust Harzburgite, chromite is a minor constituent; the unit consists of harzburgite and pyroxenite with repetitive cyclicity in the crystallisation sequence :

olivine ---> olivine + orthopyroxene ---> orthopyroxene

In the western lobe (Tankard et al., 1982) the basal rock units consist of norite and pyroxenite overlain by cyclic units of harzburgite and pyroxenite. Plagioclase is a minor cumulus mineral in the pyroxenites of the upper cyclic units and is a common intercumulus component of the lower pyroxenite layers (Tankard et al., 1982); this seems to be the equivalent of the Clapham Bronzitite of the eastern lobe. Above this there is a monomineralic pyroxenite with sequences of harzburgite and pyroxenite interlayered, which is lithologically similar to the Jagdlust Harzburgite, Rostock Bronzitite and Clapham Bronzitite units in the eastern lobe, but the pyroxenite appears much thinner in the west.

In the southeastern lobe the Lower Zone is only 45 m thick in the Bethal area - intersected in borehole KLG/2 on the farm Kaallaagte 255 IS byBuchanan (1975). It comprises olivine pyroxenites (termed orthopyroxene peridotites by Buchanan, op. cit.), with thin layers of harzburgite. The plagioclase is intercumulus, and the mafic

minerals are iron poor.

4.2.1.3 Critical Zone

The Critical Zone in the eastern lobe is divided into the Zwartkoppies pyroxenite and Winterveld norite-anorthosite, on the basis of the absence/presence of cumulus plagioclase. Major units in these lithologies can be traced 45 kilometres in a northerly direction from the Steelpoort Fault (Tankard et al., 1982). The Zwartkoppies Pyroxenite is a feldspathic bronzitite, the base of which is a "layer" forty metres thick of nearly monomineralic bronzitite interlayered with feldspathic bronzitite. Chromite appears sporadically as an important cumulus mineral in the portion of the pyroxenite above this base - at least thirteen chromite layers occur, the most important being the Steelpoort layer, which is about one metre thick and continuous along strike for eighty kilometres. Igneous layering is well developed in two of the harzburgite subunits in the Zwartkoppies Pyroxenite; the lower one, which is twenty metres thick, has been noted (Cameron and Desborough, 1969) to have 160 individual layers. The appearance of cumulus plagioclase marks the beginning of the Winterveld Norite-Anorthosite. This contact is discordant according to Cameron and Desborough (1969) - not parallel to the layering and marked by evidence of erosion, including scouring. The igneous layering in this unit is the most impressive in all of the Rustenburg Layered Suite; the individual layers can vary from a few centimetres to more than one hundred metres, and contacts can be gradational or sharp. The cumulate minerals chromite, orthopyroxene and plagioclase are present in different proportions, resulting in a diversity of layers ranging in composition from norite to monomineralic layers of chromitite, pyroxenite and anorthosite. In places there is cyclic repetition of:

chromite ---> (olivine) ---> pyroxene ---> plagioclase.

Cumulus clinopyroxene is present in only two noritic layers near the top of the Critical Zone, in the 'M' unit of Cameron (1970). The Merensky and Bastard Reef units are the most complete of the cycles;

they contain chromitite (sometimes harzburgite) and pyroxenite, norite and anorthosite, and the Merensky Unit is an economically viable source of copper, nickel and platinum group metals. In the western lobe the Critical Zone is thinner (~850 m as opposed to ~1400m in the eastern lobe (SACS, 1980)) and in the southern parts of the southeast lobe it is not present (Buchanan, 1975).

4.2.1.4 Main Zone

The Main Zone is composed of relatively homogeneous rocks, which are divided into three subzones on the basis of the cumulus minerals. The zone is characterised by an abundance of cumulus clinopyroxene, and an absence of chromite and olivine.

The Winnaarshoek Norite-Anorthosite is the lowest subzone in the east; it is somewhat similar to the underlying Critical Zone. Layering is due to the varying proportions of cumulus pyroxene and plagioclase; mottled anorthosites, with large intercumulus pyroxene grains, are common. A two hundred metre-thick "porphyritic" norite can be traced for one hundred and eighty kilometres in the west and for one hundred and twenty kilometres in the east. These norites contain large orthopyroxene crystals, approximately 5 mm in diameter, with inclusions of plagioclase (Von Gruenewaldt, 1973). The top of the subzone is at the upper anorthosite layer, which coincides with a minor reversal in the trend of the composition of cumulus orthopyroxene and plagioclase, and where inverted pigeonite first appears (Von Gruenewaldt, 1973).

The next subzone, the Leolo Mountain Gabbronorite as it is known in the east, consists of thick gabbroic layers with few variations in texture and proportions of cumulus minerals.

The Pyroxenite Marker, a pyroxenite layer approximately 1 m thick marks the division between the Leolo Mountain Gabbronorite and the overlying Mapoch Gabbronorite in the east. It is overlain by rocks similar to the Winnaarshoek Norite-Anorthosite and the Leolo Mountain Gabbronorite. In the west the sequence is similar. The Main Zone is not found in the southeastern lobe.

4.2.1.5 Upper Zone

The base of the Upper Zone is marked by the appearance of cumulus magnetite. Layering is prominent due to varying proportions of cumulus magnetite, olivine, pyroxene and plagioclase. In the eastern lobe the zone is divided into three subzones on the basis of the appearance of significant volumes of cumulus magnetite, cumulus Fe-rich olivine, and cumulus olivine with cumulus apatite (Tankard et al., op. cit.).

The Magnet Heights Gabbronorite contains the Main Magnetite Layer, approximately 1.5 metres thick. Nine other magnetite layers occur in the lower part of this lithostratigraphic unit; none is more than thirty centimetres thick. These layers have sharp basal contacts and gradational upper contacts, through feldspathic magnetite to magnetite gabbro. The Main Magnetite Layer can be traced for sixty kilometres along strike in the east. The first appearance of olivine, as a major cumulus mineral in the Upper Zone, occurs in a 5m thick troctolite layer below the Main Magnetite Layer. Two- to three hundred metres of gabbro-norite form the upper part of the subzone. This unit is homogeneous, except for a localised layer of mottled anorthosite.

The next subzone, the Ironstone Magnetite Gabbro is marked by the appearance of another five-metre thick troctolite, previously known as the Sisal Marker. The rest of the subzone is a magnetite gabbro, with seven thin magnetite layers. Cumulus olivine is found in minor amounts at various levels.

The appearance of cumulus apatite in olivine diorite marks the base of the upper subzone - the Luipershoek Olivine Diorite. The Fe-rich olivine is an important cumulus mineral, and the composition of the feldspar is andesine. Seven magnetite layers occur in the lower half of the subzone; the topmost one can be up to ten metres thick (Von Gruenewaldt, 1973). The upper half of the subzone is composed of two hundred metres of olivine-bearing diorite, overlain by a hornblende-bearing diorite, which contains intercumulus K-feldspar, quartz and scattered fayalite. The top of the subzone is overlain by

any of the following: the Transvaal Supergroup, the Rashoop Granophyre Suite, the Lebowa Granite Suite or the Rooiberg Felsite Group.

In the western lobe the Upper Zone consists of magnetite troctolite, olivine diorite and magnetite gabbro. In the southeast lobe it is divided into four subzones, which overlie the stratigraphic equivalent of the Lower Zone. The lowest subzone has only been intersected in one borehole; it consists of gabbro and norite together with anorthosite, and pegmatoid with orthopyroxene, clinopyroxene, plagioclase and magnetite. The presence of sulphides is a common feature of this subzone. The most common sulphides present are pyrrhotite, chalcopyrite and pyrite. The second subzone is gabbro and norite, the third a magnetite-rich gabbro, and the upper one a magnetite-rich diorite. The zone has a thickness of 1900 metres.

4.2.1.6 The Northern Limb

The northern limb, also known as the Potgietersrus limb, is somewhat different from the eastern and western lobes, although in general terms the same zones can be recognised.

Outcrop of the Lower and Critical Zones is exposed only south of Potgietersrus. The Lower Zone is composed of harzburgite and pyroxenite, and has chromitite layers in stratigraphic positions not matching any other lobes. Van der Merwe (1976) estimated the thickness of the Lower Zone in the northern lobe to be 4 - 6 km.

The Critical Zone was estimated to be 400 metres thick, but if the upper contact is taken at the top of the norites and anorthosites (Vermaak, in Tankard et al., 1982, page 183) overlying the platiniferous layer used by Van der Merwe (1976) to define the top of the unit, then the zone would be at least 1200 metres thick, comparable with the thickness of the Critical Zone in the eastern lobe. The Platreef, a platiniferous layer, differs from the Merensky Reef in both lithology and thickness. The base of the Platreef is a harzburgite or a lherzolite, which is rarely pegmatoidal. A

feldspathic pyroxenite overlies this basal unit, and grades upward to a porphyritic pyroxenite. Chromite blebs and veins occur at all stratigraphic levels in the Platreef (Tankard et al.,1982).

To the south of Potgietersrus the Main Zone comprises a fairly homogeneous sequence of gabbro and gabbronorite, but to the north layering is better developed due to a number of thin pyroxenite layers and a troctolite unit (Van der Merwe, 1976). De Villiers (1970) found chilled Main Zone rocks in contact with Lower Zone rocks south of Potgietersrus, and suggested that this could indicate separate magmatic pulses, but Barrett et al. (1978) proposed that it could be a faulted contact. According to Hulbert (1983) and Hulbert and Von Gruenewaldt (1986) the section of the Potgietersrus limb to the south of the town of Potgietersrus underwent four episodes of faulting, which resulted in the Lower Zone being raised to its present position as an upfaulted block.

The thickness of the Upper Zone is thought to be 1100 metres (Van der Merwe, 1976). The Upper Zone in this lobe consists of intercalations of gabbro, magnetite gabbro, anorthosite and magnetite-olivine-diorite with twenty magnetite layers.

4.2.1.7 Mafic and Ultramafic Pegmatites

Mafic and ultramafic pegmatites in the form of pipe-like bodies occur throughout the Rustenburg Layered Suite. Six main types have been recognised (Tankard et al.,1982).

1. Bronzite Pegmatites are particularly abundant in the Lower Zone, west of the Pilanesberg. The pipes are marked at surface by gossans, and below the gossans they consist of bronzite, phlogopite and nickel sulphides. The distribution of pipes coincides with faulting and fracturing on both a local and a regional scale, and with the thickest accumulation of Bushveld rocks in the area. The maximum development of pipes is in pyroxenite layers with horizontal extension immediately below harzburgite layers (Vermaak,1976).

2. Dunite pipes are found mainly in the Lower Zone, but platiniferous pipes with hortonolite dunite cores and dunite rims occur in the Critical Zone.

3. Diallagite pegmatites, which form irregular masses, anastomosing veins and pipe-like bodies transgressive to layering, are found in the Main and Upper Zones, but are more common in the Critical Zone. Olivine, hornblende, phlogopite, plagioclase and magnetite are all components of the pegmatite.

4. Pegmatites with rounded inclusions are found in the Critical Zone. The matrix consists of clinopyroxene with minor orthopyroxene and plagioclase. The most common inclusions are leucoamphibole and amphibole, others are chromitite and mottled anorthosite.

5. Magnetite pegmatites occur in the Main and Upper Zones, as circular bodies which taper at depth.

6. A vermiculite pegmatite pipe occurs in the Upper Zone of the eastern lobe. It contains coarse books of vermiculite and minor, but coarse, crystals of diallage.

4.2.2 Rashoop Granophyre Suite

This suite is composed of granophyre, microgranophyre, and porphyritic granophyre, the major minerals being quartz and feldspar with minor hornblende and biotite. The grain size ranges from fine to coarsely porphyritic. The Rashoop Granophyre Suite has five different field relations, noted in Tankard et al.(1982).

1. It occurs at the contact of the Rustenburg Layered Suite and the overlying Rooiberg Felsites. The proposed origin is the partial to complete melting of the felsite.

2. It occurs at the contact of the Lebowa Granite Suite and the overlying Rooiberg Felsites or Transvaal metasediments. Four different modes of origin have been proposed:

- crystallisation directly from a magma genetically related to that from which the Lebowa Granite Suite crystallised (Rhodes, 1975);

- crystallisation from a magma unrelated genetically to the Lebowa Granite Suite (Walraven, 1976);

- metasomatic reaction (Ianello, 1976);

- the metamorphic effect i.e., the recrystallisation of Rooiberg Felsite (De Waal, 1972).

3. It occurs associated with discontinuous lenses of meta-sediments, between the Lebowa Granites above, and the Rustenburg Layered Suite below. The origin suggested by Strauss and Truter (1944) and Kuschke (1950) is metamorphism and partial melting of metasediments.

4. It occurs within the Lebowa Granite Suite, either adjacent to cross-cutting plugs of younger granite or to intrusive basic sheets. This could be due to the metamorphic effects of intrusions (Lenthall, 1973; Lenthall and Hunter, 1977).

5. It occurs as intrusions with sharp contacts in the Rooiberg Felsite, where it is possibly of magmatic origin (Clubley-Armstrong, 1977).

4.2.3 Lebowa Granite Suite

This is a "sack name" for the granitic rocks which intrude the Rooiberg Felsites and the Rustenburg Layered Suite. There are two distinct types. The most common is the Nebo Granite (one-time Bushveld, Main and Sekhukhune Granites). It is restricted mainly to the four principal lobes. These granites have crude stratiform layering, from a coarse grey granite at the base, through medium-grained grey and red granite, through a red granophyric granite, to a granophyre at the top; the full number of layers is not always present.

The granites have a simple mineralogy of quartz and feldspar with minor hornblende and biotite. Accessory minerals include zircon, fluorite, apatite, sphene, epidote and magnetite. The alteration of primary minerals has led to the formation of secondary biotite, chlorite, saussurite, epidote, haematite and clay minerals (Tankard et al., 1982). Two types of aplitic phases occur: as irregularly shaped lenses with diffuse margins, and as an aplitic granite in dyke- and sill-like bodies with sharply defined boundaries.

To the north of Potgietersrus three granitic bodies cut across the layering of the Nebo Granite. This is the Bobbejaankop Granite, a coarse-grained red granite composed of quartz and feldspar with variable amounts of chlorite and minor amounts of biotite. It is thought to be a variety of Nebo Granite, from which it can be distinguished by its clusters of tourmaline and the redness of its feldspars. A coarse pegmatite has intruded in places along the contact of the two granites.

The second major granite type is the Makhutso Granite, (De Bruiyn and Rhodes, 1975). It is intrusive into the Nebo Granite in the Dennilton area as small dykes, sills and stocks. It is biotite-rich, and also contains quartz, sodic oligoclase, orthoclase and hornblende. It is fine grained near the margins and coarser grained to porphyritic in the centre.

4.2.4 Rooiberg Group

The Rooiberg Felsites predate the Rustenburg Layered Suite and the Nebo Granites, but the stratigraphic sequence is not well understood. Von Gruenewaldt (1968) had the Rooiberg Felsites subdivided into three zones:

- a Lower Felsite Zone, of both porphyritic and non-porphyritic felsite, which is fine-grained and micrographic, and almost glassy;

- a Middle Felsite Zone, mainly of amygdaloidal and pseudo-spherulitic felsite;

- an Upper Felsite Zone, predominantly of a red porphyritic and glassy felsite.

There is also a proposed two-fold subdivision (Rhodes and Du Plessis, 1976) of a lower felsite sequence which is homogeneous, and an upper felsite sequence which has intercalated sedimentary beds and pyroclastic beds. The top of the lower sequence is marked by quartzite xenoliths up to tens of centimetres in diameter. The base of the lower felsite is usually recrystallised, and partially mobilised due to the intrusion of the Rustenburg Layered Suite. The upper felsite is a flow unit interbedded locally with volcanic breccias, sandstones and tuffs. An agglomerate at the base of the upper unit is overlain by the 'Union Tin Shales', so called because of the occurrence of disseminated cassiterite, which was mined until a few years ago.

North of Witbank the Rooiberg Group has been divided into two sequences (Clubley-Armstrong,1977). The lower sequence, a black felsite, is mainly pseudospherulitic and amygdaloidal, and it overlies the basal micrographic felsite and granophyre. The base of the upper sequence is placed where a continuous quartzite bed appears. Above this marker is a red porphyritic felsite, which is massive, with lenses of quartzite and tuffaceous material occurring sporadically. Lenses of volcanic breccia are overlain by black felsite, which is overlain by a dark laminated mudstone - this may be correlated with the 'Union Tin Shale'. The rest of the sequence is of red porphyritic felsite. Clubley-Armstrong (1977) estimates the maximum thickness in this area to be 4000 metres.

4.3 TECTONIC SETTING

Little has been written about the tectonic setting of the Bushveld Complex. Sharpe (1986) wrote a brief review, which is summarised below. For more detail about hypotheses to account for the formation of the Bushveld Complex, the reader is referred to Lee and Sharpe (1986).

One of the pre-Transvaal tectonic events, which had significance in the evolution of the Bushveld Complex, was the development of the Limpopo Belt between the Kaapvaal and Zimbabwean Cratons about 2.5 Ga ago. Along the southern boundary of the belt runs the Palala Shear Zone, which was re-activated 2 - 2.1 Ga ago, approximately at the same time as the formation of the Bushveld. Tectonism of Transvaal age included the depression of the Kaapvaal Craton, along the "lineament" from the Great Dyke through the Bushveld, and its subsequent infilling by sediments. The Transvaal basin was extended to the south along this lineament. Sub-Transvaal basement lacks extension characteristics, therefore it seems likely that the mechanics of basin depression was either static or compressional.

There was widespread tectonism during Bushveld times. The Vredefort "dome" formed in the Witwatersrand basin along the Great Dyke - Bushveld Complex "lineament". The Crocodile River and Marble Hall "fragments" are two of the large diapiric structures formed within the Bushveld Complex. Domes formed around the edges of the Complex where the heated Transvaal sediments penetrated the basic rocks. They are elongated in the direction of 010 degrees, and have penetrative fabrics which suggest compressive stress from the direction of ~100 degrees during their evolution (Sharpe and Chadwick, 1982).

After the formation of the Complex, the central part subsided, to attain isostatic equilibium (Hattingh, 1986). Wrench movement occurred along the North Bushveld Margin (NBM) while the Waterberg basins formed. The region between the NBM and the Palala Shear Zone became anchored, and when compression was applied from the south, low amplitude folds affected the floor and layered rocks in the

vicinity of Rustenburg (Walraven and Darracott, 1986). At the NBM, the allochthon thrust to the north, deepening the structural troughs with the Waterberg sediments, folded the dolomites, and increased the dip of the layered rocks. Major faults formed along the limbs of the major diapiric "fragments", coplanar to 010 degrees and 160 degrees. These pervasive faults and lineaments were reactivated, and dykes intruded along them during Waterberg or Karoo times.

5. A REVIEW OF THE DISTRIBUTION OF OLIVINE IN SOME LAYERED ALPINE AND OPHIOLITE COMPLEXES AND RELATED BODIES

A brief overview of the occurrence of olivine in layered complexes, including ophiolites, is included here, to provide a framework for the comparison of olivine occurring in the Nooitgedacht boreholes.

5.1 BUSHVELD COMPLEX

Olivine occurs as a major cumulus mineral in the Lower, Critical and Upper Zones of the Bushveld Complex. In the Lower and Critical Zones it is Mg-rich; Wager and Brown (1968) noted olivine compositions of Fo_{88} - Fo_{60} in the Lower and lower Critical Zones, but the value of Fo_{60} cannot be regarded as representative, in the light of current data. In the eastern part of the complex the range of compositions for the Lower Zone is $Fo_{84.8}$ to $Fo_{87.2}$ (Cameron, 1980), and for the Critical Zone a range of Fo_{82} to Fo_{90} is indicated by Cameron (1978). Olivine compositions in the upper Critical Zone of the western limb fall into the range $Fo_{76.7}$ to $Fo_{81.6}$ (de Klerk, 1982). Eales and Reynolds (1986) found that the composition of olivine in the UG2 unit was in accordance with the relationship of Scoon (1985), which applies also to other units of the Complex:

$$Mg/(Mg+Fe^2)_{opx} = [Mg/(Mg+Fe^2+)_{ol} \times 0.875] + 0.125$$

where equilibrium between bronzite and olivine is assumed. Olivine compositions were found to vary from $Fo_{88.5}$ to $Fo_{79.8}$ (Eales and Reynolds, 1986). Botha (1987) found the range of compositions of olivine in the equivalent of Cameron's (1980) C_1 and C_3 units in the western part of the Complex to be $Fo_{84.3}$ - $Fo_{85.5}$ and $Fo_{84.2}$ to $Fo_{89.0}$, respectively. In the Lower Zone olivine occurs in almost monomineralic dunites, with accessory chromite, and in harzburgites where bronzite may or may not be an important cumulus phase. Where bronzite is not cumulus, it usually forms large oikocrysts, enclosing partially to almost completely resorbed olivine grains.

In the Olifants River Trough, the Lower Zone as described by Cameron (1978) is divided into a basal subzone (400 m), a lower bronzitite

subzone (400 m), a harzburgite subzone (540 m) and an upper bronzitite subzone (240 m) (the Clapham Bronzitite, Rostock Bronzitite, Jagdlust Harzburgite and Serokolo Bronzitite of SACS (1980), respectively).

The Rostock bronzitite contains an average of 98.6% bronzite, 1.0% postcumulus plagioclase and 0.6% postcumulus clinopyroxene, and has igneous lamination (Cameron, 1978). The first appearance of cumulus olivine marks the base of the (Jagdlust) harzburgite subzone. This is layered on a scale from a few centimetres to tens of metres. Layering is manifested by variations in modes and grain-size. In the upper part of the subzone one incomplete and two complete cyclic units exist. A complete cycle has olivine with accessory chromite at the base; above this is a poikilitic harzburgite with coarse (up to 3 cm in diameter) intercumulus bronzite. Above the poikilitic harzburgite is a granular harzburgite, where both olivine and bronzite are cumulus minerals, and the top of the cycle is composed of bronzitite with little or no olivine. The formation of the incomplete unit was terminated at the granular harzburgite stage. The upper (Serokolo) bronzitite subzone is similar to the lower one (Rostock Bronzitite), having similar mineralogy and internal structure. The top of the upper bronzitite subzone (and hence the top of the Lower Zone) in the area is marked by the appearance of bronzitite containing 7 - 8 % feldspar (Cameron, 1978). The feldspathic bronzitites are the basal rocks of the lower Critical Zone, which lie conformably on the Lower Zone rocks. In summary, therefore, cumulus olivine marks the base of the harzburgite subzone, and an increase in feldspar from ca. 1% to ca. 8% marks the base of the Critical Zone.

The Lower Critical Zone in the eastern Bushveld Complex is composed of bronzitites interlayered with chromitite, chromitic bronzitite and two units where olivine occurs as a major cumulus phase. The lowermost unit is a bronzitite (the B unit of Cameron, 1980). This is overlain by the C unit which is olivine-bearing. The C_1 unit is composed of regular layers of harzburgite, feldspathic bronzitite, feldspathic dunite, dunite and bronzitite. The C_2 subunit consists of feldspathic bronzitites with a few chromite-rich layers. The C_3

subunit begins with a 0.5 m interval where three to seven chromitites are layered with chromitic bronzitite at the base. There is about 4 m of interlayered bronzitite and harzburgite followed by about 2 m of poikilitic dunite; this is followed by 70 cm of a chromite-rich zone and nearly 6 m of poikilitic dunite, and it is topped by 2.5 m of harzburgite. The olivine in the poikilitic harzburgite can be partially to completely replaced by the bronzite oikocrysts. The D and E subunits contain no olivine; they are composed primarily of bronzite, and intercumulus plagioclase, clinopyroxene and phlogopite.

In the upper Critical Zone in the western Bushveld Complex olivine is seldom seen below the UG1 chromitite layer, but is locally significant between the UG1 and the Bastard Reef (Scoon and de Klerk, 1987), i.e., at the base of the UG2 pyroxenite and in the upper and lower Pseudoreefs, the Pseudoreef Marker and the Merensky and Bastard Reefs. The olivine occurs either as large anhedral grains (5 - 10 mm) or as euhedral to subhedral grains, less than 1 mm in diameter, enclosed by plagioclase in poikilitic harzburgite. In the granular harzburgite and olivine-pyroxenite small euhedral grains of olivine and orthopyroxene are enclosed by plagioclase, and reaction relationships between olivine and orthopyroxene are common. The composition of olivine in the Merensky Reef ranges from $Fo_{78.54}$ to $Fo_{80.81}$, and in the Pseudoreef from $Fo_{79.60}$ to $Fo_{81.39}$ (Scoon and De Klerk, 1987).

The "olivine gap" extends from the base of the Main Zone, where olivine no longer occurs, to about three hundred metres above the base of the Upper Zone, where it reappears as an Fe-rich variety. Subzone A of the Upper Zone does not contain olivine. Molyneux (1970, in Von Gruenewaldt, 1973) took the upper boundary of this subzone to be at the base of the olivine gabbro, about fifty metres below the Main Magnetite Layer. Von Gruenewaldt (1973) prefers the base of the Main Magnetite Layer as the boundary; the olivine gabbro was not found in the Roossenekal area where he was working at that time. The appearance of olivine in the Roossenekal area is taken as defining the base of subzone C. The lower 150 m of subzone C consists of alternating layers of olivine-gabbro, magnetite-gabbro,

anorthosite, and troctolite. The top of the subzone is taken at a fine-grained norite with cumulus, inverted pigeonite and small amounts of cumulus olivine. Subzone D is composed of olivine-diorite with 4 - 8 % cumulus apatite. Olivine-free rocks occur where there are magnetite layers. The olivine at the base of subzone C has a composition of Fo_{48} - Fo_{51} (Von Gruenewaldt, 1973), and it becomes progressively more Fe-rich towards the top of the subunit (Fo_0 according to Wager and Brown, 1968). Another major occurrence of olivine in the Bushveld Complex is in discordant ultramafic pegmatite bodies. Scoon (1985) and Viljoen and Scoon (1985) proposed a classification that differs from that given in the previous section. They dealt with the pegmatites in four groups:

1 - non-platiniferous magnesian dunite;
2 - platiniferous ultramafic pipes;
3 - iron-rich ultramafic pegmatites, of which there are two subgroups, a silicate-rich variety and an Fe-Ti oxide variety;
4 - other bodies, which include the Vlakfontein nickel pipe, orthopyroxenite pegmatites, anorthositic pegmatites, vermiculite pegmatites and amphibolite or shonkinite bodies.

Olivine occurs as a major component in the pegmatites of the first three groups. The non-platiniferous magnesian dunite is composed almost entirely of Mg-rich olivine, which is both mineralogically and texturally comparable with dunites in the cumulates (Viljoen and Scoon, 1985). One of the bodies on Clapham has olivine with a composition of Fo_{85} - Fo_{84}, and has accessory chromite. Some of these bodies have been described by Schwellnus et al. (1962), Coertze (1962, 1974) and Gain (1980).

There are only four known occurrences of the platiniferous ultramafic pipes; these are on the farms Driekop, Mooihoek, Onverwacht and Twyfelaar (not economic), in the Lower and lower Critical Zones of the Bushveld Complex. They are pipe-like bodies which are aligned approximately at right angles to the layering of the cumulates (Viljoen and Scoon, 1985). They are large cylindrical bodies of magnesium-rich dunite, with cores of pegmatitic Fe-rich dunite and wehrlite, where the platinum reserves once occurred. In

some cases there may be an outer zone of pegmatitic wehrlite or clinopyroxenite. Olivine in the cores and outer zones is more Fe-rich than that in the main body of the pipe. In the Driekop pipe, the olivine in the main body has an average composition of $Fo_{83.6}$, and olivine in the core has an average composition of $Fo_{72.7}$. Olivine from the cores of the Mooihoek and Onverwacht pipes ranges from $Fo_{72.7}$ to $Fo_{44 - 43}$ (Scoon, 1985). The Fe-rich ultramafic pegmatite bodies are abundant in the upper Critical, Main and Upper Zones, but occur rarely in the Lower and lower Critical Zones. Those that occur in the Critical Zone are usually of the silicate-rich variety, which comprises hortonolite and clinopyroxene as the main phases, and ilmenite and Ti-magnetite as accessory phases. Olivine compositions in pegmatite bodies between the UG2 and Bastard cyclic units, at Amandelbult, lie between Fo_{50} and Fo_{40} (Scoon, 1985).

5.2 GREAT DYKE

The Great Dyke of Zimbabwe used to be regarded as comprising four complexes, from north to south the Musengezi, Hartley, Selukwe, and Wedza complexes. The Hartley complex is the largest, 250 km in length and the others are between 20 and 85 km in length (Wilson, 1982). Based on more recent work, Prendergast (1987) has the Dyke divided into a northern and a southern subchamber. Of the five main rock types in the ultramafic zone of the Hartley complex (chromitite, dunite, harzburgite, olivine-bronzitite and bronzitite) olivine occurs as a cumulus mineral in all but the bronzitite. The general stratigraphy of the Great Dyke is illustrated in Figure 5.1.

Chromitite layers are taken as defining the base of each cyclic unit, but often there is a thin (5 - 50 mm) layer of dunite or harzburgite between the chromitite and the bronzite at the top of the previous unit (Wilson, 1982). In the C_1 chromitite, layers of coarse-grained chromitite alternate with an olivine-chromite in which the original margins of the olivine grains are outlined by fine cumulus chromite.

Dunite makes up about 70% of the ultramafic sequence. It is composed of cumulus olivine and chromite, with intercumulus orthopyroxene, clinopyroxene and plagioclase. There is no detectable zoning in the

olivine, but it does show undulatory extinction as a result of strain effects. Small euhedral chromite grains occur in the olivine, and larger anhedral grains occur between the olivine grains, filling in the interstices.

Harzburgite occurs as discontinuous layers towards the top of the dunite subunits. It consists of cumulus olivine and intercumulus orthopyroxene, clinopyroxene and plagioclase. There is a reaction relationship between the olivine and the orthopyroxene, which results in partial to complete replacement of olivine by orthopyroxene, giving the rock a poikilitic texture. The original shapes of the olivine grains can be seen by a mantle of chromite grains.

In the olivine-bronzitites, representing the transition from dunite to bronzitite, the texture changes from poikilitic to granular where the orthopyroxene is cumulus, and not formed by reaction between olivine and liquid or from intercumulus liquids alone. As the amount of cumulus orthopyroxene increases, the olivine becomes interstitial and the pyroxene shows a reaction relationship with the olivine (Wilson, 1982).

Overall there is Fe-enrichment upwards in the sequence. Within individual units there is strong Fe-enrichment followed by compositional reversals near the tops of the units. High-Mg olivine occurs at the base of the units, though olivine in association with chromite layers gives anomalously high Mg values, presumably as a result of sub- solidus equilibration. Compositions range from Fo_{84} - Fo_{92}, and the percentage of NiO in the olivines ranges between 0.18% and 0.45%.

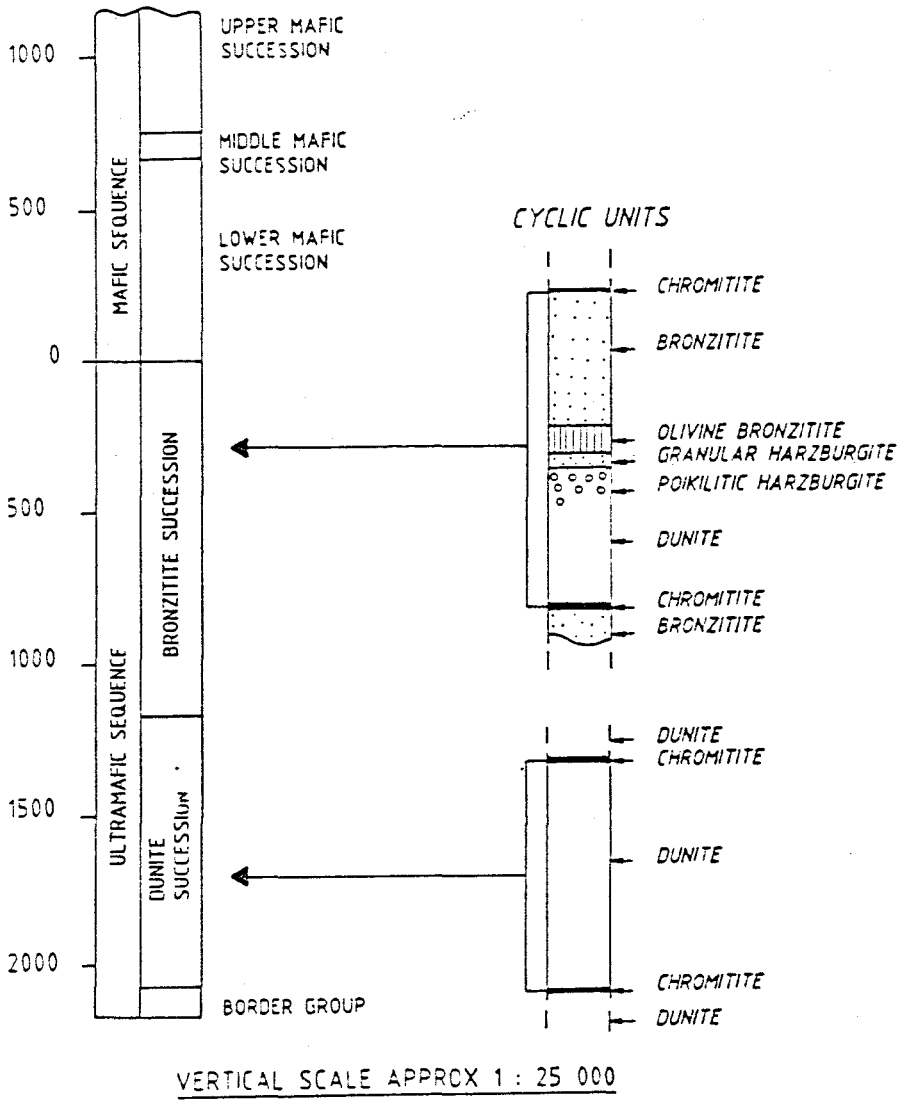

Figure 5.1: General stratigraphy of the Great Dyke (after Wilson and Tredoux, 1990).

5.3 STILLWATER COMPLEX

The Stillwater Complex in Montana, USA, is also regarded by Jackson (1967) to be similar to the Bushveld Complex in composition, structure, mineralogy and texture. The complex is divided into three main series, the Basal, Ultramafic and Banded Series, the latter being further subdivided into the Lower, Middle and Upper Banded Series. The Ultramafic Series is divided into a Lower Peridotite and Upper Bronzitite (Zientek et al., 1985). There are up to fifteen cyclic units in the Lower Peridotite, which ideally occur with chromite cumulates at the base, followed by olivine cumulates, olivine-bronzite cumulates and then bronzite cumulates. The average grain size of olivine ranges between 0.92 and 7 mm (Page et al., 1972). The grain size tends to decrease with increasing stratigraphic height throughout the olivine cumulate. The $Mg/(Mg + Fe^{2+})$ ratio in the olivines from the Lower Peridotite ranges from 0.816 to 0.898, and averages 0.84 (Page et al., 1972). Up to cyclic unit 11, there is a tendency to Mg-enrichment rather than Fe-enrichment (Jackson, 1970; Page et al.,1972), which is attributed by Jackson to crystallisation under non-equilibrium conditions.

A variety of classification systems are used for rocks of the Banded Series, and the one adopted here is that of McCallum et al. (1980). Olivine is a cumulus mineral in all the olivine-bearing layers, but in the troctolite layers it has been considerably resorbed. The five olivine-bearing subzones are complex; they are composed of a number of units, the bases of which are marked by the appearance of cumulus olivine. The sequence of the layers is different in the different subzones. In the Olivine-bearing Subzone 1 the sequence is: troctolite, anorthosite, norite, gabbronorite, and in the Olivine-bearing Subzone 4 the sequence is: troctolite, anorthosite, anorthositic troctolite, olivine-gabbro (McCallum et al.,1980). The J-M (Howland) Reef, which is rich in platinum-group elements (PGE), occurs in the olivine-bearing subzone I. MgO/(MgO + FeO) ratios in the reef range from 0.72 to 0.80 (Barnes and Naldrett, 1985, 1986) In the Banded Zone the olivine grains are often embayed and rimmed by pyroxene; in some cases the overall texture is poikilitic. The compositional ranges from the rest of the zone are between Fo_{65} and

Fo_{75}, but no systematic variation has been found in the data of McCallum et al. (1980).

5.4 RHUM COMPLEX

The Rhum layered intrusion on the Isle of Rhum off the west coast of Scotland, is roughly cylindrical, with a 7 km diameter (Dunham and Wadsworth, 1978). It is composed of alternating peridotite (olivine-rich) and allivalite (plagioclase-rich) layers. Two different stratigraphic successions have been recognised, the Eastern Layered Series (ELS) and the Western Layered Series (WLS). The exposed section of the ELS is 750 m thick, and is composed of 15 units of alternating peridotite and allivalite layers, with each unit being between 15 and 150 m thick. The WLS is up to 1400 m thick, but has only three or four cyclic units. Three units, labelled B, C and D overlie cumulates thought to be the top of another unit A. The B - D units are between 300 and 500 m thick.

Olivine, which occurs throughout the whole layered series, has a composition of Fo_{78} - Fo_{88}. There seems to be Fe-enrichment with increasing stratigraphic height in unit B of the WLS and unit 10 of the ELS, though in the B unit the most Mg-rich olivine occurs about one-third of the way up the unit (Dunham and Wadsworth, 1978). After the appearance of cumulus plagioclase the Fe-enrichment trend is more obvious, but the most Fe-rich olivines occur at about 5% (B unit) to 10% (unit 10) of the thickness of the unit below the top. Above this there is a strong reversal to Mg-enrichment to the top of the unit. The peridotite is composed of cumulus olivine and chromite, and intercumulus clinopyroxene and minor orthopyroxene. The olivines are euhedral, and are either rounded or elongate. When elongated they impart lamination to the rock. In unit 2 of the ELS the rounded olivine grains have concentrations of small chromite grains on their upper surfaces.

In the allivalites the cumulus phases are olivine and plagioclase. The olivine may or may not form lamellae in the rock, but where it is poikilitically enclosed by clinopyroxene no lamination of the rock has been detected. Plagioclase grains enclosed in clinopyroxene

are invariably smaller than those external to the poikilitic grains (Faithfull, 1985). The olivine grains are usually free of inclusions; they are anhedral and irregularly shaped. Clinopyroxene and orthopyroxene occur as interstitial minerals, as do the Fe-Ti oxides which generally occur as interstitial blebs, though in the unit 1 allivalite cumulus ilmenite occurs near the base (Faithfull, 1985).

5.5 MUSKOX INTRUSION

The Muskox intrusion of Canada is made up of four parts, two marginal zones, a layered series and a granophyric roof zone. The layered series is about 1800 m thick, and is made up of eighteen different rock types (Irvine, 1980a). On a broad scale they range from dunite at the base, to pyroxene-bearing peridotite, various pyroxenites, various gabbros and a granophyric gabbro at the top. Olivine forms more than 50% by volume of the layered series, and has associated with it 1 - 2% chromite (Irvine, 1980a). Twenty-five cyclic units have been recognised, of which there are two main types. One of these comprises peridotite-orthopyroxenite-websterite units, composed of cumulus olivine and minor chromite in the peridotite, cumulus bronzite in the orthopyroxenite, and cumulus augite and bronzite in the websterite. Chromite is usually absent from the pyroxenite units of the Muskox intrusion. All the rocks have varying proportions of plagioclase, orthopyroxene, clinopyroxene and biotite as intercumulus minerals. The grain size of the olivine in the peridotite below chromitite layers is almost twice that of the orthopyroxene above the layer; average grain size for the olivine is 1.2 to 1.5 mm. Where there are no chromite layers, the cumulus olivine and orthopyroxene grains are approximately the same size. The second type of cyclic unit is one of dunite - olivine clinopyroxenite - olivine gabbro. This is fully developed only once, but occurs in a telescoped form as paired layers of dunite and olivine clinopyroxenite. The complete unit consists of dunite with cumulus olivine and chromite, olivine clinopyroxenite with cumulus olivine and clinopyroxene, and olivine gabbro with cumulus olivine, clinopyroxene and plagioclase. No chromite occurs where there is cumulus clinopyroxene, and

orthopyroxene occurs as a minor intercumulus mineral. The composition of the olivine is Fo_{79}-Fo_{89} (from figure 8 in Irvine, 1980a).

5.6 JIMBERLANA INTRUSION

The Jimberlana intrusion of Western Australia is a dyke-like body, made up of three main series: the Upper and Lower Series, consisting of alternating sequences of layered olivine and bronzite cumulates, overlain by a plagioclase-augite-hypersthene cumulate; and the Marginal Series, which is in the lower part of the intrusion, where the olivine and bronzite cumulates overlie the plagioclase-augite-hypersthene layer, thus showing reversed fractionation (Campbell, 1977). Olivine and chromite occur as cumulus minerals in all rocks up to the point where cumulus plagioclase appears. The olivine grains have often undergone resorption, which results in variable grain sizes of 0.2 to 2 mm.

There are two main textural types in the ultramafic zone. The first is poikilitic, where plagioclase, augite and bronzite occur as poikilitic intercumulus grains up to 7 mm in diameter (Campbell, 1977). The augite and bronzite can form reaction rims around the olivine, which becomes resorbed. The second is the 'dual grain-size texture' of Campbell (1977); plagioclase and augite occur as small intercumulus grains, and the bronzite has poikilitic edges that enclose the plagioclase and augite grains. The plagioclase is zoned and augite does not form reaction rims around bronzite or olivine. Olivine shows Mg-enrichment at the bottom of the units, which corresponds with the poikilitic texture, and above, where there is the 'dual grain-size texture', the normal Fe-enrichment trend is followed. The composition of the olivine is approximately Fo_{74} to Fo_{82}.

5.7 KIGLAPAIT INTRUSION

The Kiglapait Intrusion of Canada is a part of the Nain Complex in the Labrador Province. The Nain Complex as a whole is anorthositic, but the Kiglapait Intrusion is mainly composed of troctolites. The

Kiglapait Intrusion is regarded by Morse (1979), as being a good example of fractionation of a basic magma in a closed system.

The intrusion is composed of five zones, the Outer Border Zone, Inner Border Zone, Lower Zone, Upper Zone and Upper Border Zone. The Outer Border Zone underlies the northern and northwestern part of the main intrusion. It is composed of a hornblende-bearing olivine ferrogabbro, interlayered with metasediments. The Inner Border Zone comprises a medium- to coarse-grained plagioclase-olivine orthocumulate. This grades upwards into the Lower Zone. The Lower and Upper Zones are collectively termed the Layered Group, and comprise 94% by volume of the intrusion. The Lower Zone is made up of a troctolite with an adcumulate texture; the compositions of olivine and plagioclase at the base of the zone are Fo_{74-70} and An_{70-65} respectively. The appearance of cumulus augite marks the boundary between the Lower Zone and the Upper Zone; at this boundary, the composition of olivine is Fo_{67-61}, and that of plagioclase is An_{55-51}. The Upper Zone is subdivided on the basis of the gradation of plagioclase to antiperthite and mesoperthite, and on the appearance of cumulus apatite, sulphide and titanomagnetite. At the top of the Upper Zone , olivine is pure fayalite (Fo_0), and plagioclase has a composition of An_{18-12} (Huntington, 1979, Morse, 1980). There is extreme Fe-enrichment in the upper parts of this zone, the uppermost rocks being ferrosyenite. The Upper Border Zone has a similar pattern of mineral composition as the upper 20% of the Upper Zone, except it seems to have crystallised from the roof down, resulting in a mirror image trend, and it is finer grained.

5.8 DUKE ISLAND ULTRAMAFIC COMPLEX

The Duke Island Ultramafic Complex of Alaska is one of approximately 35 bodies of ultramafic rocks along the 350-mile "pan-handle" of Alaska. The rocks in the complex range from dunite through peridotite and olivine clinopyroxenite to hornblende clinopyroxenite. No orthopyroxene or plagioclase occurs in the ultramafic rocks (Irvine, 1963). There is a tendency to Fe-enrichment from the bottom to the top of the complex. Olivine compositions range from Fo_{85} to Fo_{78}, and the clinopyroxene

composition ranges from $Ca_{45}Mg_{48}Fe_7$ to $Ca_{50}Mg_{38}Fe_{12}$ (Irvine, 1963, 1967). The dunite and peridotite contain accessory chromite and some secondary magnetite as a result of serpentinisation. Layering in the complex is mainly due to grain-size rather than to mineral density, and it is particularly evident in the olivine-bearing rocks. The layering seems to involve only olivine and clinopyroxene. Most of the layers are 2 - 10 inches (5 - 25.5 cm) thick, but the largest graded layer observed (Irvine, 1963) is 25 feet (approximately 8.5 m). In an average layer the grain-size is 4 - 10 mm at the base, decreasing to 0.2 -2 mm at the top. The bases of the graded layers are sharp, but the tops can be sharp or transitional to a finely laminated rock. Olivine tends to concentrate towards the tops of the units; it is generally finer grained than the accompanying clinopyroxene. Another type of layering occurs, which appears similar to the "inch-scale layering" of Hess (1960) in the Stillwater Complex. The layering is marked by alternation of olivine and pyroxene, and thin discontinuous bands of dunite (Irvine, 1963).

5.9 CANYON MOUNTAIN OPHIOLITE

The Canyon Mountain Ophiolite of Oregon consists of four units: a harzburgite tectonite, a metacumulate, a cumulate and a sheeted dyke unit (Himmelberg and Loney, 1980). The harzburgite tectonite consists primarily of harzburgite (grain-size 4-5 mm, xenoblastic granular texture), with plagioclase at the contact with the metacumulates. Irregular dunite bodies with or without podiform chromite occur within the harzburgite, and may range in size from tens to hundreds of metres. These are thought, on the basis of composition, to be derived from the metacumulates. Dunite also occurs as veins, dyke-like bodies and irregular bodies in the harzburgite, which may be the result of metasomatism.

The metacumulate layer, consisting of interlayered ultramafic (grain-size 2-3 mm, allotriomorphic granular texture) and gabbroic rocks, is so called because of the strong foliation and lineation imposed on the original cumulus texture. The ultramafic rocks are mainly olivine and clinopyroxene cumulates. Associated with some of the dunites are podiform chromite deposits, which were found by

Thayer (Himmelberg and Loney, 1980) to be from a few kilograms to one hundred and twenty-five thousand tons in size. The gabbroic and ultramafic rocks are interlayered on a scale of a few centimetres to tens of metres. The olivine composition ranges from $Fo_{92.8}$ in dunite to $Fo_{68.1}$ in gabbro (Himmelberg and Loney, 1980).

The cumulates are broadly folded, and are composed of gabbros and gabbronorites with wehrlite lenses. There is rhythmic layering within the gabbros, of varying plagioclase - pyroxene ratios. The wehrlite lenses, which are up to tens of metres thick, show no layering. The overall range of olivine compositions is $Fo_{92.8}$ - $Fo_{68.1}$. (Himmelberg and Loney, 1980).

Plagioclase from cumulate and metacumulate ultramafic rocks has a composition range of An_{96} - An_{73}. There seems to be no good correlation between the An number (An/An+Ab+Or) of plagioclase and the MMF (MgO/MgO+FeO) of co-existing mafic silicates. There are significant amounts of Mg and Fe present in all the analysed plagioclase; it is suggested (Himmelberg and Loney,1980) that the iron present is Fe3+ substituting for Al, while Mg substitutes for Ca.

5.10 TROODOS OPHIOLITE

The Troodos ophiolite of Cyprus can be divided into four units, from bottom to top: peridotites, transition zone, sheeted diabases and pillow lavas. The peridotites occur as small irregular bodies, and there are no exposed contacts between these and the older autochthonous rocks. The peridotite is made up of harzburgite with minor dunite. The contacts are steeply inclined, and mineral banding, which consists of varying quantities of olivine and clinopyroxene, is discontinuous. The banding and elongated chromite lenses within the dunite trend in a north-south direction (Coleman, 1977).

The dunites have a xenomorphic granular fabric, and consist of olivine and chromite. The harzburgite has the same texture, but is composed of about 80% olivine, 20% orthopyroxene and accessory chromite. Small plagioclase-lherzolite masses occur within the

harzburgite near its boundary with the dunite. They consist of 65% olivine, 15% orthopyroxene, 10% clinopyroxene, 8% plagioclase and 2% spinel. The olivine composition is Fo_{90} to Fo_{92} (Coleman, 1977). Serpentinisation occurs throughout the peridotite unit - it can be up to 100% in some rocks. On the western and southern sides of Mount Olympus there are outcrops of ultramafic cumulates, which seem to have crystallised in the following sequence, from bottom to top:

chromite; olivine + chromite; olivine + clinopyroxene;
olivine + clinopyroxene + orthopyroxene + plagioclase;
clinopyroxene + orthopyroxene + plagioclase.

There is no sharp boundary between the peridotite and the transition zone, the basal cumulate rocks of which are gabbro-norite, troctolite, wehrlite, pyroxenite and dunite; these are overlain by clinopyroxene-bearing gabbros and gabbro-norites. The composition of plagioclase in the upper gabbros is in the range An_{72} - An_{92}.

5.11 OMAN MOUNTAINS

The Semail ophiolite complex of Oman and the United Arab Emirates forms part of the Oman Mountains and the Middle East alpine mountain chain. It is divided into six units, from bottom to top: a metamorphic zone, peridotite zone, transition zone, gabbro zone, dyke section and volcanic zone (Coleman, 1977). This ophiolite is composed of a number of individual plates, rather than a continuous sheet or nappe. Tectonic repetition of the ophiolite sequence has been caused by low-angle thrust faults.

The peridotites make up about 60% of the outcrop of the ophiolite. They have undergone considerable alteration, with serpentinisation affecting from 60 - 100% of the rock. The harzburgite consists of 60% to 80% olivine (Fo_{90}), 10% to 25% orthopyroxene (En_{90} - En_{91}) and accessory chromite (Coleman,1977). Lenses of dunite occur in the harzburgite, which can contain chromite concentrations. Orthopyroxene dykes and magnesite veins cut across the harzburgite and dunite; above this is a 200 m thick zone of dunite, composed of cumulus olivine and chromite. The contact between the peridotite

zone and the transition zone is not clear. In the transition zone occurs the first of the rocks with cumulus plagioclase; this zone is characterised by alternating dark and light bands. The dark bands are made up of cumulus olivine and clinopyroxene and the light bands of anorthosite, troctolite, gabbro and norite. In the banded rocks the olivine is more Fe-rich (Fo_{85} - Fo_{88}) than in the peridotite zone, and the plagioclase and clinopyroxene are higher in calcium (An_{81}-An_{92}, and $Fe_{5.8}Mg_{50}Ca_{44.2}$) respectively; (Reinhardt, 1969 in Coleman, 1977). Gabbro, troctolite and anorthosite dykes cut the transition zone, and brecciated areas are invaded by leucogabbros. The layering tends to be discontinuous and pinches out over several metres. The transition zone grades upwards into layered then massive gabbros of the gabbro zone. Plagioclase compositions range from An_{92} - An_{65}, and olivine compositions from Fo_{72} - Fo_{85} (Coleman, 1977).

5.12 THE TWIN SISTERS DUNITE

The Twin Sisters Dunite, in Washington State, USA, is composed of an enstatite-bearing dunite, which is reddish-brown in colour. The dunite is composed of four minerals, olivine, orthopyroxene, clinopyroxene and chromite. The olivine has a composition of about Fo_{90}, which changes very little throughout the body. The orthopyroxene (enstatite), has a similar Fe/Mg ratio to that of the olivine (Ragan, 1967). Overall, chromite averages 1 - 2 % of the rock, but there are greater concentrations of local significance. The clinopyroxene, a chromium diopside, occurs in trace amounts.

Primary textures in the dunites, such as coarse, interlocking anhedral olivine grains, with interstitial orthopyroxene and disseminated euhedral to subhedral chromite grains, indicate a magmatic origin. The texture of the dunitic mass varies fairly widely. In some places the olivine grains are coarse (up to 5 cm in length), and anhedral, having interlocking boundaries. Enstatite with clinopyroxene exsolution lamellae occurs between olivine grains, either as thin intercumulus grains partially surrounding the olivine grains, or as large isolated subhedral crystals (Ragan, 1967). Chromite occurs either as disseminated euhedral to subhedral grains,

or as concentrations in bands.

There can be a strong preferred crystallographic orientation in the olivine; this has been particularly noted in grains which are 5 - 10 mm in length, where the (100) plane is statistically oriented parallel to visible structures. Partial recrystallisation is indicated by areas of fine-grained olivine, with a mosaic texture, occurring between large primary olivine grains, which show undulatory extinction (Ragan, 1967). There is a tendency for these zones of recrystallised material in the core of the dunite to lie parallel to the long axis of the body, and at the edges of the body the zones run parallel to the contacts.

5.13 SUMMARY

The aim of this review is to summarise the mode of occurrence of olivine-bearing rocks in different types of intrusions, and the composition and the relationship of olivine to co-existing minerals in the different intrusions.

The compositions of olivine and plagioclase in the layered intrusions discussed above are presented in Figure 5.2. The majority of ultramafic complexes discussed in this review have a characteristic association of magnesian olivine and calcic plagioclase. Two notable exceptions are the Bushveld Complex and the Kiglapait intrusion. The Kiglapait intrusion is highly differentiated, and hosts pure fayalite, as does the Upper Zone of the Bushveld Complex. The most sodic plagioclase would be expected to occur with the Fe-rich olivines, as it does in the Kiglapait intrusion. In the Bushveld Complex, however, the most sodic plagioclase occurs in the lower Critical and Lower Zones (Figure 5.2), as an intercumulus phase .

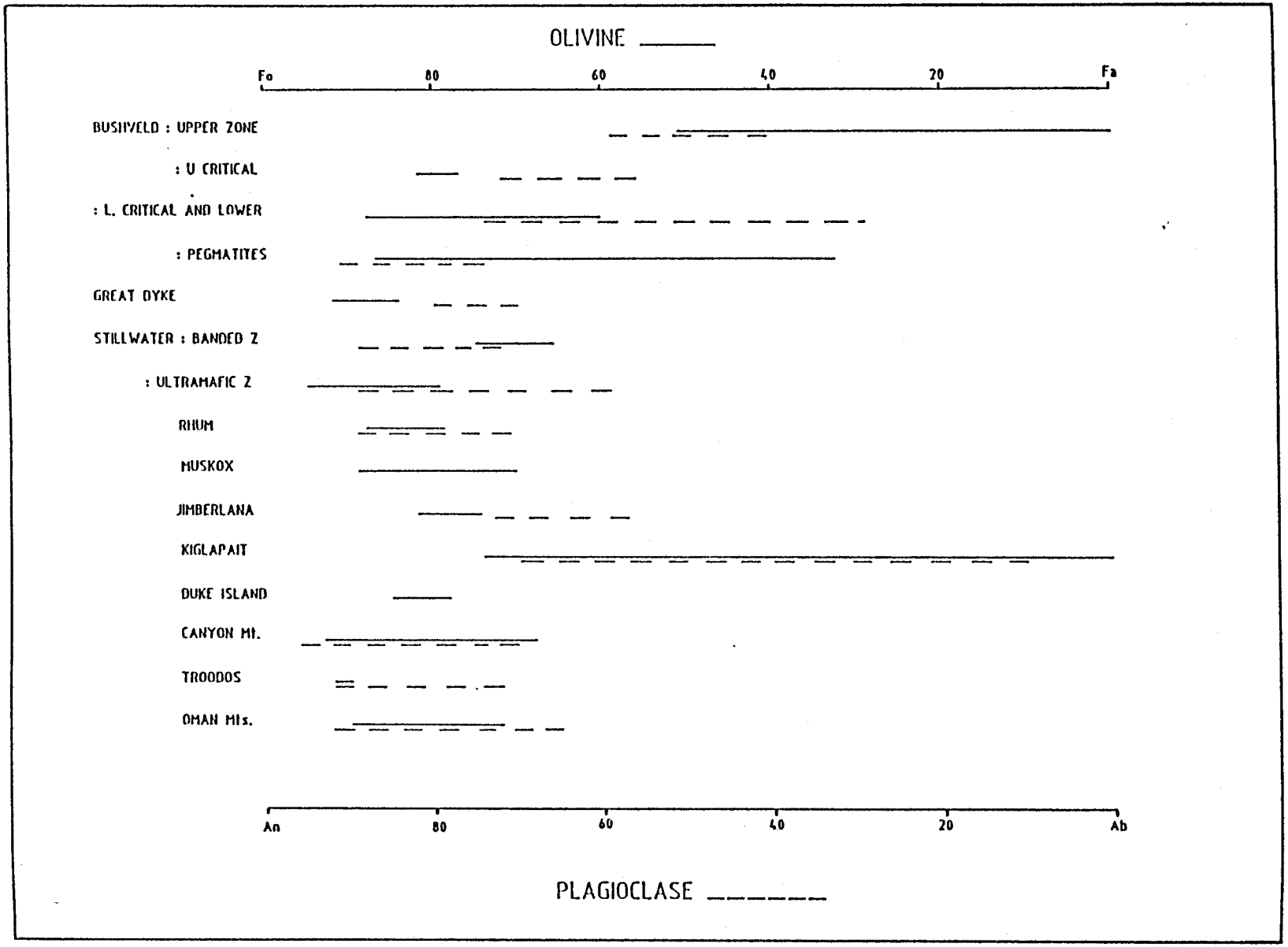

Figure 5.2: Ranges of olivine and plagioclase compositions in some layered intrusions.

6. PETROGRAPHY OF THE OLIVINE-RICH CUMULATES INTERSECTED BY THE NOOITGEDACHT BOREHOLES

6.1 INTRODUCTION

The petrography of the olivine-bearing rocks in boreholes NG1 and NG2 is discussed in this chapter. The petrographical study was based on approximately 230 thin sections, therefore in order to avoid excessive length and repetition in description, generalisation has been necessary. Certain samples have been specifically mentioned where they either display unique features, or characterise the general texture of the group. A brief review of cumulus textures is given first, including some ideas as to how they could form. Their implied significance is discussed. A description of the rocks of this study then follows.

6.2 THE TEXTURES OF CUMULATE ROCKS

The cumulate terminology of Wager et al. (1960) was originally proposed in conformity with a crystal settling model. The settling model is now not entirely accepted, but the names given to the different textures are still retained. Those most commonly used are orthocumulate, mesocumulate and adcumulate; the ortho- and adcumulates being the end members of a continuum of textures. Figure 6.1 illustrates diagrammatically the appearance of these textures in a plagioclase cumulate. Wager et al. (1960) also proposed the term heteradcumulate, for textures dominated by poikilitic, unzoned crystals having the same composition as they would have had as cumulate grains, enclosing numerous smaller primocrysts of a different phase. They considered that the rocks are genetically related to adcumulates, hence the name linking the two. The name has tended to fall away, however, in favour of the more descriptive term "poikilitic" as proposed by Irvine (1982). Irvine (op. cit.) also proposed a general rule for the classification of textures into the three main groups. He allowed that the exact percentage limits would depend on the grain-size and type of the minerals involved, but suggested that intercumulus minerals make up 25-50% of orthocumulates, 7-25% of mesocumulates and 0-7% of adcumulates.

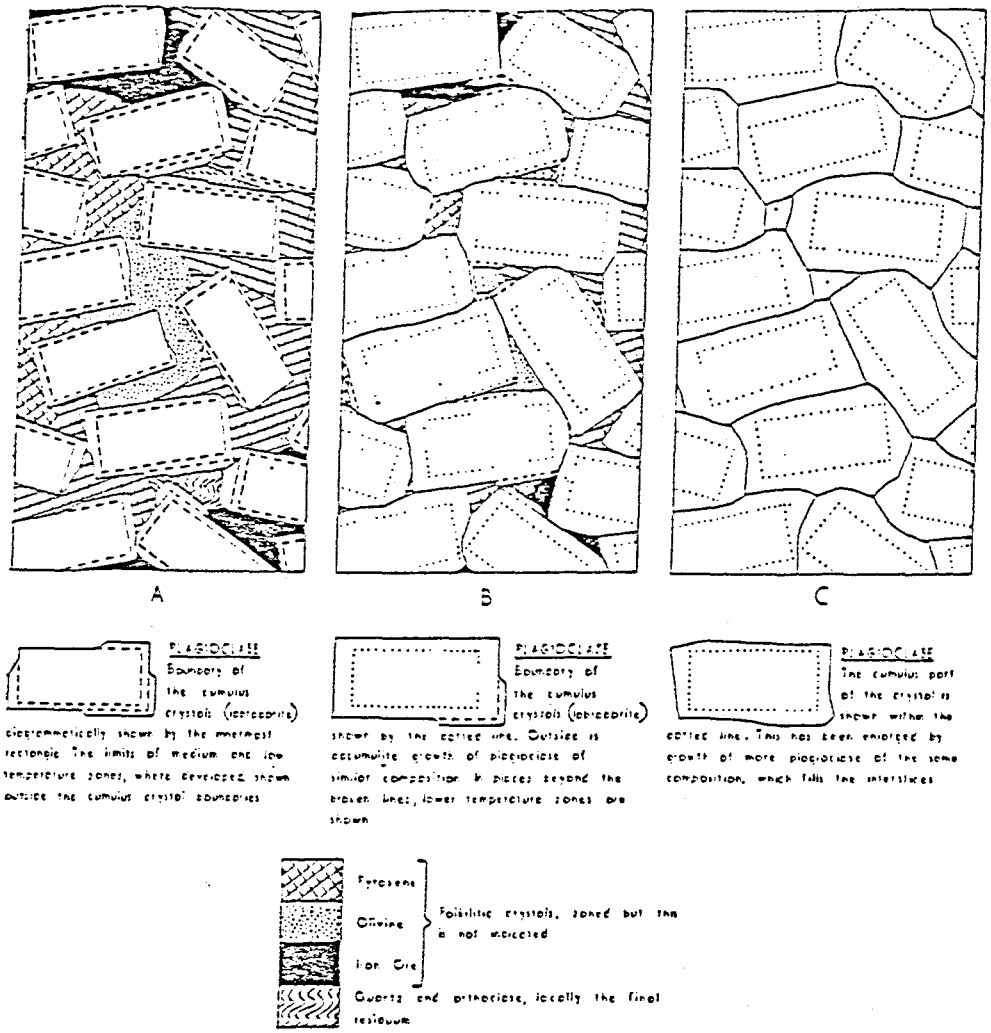

Figure 6.1: Ortho-, meso- and adcumulate textures in a feldspathic rock (Wager and Brown, 1968).

6.2.1 Adcumulates

Adcumulate rocks often tend towards monomineralic compositions (e.g., dunites or anorthosites), but this is not a prerequisite. They are, however, composed almost exclusively of cumulus grains, with very little intercumulus material. Hess (1939, in Wager and Brown 1968) suggested that diffusion took place between the overlying magma and the intercumulus liquid, thus replenishing the intercumulus liquid in contact with the crystallising phase. This would then enable the cumulus phase to grow, the new parts having the same composition as the original cumulus grain. Wager et al. (1960) and Wager and Brown (1968) proposed that the growth of the cumulus crystals took place at the same temperature as their original formation, because the overgrowth is usually of the same

composition as the core. They also suggested that the intercumulus liquid is mechanically forced out by the growing grains, thus resulting in a rock with very little intercumulus minerals.

Irvine (1980b) put forward a theory of adcumulus growth by filter pressing and infiltration metasomatism. Briefly, he proposed that intercumulus liquid is forced upward by the compaction of the cumulates during the accumulation process, and by the enlargement of cumulate phases, thus reducing the size of the primary pore-spaces. He suggested that the cumulus minerals recrystallise through reaction with the migrating intercumulus fluid. Allowing that this process results mainly in mesocumulates, Irvine suggested that one or more of the following five processes is necessary as well:

1. incorporation of components of the intercumulus liquid in solid solution in the cumulate phase,
2. removal of some of the constituents, by diffusion through the intercumulus liquid,
3. intercumulus fractionation by double diffusive convection, where components of the intercumulus liquid, and heat, in density stratified layers, diffuse between the layers,
4. leaching of extra components by an infiltrating vapour phase,
5. mechanical removal of intercumulus liquid as a result of tectonic deformation (Irvine,1980b).

Tait et al. (1984) suggested that compositional convection could be an alternative mechanism in the formation of adcumulate rocks, particularly of mafic adcumulate rocks. With the crystallisation of minerals the residual magma adjacent to the crystals is depleted in the components that make up the mineral, therefore the density of the magma is altered. It becomes either more dense, if the crystals are felsic, or less dense if the crystals are mafic. The density difference could then cause convection in the residual magma and convective exchange between the pore fluid and an overlying magma chamber. This could bring fresh magmatic liquid, which is similar to the magma from which the cumulates initially formed, into contact with the crystals, allowing them to grow, without any significant change in composition. A constraint on adcumulus growth by this

process is the balance between the removal of components of the melt by crystal growth, and the flux of those components through the convecting residual magma. The rate of crystallisation is proportional to the cooling rate, therefore if the cooling rate is rapid mesocumulates or orthocumulates could form, even if the density differences are suitable for convection (Figure 6.2).

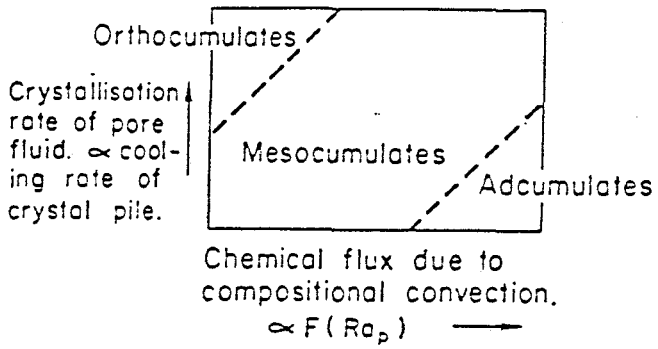

Figure 6.2: The influence of the rate of cooling on texture (Tait et al., 1984).

Laboratory experiments carried out by Sparks et al. (1985) with glass balls and aqueous solutions of $CuSO_4$ and Na_2SO_4 showed that:

- vigerous compositional convection can occur when a system is thermally stable

- convective patterns can be different in compositional convection than in thermal composition

- boundary layer thicknesses are less for compositional convection than for thermal convection

- adcumulus growth can occur within a porous medium.

Morse (1986) suggested that the two mechanisms (convection and

diffusion), by which rejected intercumulus liquid can be exchanged for liquid containing elements needed for crystal growth, are both important in the formation of adcumulates. He suggests that the rejected solute (containing elements incompatible with the crystallising minerals) moves away from the crystallising phases due to density differences, and convection currents within the magma aid by flushing away the rejected solute. The stability of the rejected solute depends on the crystallising phases, as mentioned above. If crystallisation is taking place along a sloping surface, rejected solute that is more dense than the original magma may flow down the sloping floor. These currents can have velocities from kilometres per year to kilometres per day (Morse, 1986). Morse (op. cit.) also defends the role of diffusion in the formation of felsic adcumulates at floor level where rejected solute could not flow. The rejected solute would have had a higher density than the original magma, and hence, if the floor did not slope, conditions would have been stagnant. The process of diffusion could therefore be a likely mechanism whereby incompatible elements are exchanged for compatible ones in the fluid. Morse (op. cit.) rejects the infiltration metasomatism model of Irvine (1980) on the basis that processes giving rise to orthocumulates also give rise to mesocumulates. He also discounts the role of double diffusive convection in the formation of adcumulates, because the rejected solute from mafic cumulates would rise freely and not cause double diffusion, and that from felsic cumulates would be too dense to be overturned by the latent heat of fusion from below.

6.2.2 Orthocumulates

The cumulus theory of Wager and Brown (1968) had crystals settling to the bottom of a magma chamber, and if the accumulation rate was rapid, intercumulus liquid would be trapped, and would crystallise in situ giving rise to orthocumulates. Tait et al.(1984) suggest that the intercumulus liquid could be trapped for a number of reasons. It could be due to the intercumulus liquid increasing in density as a result of crystallisation of felsic minerals, leading to a stable density distribution, and no convection would take place. If the density distribution was suitable for convection, the

cooling rate and associated increase in viscosity would inhibit convection, and thus trap the intercumulus liquid. Morse (1986), having disputed Irvine's (1980) infiltration metasomatism model for the formation of adcumulates, supports it as a mechanism for the formation of orthocumulates and mesocumulates.

6.2.3 Mesocumulates

Mesocumulates are the 'in-between' rocks within the orthocumulus-adcumulus spectrum. They form when the rival processes of adcumulus and orthocumulus growth are taking place, but neither process is sufficiently dominant to yield the extreme cases.

6.3 A BRIEF DESCRIPTION OF THE NOOITGEDACHT CORE

The rocks encountered in boreholes NG1 and NG2 range from dunites through harzburgites to pyroxenites, with numerous chromitite layers and one norite layer. As this report is primarily about the olivine-bearing rocks, emphasis will be placed on dunite, harzburgite and olivine-pyroxenite. The other rocks are mentioned for the sake of completeness, but these are dealt with by Teigler (1991). The full descriptive log of NG1 and NG2 is presented in Appendix 1.

The log of NG1 (with sampling positions) is presented in Figure 6.3, and that of NG2 in Figure 6.4. NG1 is collared in medium-grained feldspathic pyroxenites, which continue to a depth of 745 m. Within this sequence, there are 10 chromite-rich and 5 olivine-rich units. The chromite-rich units range from disseminated oxide grains in the silicate rocks, to a 1.04 m thick chromitite layer 255 m below the collar, which has been correlated with the LG6 chromitite layer. The thickest of the olivine-rich units (30 m) starts about 420 m below the collar. From 745 m to the base of NG1 at 830.15 m the rock is mainly dunitic, with a small proportion of intercumulus plagioclase, variable proportions of poikilitic pyroxene, and ubiquitous disseminated chromite, which becomes more concentrated at 779.5 - 787.5 m and 808.5 - 824.5 m.

NG2 is collared in the dunitic unit intersected at the base of NG1. Here it extends to a depth of 91 m. Below there is an approximately 280 m pyroxenite unit, with one 40 m harzburgite unit, a sequence of interlayered dunite, harzburgite and pyroxenite and a 3 m norite layer 300 m below the collar. A predominantly olivine-bearing unit extends from 372 m to 531 m (limit of the core available for this study); the unit is composed of dunite, harzburgite and pyroxenite interlayered on both fine and massive scales (for the complete log see Teigler, 1991).

6.3.1 Correlation with other sections

According to SACS (1980) nomenclature NG1 is collared in the Ruighoek Pyroxenite, which extends to a depth of 570 m. Below this unit is the Tweelaagte Pyroxenite, an almost monomineralic bronzitite which extends from 570 m to 745 m. From 745 m to the end of the hole at circa. 830 m are rocks of the Groenfontein Harzburgite unit, composed mainly of harzburgite and dunite. NG2 is collared in the Groenfontein Harzburgite which extends for about 250 m. Below the harzburgite unit, extending for about 100 m, is the Makgope Bronzitite, which is similar to the Tweelaagte Pyroxenite. From approximately 350 m to the base of the hole (where the Transvaal Sequence is intersected) is the Eerlyk Bronzitite which comprises multiple intercalations of olivine-rich cumulates with pyroxenites.

The correlation of NG1 with other sections from both the eastern and western Bushveld Complex is illustrated in Figure 6.5. The LG6 chromitite layer is taken as the datum line, following the convention of Hatton and Von Gruenewaldt (1987) and others, and because it is usually a prominent and easily recognised horizon. The olivine-rich rocks, C_1 and C_3 of Cameron (1980) (in the Ruighoek Pyroxenite of SACS (1980)), and the Lower Group chromitite horizons are used as markers, as they seem to occur in most of the published sections.

The whole NG sequence compared with the type sequence in the western Bushveld Complex is illustrated in Figure 6.6. This is included

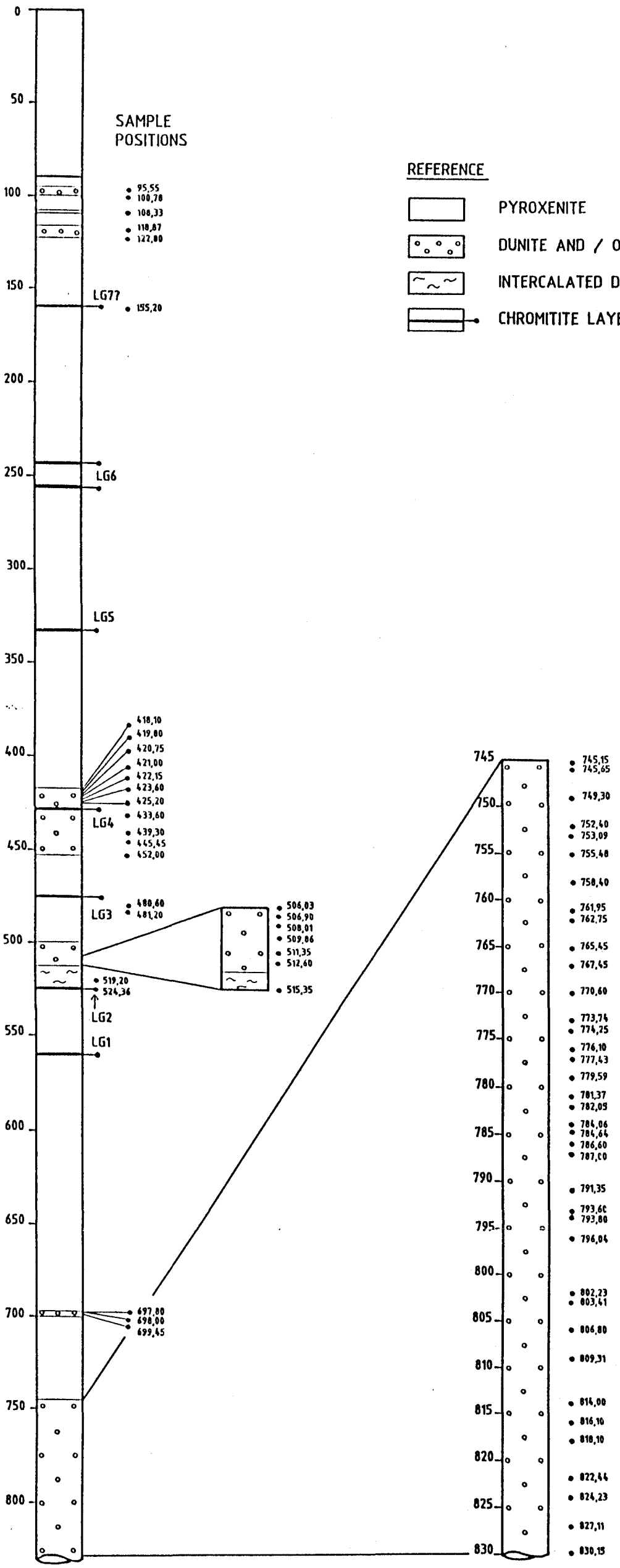

Figure 6.3: Log of borehole NG1 showing sampling positions.

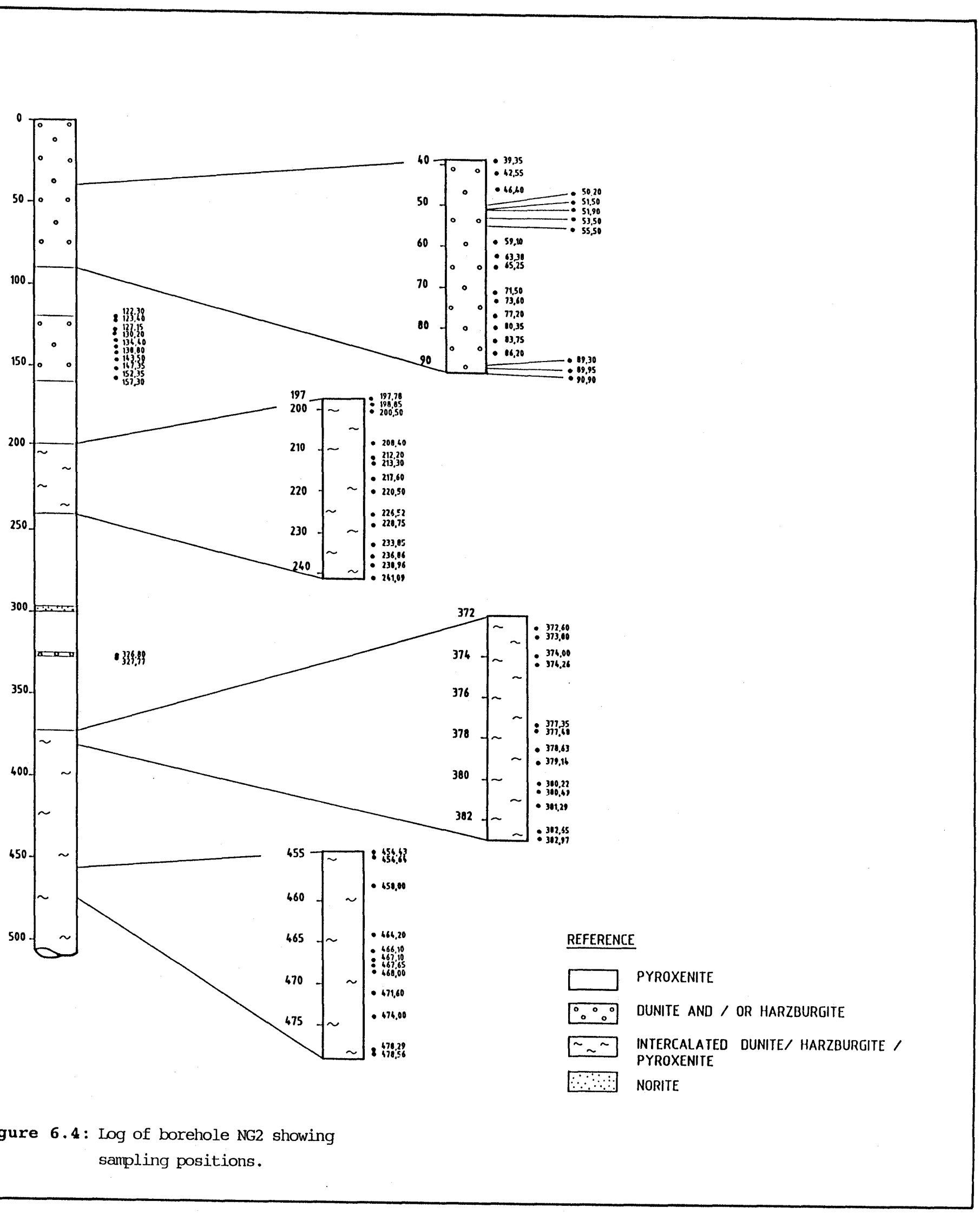

Figure 6.4: Log of borehole NG2 showing sampling positions.

merely for completeness, as NG3 and the last approximately 300m of NG2 were not available for this study.

6.4 ROCK DESCRIPTIONS

According to the IUGS classification system for plutonic rocks (Le Maitre et al., 1989), ultramafic rocks consist of greater than 90% mafic minerals. The rocks are classified and named according to the proportions of the main mineral constituents. Those that are relevant to the rocks of this study are olivine, orthopyroxene and clinopyroxene (Figure 6.7). The majority of the rocks dealt with here fall within the harzburgite range, with fewer in the dunite and olivine-pyroxenite ranges. The modal proportions of the minerals comprising the rocks, as determined by point counting, are presented in Appendix 2.

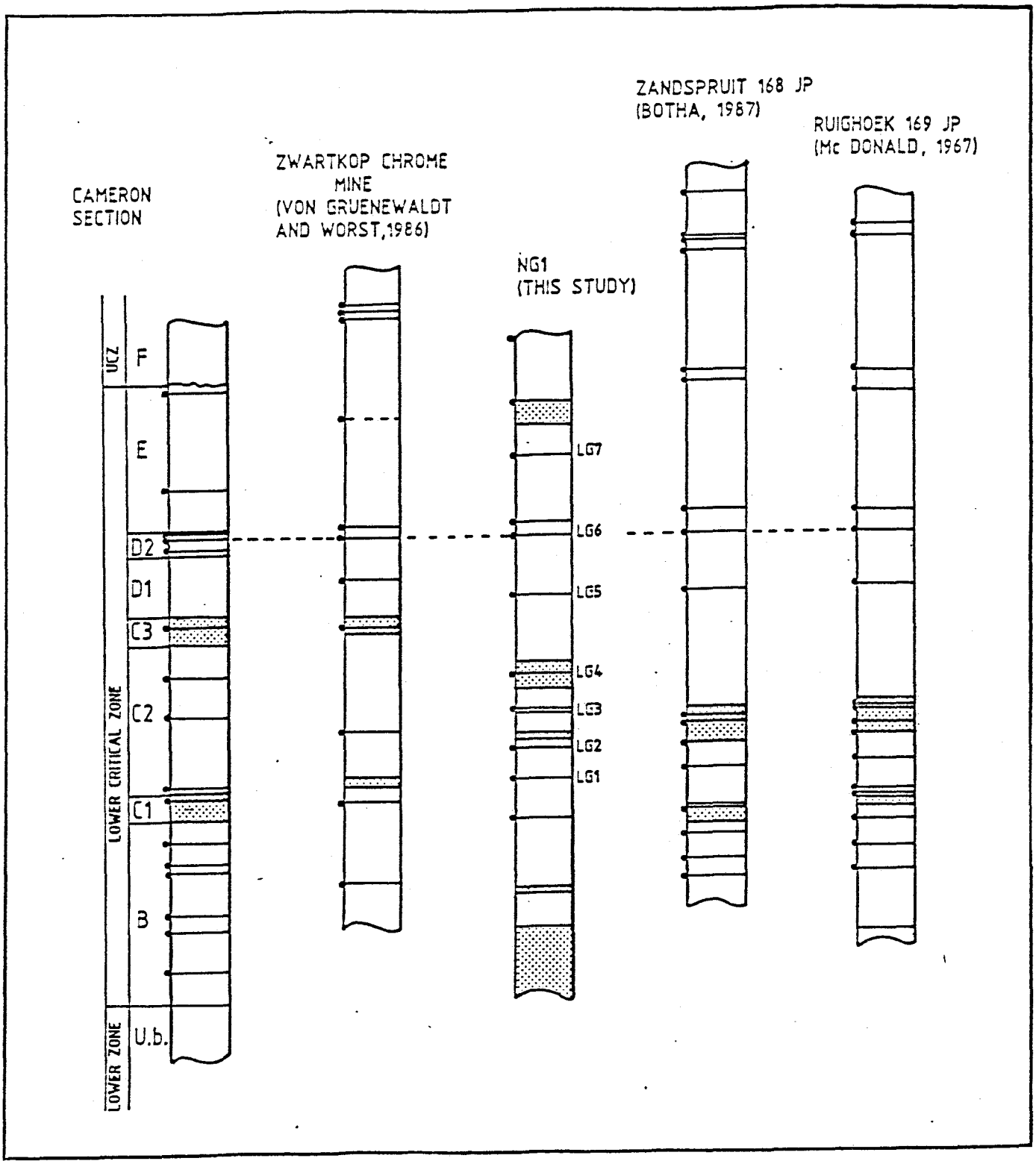

Figure 6.5: The correlation of borehole NG1 with other sections in the complex.

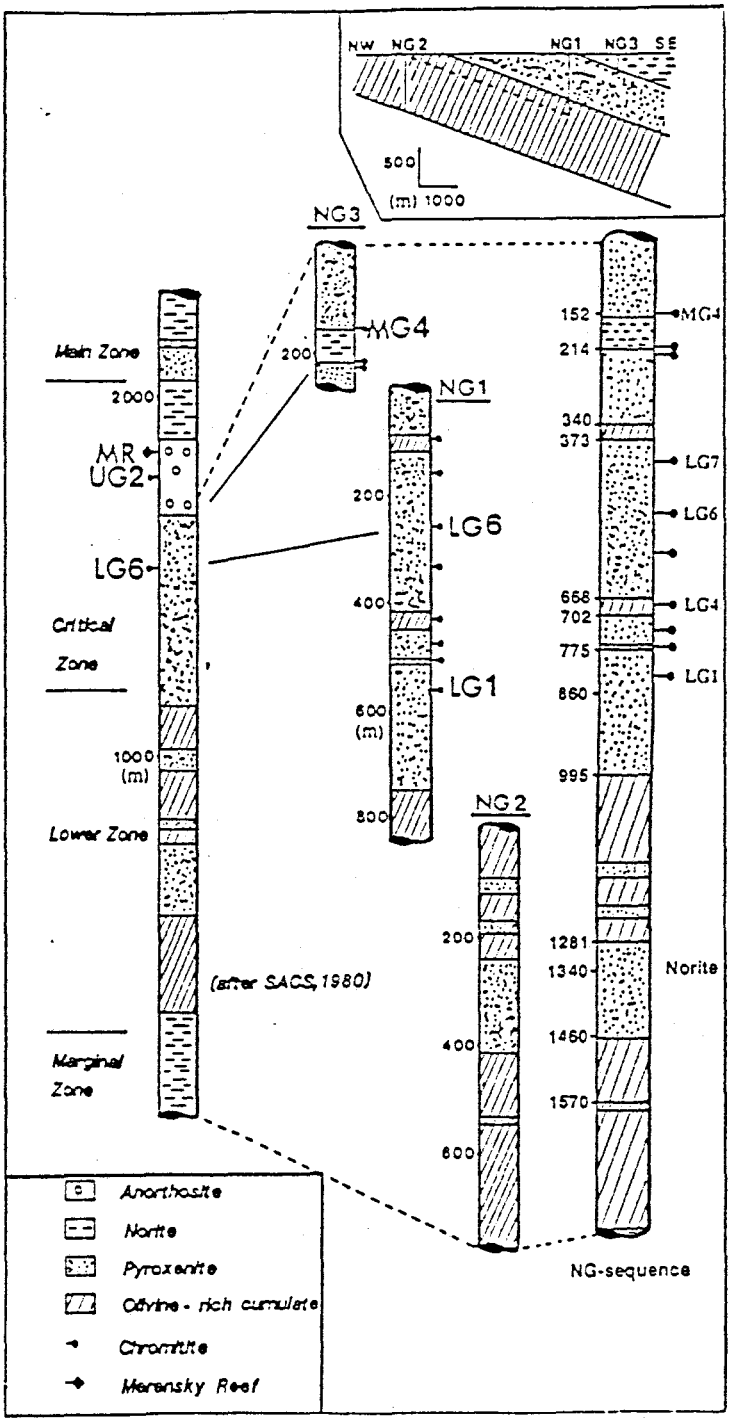

Figure 6.6: The NG boreholes and the full NG-sequence compared with the type sequence of the western Bushveld Complex. Note the different scales (after Teigler, 1991).

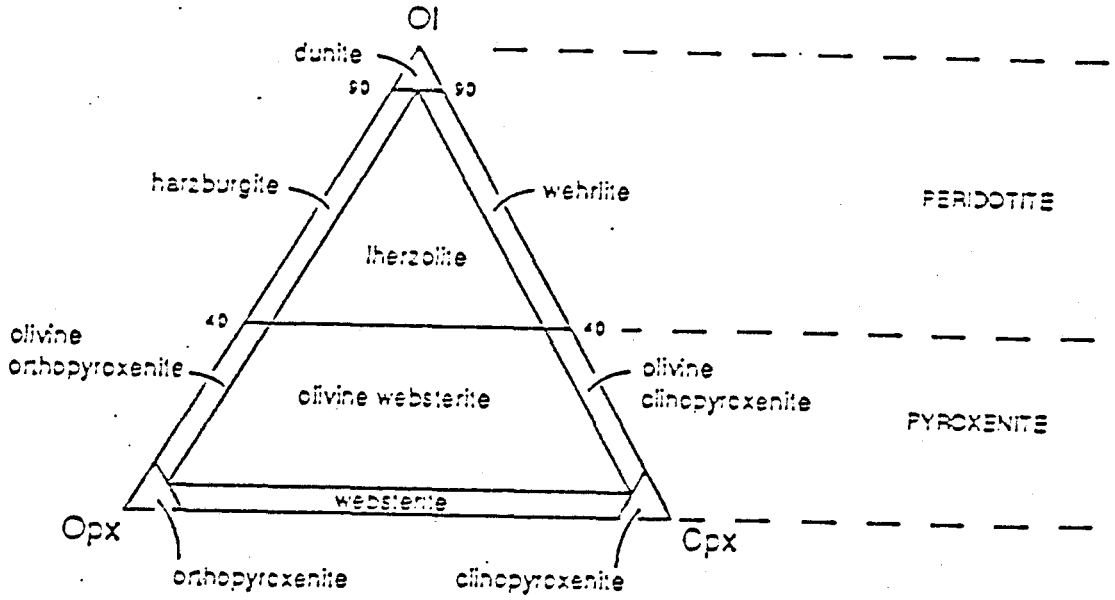

Figure 6.7: IUGS classification of ultramafic rocks (Le Maitre et al., 1989).

6.4.1 Dunites

Textures in the dunites vary from adcumulate to mesocumulate. The more the texture tends towards that of an orthocumulate, the more pyroxene the rock contains, yielding a gradation to a harzburgite. Where chromite is no longer an accessory phase, chromite-dunites are dealt with separately.

6.4.1.1 Adcumulate Dunites

Samples which have an adcumulus texture include:

NG1 : 791.35; 793.60
NG2 : 53.50; 69.42B

The adcumulate dunites are composed primarily of two minerals, olivine and accessory chromite. The olivine grains are anhedral, and meet along straight grain boundaries and at triple points (Figure 6.8). The grain-size is approximately 1 mm which is markedly different from that in the mesocumulates.

Chromite is a ubiquitous accessory mineral, which occurs both between olivine grains, and within olivine grains. The grains are discrete, and commonly subhedral, though occasional euhedral octahedral grains are present (Figure 6.9). The relationship between olivine and chromite varies. In sample NG1-793,60, most of the chromite appears to have formed at the same time as, or after the olivine, being external to the olivine grains. In sample NG2-53.50 the larger chromite grains occur outside of olivine, but the olivine is peppered with tiny rounded chromite grains, about 10 microns in diameter.

Intercumulus minerals occur sporadically, and include plagioclase, biotite or orthopyroxene or, more rarely, clinopyroxene. These intercumulus minerals have crystallised in the interstices between grains. Ideal adcumulate textures are not pervasive in the dunites, as sporadic oikocrysts of pyroxene occur; these are usually orthopyroxene, but occasionally clinopyroxene. This texture overlaps with that of a poikilitic harzburgite, and classification depends on the size and number of the oikocrysts.

Figure 6.8: Photomicrograph of an adcumulate dunite showing olivine crystals meeting along straight grain boundaries and at triple points.
Crossed nicols.
Bar Scale: 1mm

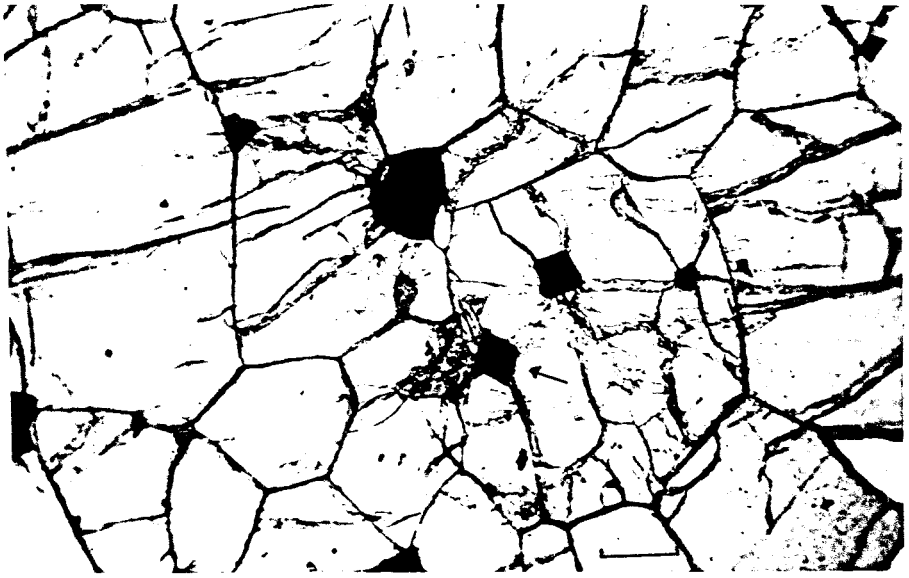

Figure 6.9: Photomicrograph of an adcumulate dunite with three different types of chromite occurrence: euhedral (octahedral) crystals (arrowed); large subhedral cyrstals between olivine crystals and very fine chromite crystals within olivine.
Plane light.
Bar Scale: 1mm

Figure 6.10: Photomicrograph of a mesocumulate dunite showing an orthopyroxene oikocryst (opx) with very fine exsolution lamellae, and a partially resorbed olivine chadacryst (ol).
Crossed nicols.
Bar Scale: 2mm

6.4.1.2 Mesocumulate Dunites

Samples with a mesocumulate texture include:

NG-1 : 423.60; 508.01; 509.86; 779.59; 787.00
NG-2 : 86.20; 123.40; 138.80; 152.35

Mesocumulate dunites are composed of olivine, chromite, plagioclase and orthopyroxene, and in some cases clinopyroxene and biotite as well. The average grain-size ranges from 2.1 - 2.8 mm, considerably larger than that of adcumulus dunites. The olivine grains are mainly subhedral, but may be euhedral, or, when partially resorbed, anhedral. Many of the grains meet along straight grain boundaries and in triple points, but not to the same extent as in the adcumulates.

Orthopyroxene occurs both as an intercumulus phase and as a cumulus phase, though the latter is not common in the dunites. Where the orthopyroxene is cumulus it has a similar morphology to the olivine described above. As an intercumulus mineral it has the form either of large oikocrysts, which poikilitically enclose olivine and chromite, or of small anhedral grains, which have crystallised in the spaces between the cumulus grains. The small anhedral grains show no evidence of exsolution, whereas the oikocrysts may or may not have exsolution lamellae. The orthopyroxene with exsolution lamellae has very fine dark and light striations, resulting in incomplete extinction of the grain in all orientations (Figure 6.10). All the oikocrysts have resorbed their olivine chadacrysts to some extent (Figure 6.10), and, in some cases, chromite grains which once surrounded the olivine grain remain as indicators of the original size of the grain (Figure 6.11).

Plagioclase occurs only as an intercumulus mineral in the mesocumulate dunites. It is found as small irregular grains between the cumulus minerals, and in samples NG1 508.01, 509.86, 779.59, 787.00, 824.23 and NG2 138.80, 152.35 it occurs as larger oikocryst-like grains, or as a number of optically continuous grains (Figure 6.12). Twinning in the plagioclase takes a number of forms. Albite

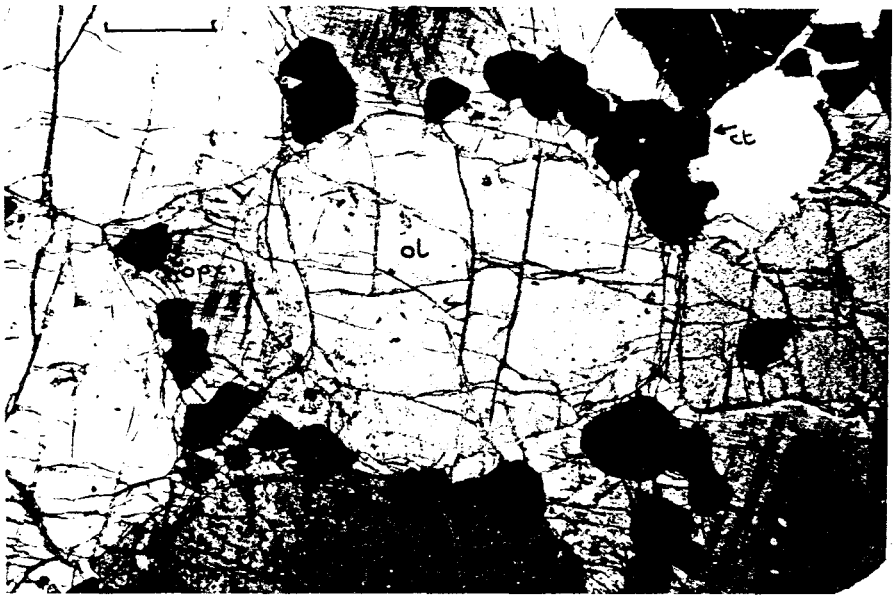

Figure 6.11: Photomicrograph of a mesocumulate dunite showing a partially resorbed olivine chadacryst (ol) in an orthopyroxene oikocryst (opx), with a rim of chromite cyrstals (ct) indicating the original outline of the olivine crystal.
Crossed nicols.
Bar scale: 2.5mm

Figure 6.12: Photomicrograph of a mesocumulate dunite with intercumulus plagioclase forming a number of optically continuous grains (plag) around cumulus olivine (ol).
Crossed nicols.
Bar scale: 2mm

Figure 6.13: Photomicrograph of a mesocumulate dunite with a rare biotite oikocryst (bi) enclosing olivine (ol) and chromite (ct) chadacrysts.
Crossed nicols.
Bar scale: 2mm

twinning is almost always present. It occurs in combination with Pericline twinning, and with Carlsbad and Pericline twinning.

Chromite is ubiquitous and accessory, and as in the adcumulus dunites, it occurs both between and within the cumulate olivine grains, and also has the same morphology as described in section 6.4.1.1 above. In samples NG1 423.60 and 508.01 clusters of chromite grains outline the original shapes of the cumulate olivine grains.

Clinopyroxene occurs as an intercumulus phase in the form of oikocrysts in samples NG1 423.60, NG2 123.40, 152.35 and 138.80. As with the orthopyroxene oikocrysts, the clinopyroxene contains partially resorbed olivine and chromite chadacrysts, and in all four samples exsolution lamellae are present.

Biotite occurs in most of the fresh samples as an intercumulus mineral. In samples NG1 779,59, NG2 86.20 and 123.40 it occurs as oikocrysts, poikilitically enclosing olivine and chromite (Figure 6.13).

6.4.1.3 Chromite-Dunite

Samples of chromite-dunite include:

NG1 : 425.20; 429.90; 481.30

The chromite-dunites consist essentially of two cumulus phases, olivine and chromite, but in the latter two samples olivine has undergone complete alteration to serpentine and iddingsite. The olivine grains are subhedral and usually entirely surrounded by chromite. Much of the chromite has annealed, though some discrete grains are still discernible. Stringers of alteration products cut across the chromite as well as the olivine.

6.4.2 Harzburgites (including Olivine-Pyroxenites)

According to the IUGS classification system (Le Maitre et al., 1989) harzburgites are composed of olivine and orthopyroxene, with up to

5% clinopyroxene, and olivine-pyroxenites have a similar composition, but with less than 40% olivine (Figure 6.6). The olivine-pyroxenites are included here, as they have similar textures to the true harzburgites. For the purposes of description, the harzburgites have been divided into four groups:

- adcumulate harzburgite
- mesocumulate harzburgite
- poikilitic harzburgite
- chromite-harzburgite

6.4.2.1 Adcumulate Harzburgite

Samples with adcumulate texture include:

NG1 : 752.54B; 753.09; 755.45; 758.4; 761.95; 762.75; 765.45
767.45; 774.25; 793.80; 803.41; 827.11
NG2 : 65.25; 198.85; 228.75

The adcumulate harzburgites are composed of three main minerals, olivine, orthopyroxene and chromite. As in the case of the adcumulate dunites, the olivine grains are anhedral, and meet along straight grain boundaries and in triple points. The orthopyroxene grains have a similar morphology to that of the olivine grains. Olivine and orthopyroxene grains meet along either straight or slightly curved grain boundaries, and in triple points with inter-mineral angles close to 120°. The overall grain-size is slightly coarser than its dunitic counterpart, being on average 1.75 mm.

Chromite is once again a ubiquitous accessory mineral. The grain-size ranges from 0.5 mm to micron-sized particles. The coarser grains tend to be in the spaces between the olivine and orthopyroxene, whereas the finer grains are more commonly included in other cumulate grains. The grains have a wide range of shapes, from euhedral grains through subhedral grains with silicate inclusions to anhedral grains in the interstices between cumulate grains (Figure 6.14).

Intercumulus minerals are rare. Where present, they include orthopyroxene, clinopyroxene or biotite and are very small. Biotite is found only in samples NG1 803.41 and NG2 65.25 and 228.75. In the latter it is oikocrystic, whereas in the former two it occurs as small discrete grains.

6.4.2.2 Mesocumulate Harzburgite

Samples with a mesocumulate texture include:

NG1 : 100.70; 118.87A; 418.10; 420.75; 452A; 480.60A;
506.05A; 512.60; 745.65; 784.64(12); 814.00; 822.44
NG2 : 39.35; 42.55; 46.40; 55.50; 63.35; 69.42A; 77.20;
80.35; 89.30; 122.30; 134.40; 143.35; 200.50; 236.86

The mesocumulate harzburgites are composed of cumulus olivine, orthopyroxene and chromite, and of intercumulus orthopyroxene, clinopyroxene, plagioclase and biotite. The overall grain-size is coarser than that of the adcumulates, being on average 2.12 mm. The olivine grains are euhedral to subhedral, and are commonly strained (Figure 6.15); all have unoriented fractures running through them. Serpentinisation has taken place along most of the fractures, but the alteration is not pervasive. The fractures and alteration are not restricted to olivine, but are also found extensively in the associated cumulus orthopyroxene. In sample NG2 55.50 there seem to be two generations of cumulus orthopyroxene: a coarse-grained variety, with an average grain-size of 4 mm, and a finer type with a more adcumulate habit, and an average grain-size of 0.5 mm. Chromite is once again ubiquitous, occurring as both inter- and intracumulus grains, and having a habit ranging from euhedral to anhedral.

Plagioclase is the main intercumulus mineral. In NG1 506.05A and NG2 39.35 there are a number of seemingly discrete grains which are in optical continuity. In samples NG2 143.35 and NG2 236.86 a rounded grain of plagioclase occurs within an olivine grain. This is an unusual feature in these rocks. Some intercumulus plagioclase is in the form of small oikocrysts, encompassing a few of the cumulate grains, but too small to give the rock a poikilitic texture.

Figure 6.14: Photomicrograph of an adcumulate harzburgite with a subhedral chromite grain which has a silicate inclusion (arrowed).
Plane light.
Bar scale: 1mm

Figure 6.15: Photomicrograph of a mesocumulate harzburgite showing a strained olivine crystal (ol).
Crossed nicols.
Bar scale: 1mm

Biotite occurs in almost all sections in varying degrees. It is a late-stage mineral, and is always anhedral. It can occur either as discrete grains or as oikocrysts. Ortho- and clinopyroxene occur as small oikocrysts, poikilitically enclosing olivine and chromite; both pyroxenes may exhibit exsolution lamellae. The oikocrysts are different from those of the poikilitic harzburgites, in that they are smaller, and have resorbed their chadacrysts to a much lesser extent, hence the poikilitic texture is not imposed on the whole rock.

6.4.2.3 Poikilitic Harzburgite

Samples with a poikilitic texture include:

NG1 : 439.80; 445.45; 511.35; 784.06; 816.20; 822.44; 830.15
NG2 : 59.10; 127.15; 130.20; 143.35; 213.30; 217.60

The most remarkable feature of the poikilitic harzburgites is the large size of the oikocrysts which dominate the rock. The majority of the oikocrysts occurring in the rock are orthopyroxene. In only two of the samples noted above (NG1 816.20 and 830.15) do clinopyroxene oikocrysts occur, and these are juxtaposed to orthopyroxene oikocrysts. The cumulus minerals are once again olivine, chromite and to a lesser degree orthopyroxene, and the intercumulus minerals are orthopyroxene, plagioclase, clinopyroxene and accessory biotite.

In many cases olivine chadacrysts within orthopyroxene oikocrysts appear to have been strongly resorbed, and to employ a sedimentological term, have a high degree of roundness, and often of sphericity as well. The chromite grains do not appear to have been affected by the growth of the oikocrysts, and many still retain their euhedral form. Once again clusters of chromite grains outline the original olivine grains. Where the oikocrysts are composed of clinopyroxene, the degree of resorption of olivine and orthopyroxene appears less extensive than in the orthopyroxene oikocrysts, and the original texture of the rock can still be determined.

Plagioclase is a minor but ubiquitous intercumulus mineral, and has the same appearance as in all the other harzburgites. Biotite, too, occurs in all the samples, but only as one or two small grains per slide.

6.4.2.4 Chromite-Harzburgites

Samples include:

NG1 : 430.20; 433.6; 439.30

The chromite-harzburgites all tend to be poikilitic harzburgites with large orthopyroxene oikocrysts, which include both olivine and chromite. The olivine has been resorbed, and as in the cases of the samples with smaller amounts of chromite, the chromite outlines the original size and shape of the olivine grains. Most of the chromite grains have not been annealed to any great extent, but there is evidence of sintering between some.

6.5 DISCUSSION

The textures of the rocks of this study are almost entirely adcumulate, mesocumulate or poikilitic. It would appear that the rate of crystallisation and cooling could not have been rapid as this would have resulted in the entrapment of intercumulus liquids on a large scale, resulting in orthocumulus textures.

Some postcumulus processes such as those discussed in section 6.2.1 must have been in motion during the formation of the adcumulates as no zoning was detected in any of the cumulus grains analysed. The density of the rejected solute would have been reduced, and could then have been exchanged with more mafic fluids, resulting in the continuous growth of cumulate phases without a change in composition. The sizes of the adcumulate grains vary from about 0.1 mm to 1.2 mm, but in no instance do they show the sintering effects as seen in the magnetite layers studied by Reynolds (1985). In many, but not all cases, the poikilitic texture seems to be a secondary feature, where the primocrysts have been partially to completely

resorbed, resulting in large oikocrysts of a few centimetres in size.

There is no conclusive evidence pointing to crystal settling as a mode of crystal accumulation. There is no zoning of crystals which would have grown as they settled down through the fluid magma, and there are no "way-up" structures such as the accumulation of chromite grains against the top surfaces of olivine grains, as occurs in the Rhum Complex (Butcher. pers comm.).

7. MINERAL CHEMISTRY

7.1 INTRODUCTION

This chapter is devoted to the presentation of analytical data on olivine, pyroxene, chromite and plagioclase, and to the illustration of the chemical variations that are manifested. In all, 25 polished sections were made from NG1 and 38 from NG2. For the purposes of discussion the samples have been grouped into six intervals, referred to here as the olivine-bearing intervals 6 to 1 (OBI6 to OBI1); the divisions are illustrated in all plots of data against stratigraphic height eg. Figures 7.2 and 7.5.

7.2 OLIVINE

7.2.1 A brief review of olivine

Olivine is an orthosilicate consisting of independent SiO_4 tetrahedra joined by divalent atoms in octahedral co-ordination (Deer et al., 1982). Complete substitution between Mg^{2+} and Fe^{2+} results in the forsterite (Mg_2SiO_4) - fayalite (Fe_2SiO_4) solid solution series; substitution between Fe2+ and Mn2+ results in the fayalite - tephroite (Mn_2SiO_4) solid solution series. Ca-rich minerals are monticellite ($CaMgSiO_4$), glaucochroite ($CaMnSiO_4$) and kirschsteinite ($CaFeSiO_4$), but the Ca-rich varieties do not have an olivine structure. The terms forsterite and fayalite sensu stricto only apply to the end-members of series. The names of the intermediate members are given in Figure 7.1.

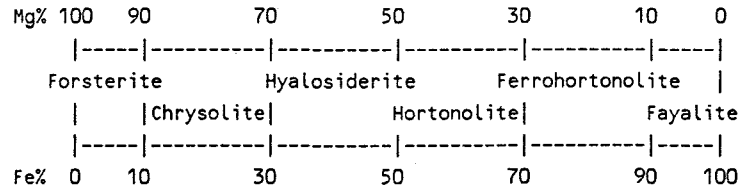

Figure 7.1: The members of the Mg - Fe olivine series.

Ni is a common component of Mg-rich olivine, and varying amounts of Mn and Ca can be present in both Mg- and Fe-rich olivine. Occasionally, small plates of opaque minerals are found in olivine grains, these are usually Cr- or Fe-oxides. Olivine is readily altered by hydrothermal processes, low-grade metamorphism and weathering. The more common alteration minerals are serpentine, iddingsite, bowlingite, chlorite, amphibole, talc, carbonates and iron oxides (Deer et al., 1982).

7.2.2 The Olivines of this study

This discussion will be restricted to olivines of the forsterite - fayalite series as Ca and Mn are trace components of the olivines of this study. Averaged olivine analyses are presented in Table 7.1, and plots of the main components of olivine against stratigraphic height are shown in Figure 7.2. Alteration products of olivine encountered are mainly serpentine, iddingsite, bowlingite and magnetite.

The iron-magnesium ratio in olivine is expressed as MMF (Mg/Mg+Fe), i.e. as an atomic ratio. This gives a useful indication of the character of the melt from which the olivine crystallised. The earliest formed olivines are usually Mg-rich. With fractionation of the melt they would be expected to become progressively more Fe-rich, i.e. the MMF decreases with an increasing degree of fractionation. In Figure 7.2 this trend is seen over the length of the two boreholes, however, within the different olivine-bearing intervals, excepting the uppermost one in NG1 and the lowermost one in NG2, there is a distinctive trend of Mg-enrichment from the base to the top of each interval.

The manganese content of the olivine varies from 400 ppm to 1900 ppm (Table 7.1). There is an overall trend of decreasing MnO in the olivine with increasing stratigraphic height, but the pattern of MnO distribution within each interval is random.

Nickel values vary between 2100 ppm and 4900 ppm (Table 7.1) The distribution of nickel in olivine shows an overall decrease from the

Table 7.1: Averaged olivine compositions (microprobe analyses) from borehole NG1

SAMPLE	108.33	122.8	155.2	420.8	430.55	445.45	452.75	480.6	506.05	506.9	508	515.15	697.8	753	761	770	773.74	779	784.64
SiO2	38.32	39.58	39.22	39.57	39.87	39.73	40.23	40.22	39.88	39.85	39.88	38.99	39.42	39.92	39.88	40.11	40.39	40.11	39.99
FeO	18.17	16.29	16.76	13.86	12.15	14.09	12.55	13.43	14.11	13.60	14.10	15.63	14.90	11.71	12.70	11.91	12.55	12.42	12.40
MnO	0.04	0.07	0.07	0.16	0.14	0.15	0.05	0.17	0.17	0.05	0.14	0.11	0.12	0.15	0.10	0.07	0.18	0.10	0.06
NiO	0.26	0.32	0.37	0.27	0.28	0.24	0.30	0.27	0.21	0.27	0.24	0.25	0.31	0.28	0.22	0.24	0.28	0.32	0.31
MgO	43.25	43.52	43.42	46.04	47.36	45.88	46.89	45.88	45.51	46.37	45.45	44.87	45.20	48.02	46.72	47.72	46.58	47.04	47.25
CaO	0.02	0.02	0.00	0.00	0.01	0.01	0.00	0.01	0.02	0.00	0.01	0.02	0.01	0.01	0.01	0.01	0.00	0.02	0.01
TOTAL	100.07	99.79	99.83	99.90	99.82	100.10	100.03	99.98	99.90	100.15	99.82	99.87	99.96	100.08	99.62	100.07	99.99	100.01	100.02
CATIONS PER 4 OXYGEN																			
Si	0.9791	1.0022	0.9959	0.9910	0.9915	0.9935	0.9987	1.0029	0.9987	0.9934	0.9994	0.9855	0.9915	0.9883	0.9952	0.9930	1.0030	0.9961	0.9929
Fe2	0.3883	0.3450	0.3559	0.2904	0.2528	0.2947	0.2606	0.2800	0.2956	0.2837	0.2955	0.3304	0.3134	0.2424	0.2650	0.2466	0.2606	0.2580	0.2574
Mn	0.0009	0.0014	0.0014	0.0034	0.0030	0.0032	0.0011	0.0035	0.0036	0.0011	0.0030	0.0023	0.0026	0.0031	0.0021	0.0015	0.0037	0.0021	0.0013
Ni	0.0053	0.0064	0.0076	0.0055	0.0056	0.0048	0.0061	0.0054	0.0042	0.0055	0.0048	0.0051	0.0062	0.0056	0.0043	0.0048	0.0056	0.0064	0.0062
Mg	1.6468	1.6423	1.6433	1.7187	1.7553	1.7100	1.7348	1.7050	1.6988	1.7228	1.6978	1.6906	1.6945	1.7720	1.7378	1.7606	1.7240	1.7409	1.7490
Ca	0.0006	0.0005	0.0001	0.0001	0.0003	0.0004	0.0001	0.0004	0.0005	0.0001	0.0002	0.0005	0.0003	0.0004	0.0003	0.0004	0.0001	0.0004	0.0002
TOTAL	3.0209	2.9978	3.0041	3.0090	3.0085	3.0065	3.0013	2.9971	3.0013	3.0066	3.0006	3.0145	3.0085	3.0117	3.0048	3.0070	2.9970	3.0039	3.0071
MMF	0.8092	0.8264	0.8220	0.8555	0.8741	0.8530	0.8694	0.8590	0.8518	0.8586	0.8518	0.8365	0.8439	0.8797	0.8677	0.8771	0.8687	0.8709	0.8717
N	3	3	3	15	3	3	3	5	5	3	10	3	10	10	5	3	3	3	10

SAMPLE	793.5	803	809.1	816.1	818.8	830.15
SiO2	40.20	40.10	40.28	40.00	40.28	39.79
FeO	11.23	12.28	12.35	12.42	12.11	13.56
MnO	0.10	0.09	0.12	0.15	0.11	0.13
NiO	0.35	0.32	0.33	0.31	0.32	0.29
MgO	48.18	47.20	46.88	47.11	47.09	46.21
CaO	0.01	0.01	0.01	0.01	0.00	0.00
TOTAL	100.07	100.00	99.96	99.99	99.91	99.98
CATIONS PER 4 OXYGEN						
Si	0.9927	0.9952	0.9998	0.9939	0.9993	0.9940
Fe2	0.2319	0.2549	0.2563	0.2581	0.2514	0.2832
Mn	0.0022	0.0019	0.0025	0.0031	0.0022	0.0027
Ni	0.0070	0.0064	0.0066	0.0061	0.0063	0.0058
Mg	1.7735	1.7462	1.7346	1.7446	1.7415	1.7203
Ca	0.0002	0.0002	0.0003	0.0002	0.0001	0.0000
TOTAL	3.0073	3.0048	3.0002	3.0061	3.0007	3.0060
MMF	0.8844	0.8726	0.8712	0.8711	0.8739	0.8586
N	8	10	8	3	5	5

MMF: $Mg/(Mg+Fe^{2+})$

N : number of analyses averaged

Table 7.1 (cont): Averaged olivine compositions (microprobe analyses) from borehole NG2.

SAMPLE	39.35	42.55	43.35	50.20	55.50	65.25	73.60	80.35	83.75	122.30	123.40	127.55	134.40	153.35	157.50	158.6	165.62	197.75	200.5
SiO2	40.22	39.83	39.60	39.84	40.22	39.66	40.04	39.75	39.92	39.89	40.17	39.73	40.24	39.43	39.54	39.81	39.59	40.10	39.49
FeO	12.66	12.78	13.22	12.78	13.12	13.39	13.55	14.06	14.30	13.27	12.64	13.04	13.84	14.73	14.86	11.95	15.13	13.67	14.49
MnO	0.17	0.17	0.17	0.17	0.15	0.16	0.14	0.18	0.18	0.16	0.17	0.15	0.17	0.19	0.18	0.14	0.18	0.15	0.18
NiO	0.25	0.29	0.32	0.28	0.30	0.32	0.30	0.30	0.29	0.31	0.30	0.31	0.34	0.34	0.33	0.36	0.29	0.35	0.41
MgO	46.77	46.88	46.43	46.86	46.64	46.50	46.33	45.72	45.23	46.50	46.70	46.70	45.60	45.19	45.03	47.95	44.84	45.57	45.44
CaO	0.00	0.01	0.01	0.00	0.00	0.00	0.00	0.00	0.01	0.01	0.01	0.00	0.00	0.00	0.00	0.00	0.00	0.00	0.00
TOTAL	100.07	99.96	99.75	99.92	100.44	100.03	100.35	100.02	99.93	100.14	99.99	99.94	100.19	99.89	99.96	100.22	100.02	99.85	100.01
CATIONS PER 4 OXYGEN																			
Si	0.9987	0.9919	0.9908	0.9923	0.9974	0.9901	0.9962	0.9949	1.0004	0.9937	0.9986	0.9911	1.0032	0.9921	0.9944	0.9861	0.9956	1.0028	0.9915
Fe2	0.2630	0.2662	0.2767	0.2662	0.2721	0.2796	0.2819	0.2944	0.2998	0.2764	0.2629	0.2719	0.2887	0.3099	0.3126	0.2477	0.3182	0.2858	0.3044
Mn	0.0036	0.0036	0.0035	0.0035	0.0031	0.0034	0.0029	0.0039	0.0038	0.0033	0.0036	0.0032	0.0036	0.0041	0.0039	0.0029	0.0038	0.0032	0.0038
Ni	0.0050	0.0059	0.0065	0.0055	0.0060	0.0065	0.0060	0.0060	0.0058	0.0062	0.0060	0.0063	0.0067	0.0069	0.0067	0.0072	0.0058	0.0071	0.0082
Mg	1.7309	1.7403	1.7314	1.7400	1.7239	1.7303	1.7168	1.7059	1.6896	1.7265	1.7302	1.7364	1.6946	1.6948	1.6879	1.7699	1.6809	1.6983	1.7005
Ca	0.0001	0.0002	0.0001	0.0001	0.0001	0.0001	0.0001	0.0001	0.0002	0.0001	0.0003	0.0001	0.0001	0.0001	0.0001	0.0001	0.0001	0.0001	0.0001
TOTAL	3.0013	3.0081	3.0092	3.0077	3.0026	3.0099	3.0038	3.0051	2.9996	3.0063	3.0014	3.0089	2.9968	3.0079	3.0056	3.0139	3.0044	2.9972	3.0085
MMF	0.8681	0.8673	0.8622	0.8673	0.8637	0.8609	0.8590	0.8528	0.8493	0.8620	0.8681	0.8646	0.8545	0.8454	0.8437	0.8772	0.8408	0.8560	0.8482
N	14	11	9	18	2	13	7	18	13	10	27	11	7	5	11	8	5	6	23

SAMPLE	206.3	212.2	213.3	236.86	238.9	241.09	326.86	372.6	374	376.1	382.97	399.5	436.58	438.29	466.1	474	478.56	480.8	493.19
SiO2	40.11	39.80	39.34	39.71	39.82	39.80	39.98	39.25	39.72	40.14	39.94	39.46	40.37	40.10	39.75	40.28	39.80	39.44	40.35
FeO	13.66	14.81	14.83	15.10	13.86	15.08	14.09	14.77	14.26	13.91	13.79	14.60	12.38	13.48	13.29	12.84	13.17	13.30	12.11
MnO	0.15	0.17	0.18	0.17	0.15	0.15	0.15	0.16	0.17	0.15	0.16	0.17	0.13	0.16	0.13	0.15	0.14	0.14	0.14
NiO	0.43	0.38	0.35	0.38	0.38	0.34	0.45	0.36	0.31	0.42	0.30	0.35	0.31	0.37	0.39	0.31	0.42	0.37	0.34
MgO	45.85	44.78	45.40	44.99	46.04	44.63	45.46	45.55	45.65	45.39	45.87	45.51	46.73	45.62	46.45	46.48	46.53	46.84	47.16
CaO	0.00	0.00	0.00	0.01	0.00	0.01	0.00	0.01	0.01	0.01	0.01	0.00	0.00	0.01	0.01	0.01	0.01	0.01	0.01
TOTAL	100.20	99.94	100.10	100.35	100.27	100.01	100.14	100.09	100.12	100.02	100.07	100.09	99.92	99.73	100.03	100.06	100.07	100.11	100.11
CATIONS PER 4 OXYGEN																			
Si	0.9999	1.0002	0.9885	0.9955	0.9937	1.0003	0.9996	0.9863	0.9942	1.0033	0.9975	0.9902	1.0022	1.0030	0.9920	1.0010	0.9923	0.9845	0.9993
Fe2	0.2848	0.3111	0.3116	0.3165	0.2892	0.3169	0.2946	0.3105	0.2985	0.2908	0.2881	0.3063	0.2571	0.2819	0.2774	0.2669	0.2746	0.2777	0.2508
Mn	0.0032	0.0036	0.0038	0.0035	0.0032	0.0032	0.0032	0.0033	0.0037	0.0032	0.0033	0.0037	0.0027	0.0034	0.0028	0.0032	0.0029	0.0031	0.0029
Ni	0.0086	0.0077	0.0071	0.0077	0.0077	0.0070	0.0091	0.0072	0.0062	0.0084	0.0061	0.0071	0.0061	0.0074	0.0078	0.0062	0.0083	0.0074	0.0067
Mg	1.7035	1.6771	1.7004	1.6810	1.7124	1.6720	1.6938	1.7061	1.7030	1.6909	1.7074	1.7023	1.7295	1.7009	1.7277	1.7216	1.7292	1.7427	1.7408
Ca	0.0001	0.0000	0.0001	0.0003	0.0001	0.0003	0.0001	0.0002	0.0002	0.0002	0.0002	0.0000	0.0001	0.0004	0.0004	0.0001	0.0003	0.0001	0.0002
TOTAL	3.0001	2.9998	3.0115	3.0045	3.0063	2.9997	3.0004	3.0137	3.0058	2.9967	3.0025	3.0098	2.9978	2.9970	3.0080	2.9990	3.0077	3.0155	3.0007
MMF	0.8568	0.8435	0.8451	0.8416	0.8555	0.8407	0.8519	0.8460	0.8509	0.8533	0.8556	0.8475	0.8706	0.8578	0.8616	0.8658	0.8630	0.8626	0.8741
N	6	5	4	4	15	5	6	5	5	5	5	5	5	3	8	5	8	3	5

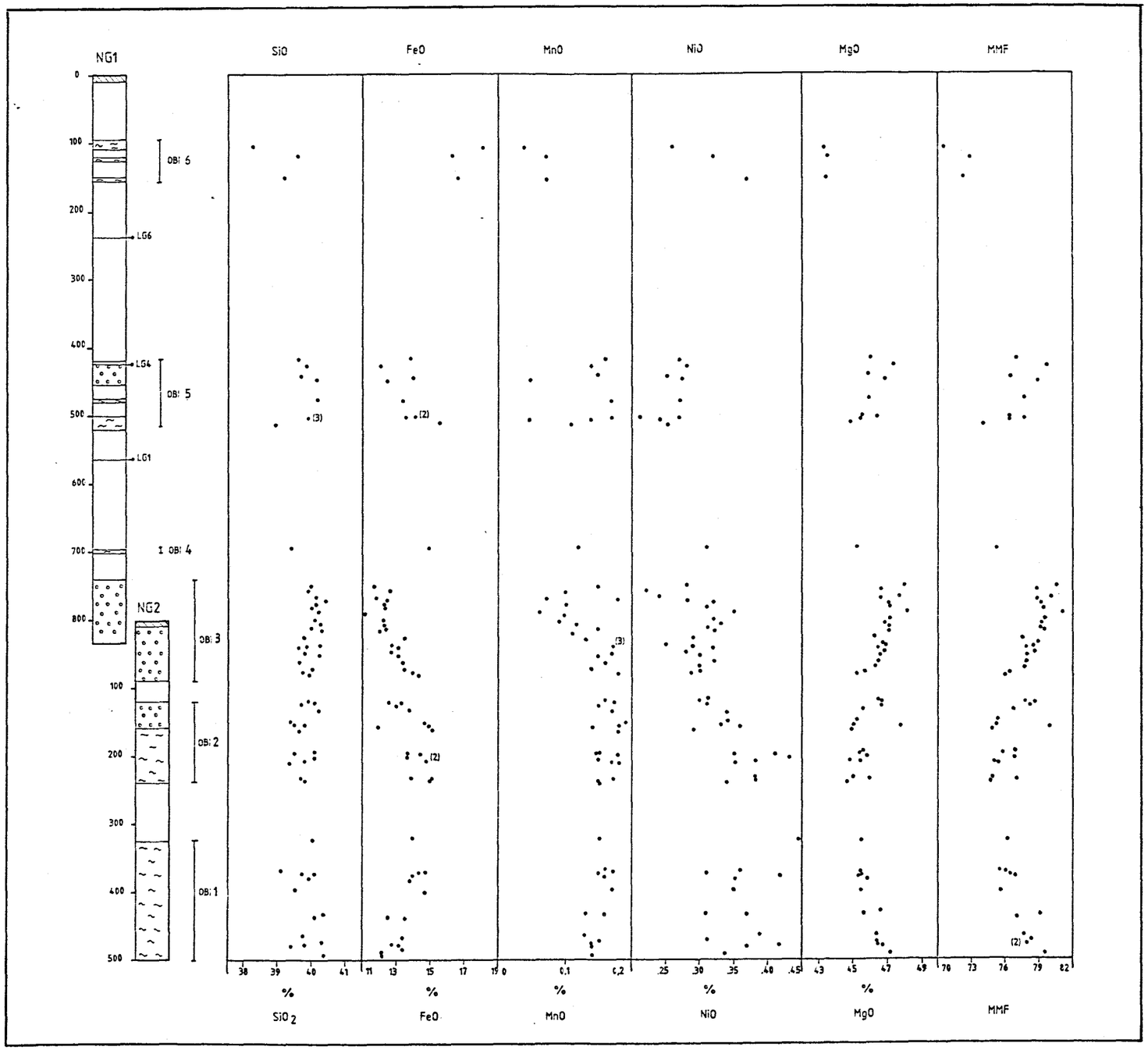

Figure 7.2: Plot of olivine compositions in the olivine-rich cumulates of the NG boreholes. The numbers in brackets indicate the number of datum points which have plotted in the same place. Ornamentation is the same as in Figures 6.3 and 6.4.

base of OBI1 to the top of OBI5 (Figure 7.2) The scatter, however, in the individual intervals is large, particularly so in OBI6 and OBI1.

7.2.3 Comparisons with other studies

Analyses of olivine from other studies are included here for comparison, and are presented in Table 7.2. The three sets of analyses from the eastern Bushveld were chosen because they are from positions close to or stratigraphically similar to those of the NG boreholes. The analyses from the western Bushveld were selected as they lie stratigraphically above the section covered by this study. Analyses from the Stillwater and Rhum Complexes were chosen because in the case of the former the complexes have some characteristics in common, while in the case of the Rhum Complex, the olivine occurs in a different association.

The FeO and MgO compositions from the NG boreholes are similar to those from the Olifants river trough, the Central sector and the Clapham Section of the eastern Bushveld. Fe is relatively depleted, and Mg relatively enriched in the NG olivines compared with that from the stratigraphically higher Union and Amandelbult Sections of the western Bushveld Complex. The NG olivines have similar SiO_2 values to olivines from both the Stillwater and Rhum Complexes, but all the other chemical parameters are quite distinctly different. The olivine from Gish Mine in the Stillwater Complex is chemically more evolved than that from the NG boreholes, but is less evolved than the olivine from the Union and Amandelbult Sections. Olivine from the Rhum Complex has a very much higher CaO content than the Bushveld olivines, and a considerably higher MnO content. The FeO and MgO values of olivine from Rhum are in the range of the Bushveld olivines.

Table 7.2: Olivine analyses from some layered intrusions.

	BUSHVELD COMPLEX						STILLWATER COMPLEX	RHUM COMPLEX	
	EASTERN			WESTERN					
	Olifants River Trough	Central Sector	Clapham Section	Union Section	Amandelbult Section	Nooitgedacht	Gish Mine	Eastern	Western
	1	2	3	4	4	5	6	7	7
SiO_2	40	39.72	40.16	39.24	39.06	39.84	39.64	39.88	40.06
FeO	13.23	12.98	14.44	18.58	18.3	13.62	16.73	15.26	14.13
MnO	0.18	0.16	b 0.25	0.2	0.23	0.14	0.16	0.27	0.26
NiO	a 0.33	0.26	0.57	0.38	0.37	0.32	c 0.19	d 0.27	0.33
MgO	46.84	46.71	45.43	41.76	41.7	46.09	44.22	44.53	45.3
CaO	0.01	n.d.	n.d.	0.02	0.02	0.01	0.03	0.13	e 0.11
Total	100.68	99.83	100.65	100.18	99.68	100.02	100.97	100.34	100.21
N	7	3	33	7			15	65	116
Intersection	Lower Zone	lower Critical Zone	Lower Zone	Upper Critical Zone	Upper Critical Zone	lower Critical and Lower Zone			

Sources of Data:
1: Cameron (1978)
2: Cameron (1980)
3: Lee and Wadsworth (in prep.)
4: Eales et al. (1986)
5: This study
6: Nicholson and Lipin (1984)
7: Dunham and Wadsworth (1978)

a: 2 samples
b: 10 samples
c: 1 sample
d: 44 samples
e: 33 samples

7.3 PYROXENES

7.3.1 A brief review of the pyroxenes

The pyroxene group comprises orthopyroxenes and clinopyroxenes, having orthorhombic and monoclinic symmetry respectively. The general formula for the group can be expressed as:

$$X_{1-p}Y_{1+p}Z_2O_6$$

where: X = Ca, Na
Y = Mg, Fe^{2+}, Mn, Li, Ni, Al, Fe^{3+}, Cr, Ti
Z = Si, Al

For the orthopyroxene series p is approximately equal to one, and the content of trivalent ions in the Y position is small. For the clinopyroxenes the value of p ranges between one and zero. An example where p = 0 is diopside ($CaMgSi_2O_6$) and where p = 1 is spodumene ($LiAlSi_2O_6$) (Deer et al., 1966). It has been found, however, that this general formula dictates a rigid partitioning of cations into the sites; the formula used by Cameron and Papike (1980) is probably more applicable as it is more flexible. The formula is:

$$XYZ_2O_6$$

where: X = Na, Ca Mn^{2+}, Fe^{2+}, Mg, Li in the octahedral and cubic co-ordinated M_2 sites
Y = Mn^{2+}, Fe^{2+}, Mg, Fe^{3+}, Al, Cr, Ti in the octahedral M_1 sites
Z = Si, Al in tetrahedral sites

The composition of the pyroxenes is traditionally presented on a triangular plot with the end members being $MgSiO_3$, $FeSiO_3$ and $CaSiO_3$. The pure Ca end member, wollastonite ($CaSiO_3$) does not have the structure of a pyroxene, and therefore the ternary plot is usually terminated at a Ca value of 50%, the maximum amount of Ca that can be accommodated in the pyroxene structure. Those pyroxenes

with a Ca content of greater than 5% are clinopyroxenes, their symmetry being modified as a result of having to incorporate the larger Ca2+ ion. There is a complex system of exsolution of lamellae of clinopyroxene within orthopyroxene grains, where, with cooling and re-equilibration to lower pressures, the high calcium content of a pyroxene cannot be accommodated, and the two phases unmix.

7.3.2 The Orthopyroxenes of this study

Orthopyroxene occurs predominantly as a cumulus phase, but orthopyroxene oikocrysts also occur. Only cumulus grains were selected for microprobe analysis in this study. Teigler (1991) found that orthopyroxene compositions plotted in a well defined field regardless of their textural habit. Core and rim analyses revealed little zoning of the grains. The orthopyroxenes plot within the bronzite field, having a maximum CaO content of 2.23%, and having an En value between 80% and 90%. The average values of orthopyroxene analyses are presented in Table 7.3, and plots of the main components of orthopyroxene against stratigraphic height in Figure 7.3. The clearest chemical trends are seen in OBI1, where the sampling was densest. The following patterns can be determined.

1- SiO_2, TiO_2, and MgO decrease in opx towards the top of the interval
2- Al_2O_3, Cr_2O_3, and FeO in opx increase towards the top of the interval

The behaviour of MgO and FeO is repeated at the top of OBI3, and is as would be expected in a normal fractionation trend. The Na and Ni contents vary erratically, but both these elements occur in the lowest abundances of the trace elements analysed. CaO in OBI2 shows a distinct decrease with stratigraphic height, which is mirrored by Al_2O_3, however, the same relationship is not evident in OBI3. Inter-element plots have revealed no relationships other than those already evident from the plots of elements against stratigraphic height.

Table 7.3: Averaged orthopyroxene compositions (microprobe analyses) from borehole NG1.

SAMPLE	108.00	122.00	155.00	445.00	452.00	505.00	506	515.35	773.74	784.64	779	793
SiO2	55.05	55.59	55.49	56.11	56.88	55.74	56.09	55.63	56.93	56.50	57.03	57.35
TiO2	0.19	0.11	0.10	0.06	0.06	0.08	0.06	0.06	0.09	0.12	0.07	0.05
Al2O3	1.39	1.55	1.46	1.27	1.09	1.21	1.26	1.28	1.18	1.30	1.00	1.05
Cr2O3	0.36	0.49	0.39	0.51	0.55	0.41	0.46	0.44	0.44	0.39	0.28	0.36
FeO	10.81	9.58	10.05	8.03	7.04	9.25	8.76	9.32	7.88	7.58	7.76	7.26
MnO	0.24	0.16	0.20	0.21	0.17	0.22	0.22	0.22	0.18	0.18	0.17	0.18
NiO	0.08	0.07	0.08	0.05	0.04	0.08	0.06	0.05	0.06	0.07	0.05	0.07
MgO	29.82	29.68	30.47	31.31	32.81	31.42	31.97	31.31	31.82	32.47	32.59	33.11
CaO	1.01	2.23	1.61	2.14	1.25	1.30	1.31	1.40	1.44	1.19	0.92	0.68
Na2O	0.02	0.04	0.01	0.05	0.03	0.03	0.03	0.04	0.04	0.04	0.03	0.02
TOTAL	98.96	99.47	99.83	99.71	99.92	99.72	100.20	99.75	100.07	99.84	99.90	100.13
CATIONS PER 6 OXYGEN												
Si	1.9645	1.9673	1.9589	1.9675	1.9751	1.9619	1.9601	1.9589	1.9809	1.9683	1.9831	1.9837
Ti	0.0050	0.0028	0.0025	0.0016	0.0016	0.0021	0.0016	0.0017	0.0023	0.0031	0.0018	0.0013
Al	0.0585	0.0647	0.0605	0.0523	0.0446	0.0500	0.0518	0.0532	0.0484	0.0534	0.0410	0.0430
Cr	0.0107	0.0144	0.0114	0.0148	0.0160	0.0119	0.0133	0.0129	0.0129	0.0114	0.0081	0.0105
Fe	0.3226	0.2834	0.2966	0.2353	0.2046	0.2723	0.2559	0.2745	0.2292	0.2208	0.2257	0.2099
Mn	0.0071	0.0046	0.0060	0.0061	0.0049	0.0064	0.0064	0.0064	0.0054	0.0054	0.0050	0.0052
Ni	0.0023	0.0019	0.0023	0.0014	0.0011	0.0023	0.0016	0.0015	0.0018	0.0020	0.0014	0.0019
Mg	1.5859	1.5654	1.6033	1.6363	1.6975	1.6483	1.6651	1.6432	1.6501	1.6861	1.6891	1.7068
Ca	0.0386	0.0847	0.0608	0.0803	0.0469	0.0488	0.0492	0.0526	0.0538	0.0443	0.0343	0.0251
Na	0.0014	0.0024	0.0008	0.0034	0.0019	0.0020	0.0019	0.0027	0.0029	0.0026	0.0020	0.0015
TOTAL	3.9966	3.9916	4.0030	3.9990	3.9940	4.0061	4.0068	4.0077	3.9876	3.9975	3.9915	3.9890
EN #	0.8145	0.8096	0.8177	0.8383	0.8710	0.8369	0.8451	0.8340	0.8536	0.8641	0.8666	0.8789
FS #	0.1657	0.1465	0.1513	0.1206	0.1050	0.1382	0.1299	0.1393	0.1186	0.1132	0.1158	0.1081
WO #	0.0198	0.0439	0.0310	0.0411	0.0240	0.0248	0.0250	0.0267	0.0278	0.0227	0.0176	0.0130
N	2	2	2	2	4	2	6	10	7	13	1	5

N : number of analyses averaged

Table 7.3 (cont): Averaged orthopyroxene compositions (microprobe analyses) from borehole NG2.

SAMPLE	157.50	165.62	200.5	213.30	236.86	372.6	374.55	376.1	382.97	399.5	436.58	438.29	466.1	474	478.56	480.8	493.19
SiO2	56.20	56.57	56.49	56.21	56.23	56.69	56.55	56.76	56.12	56.11	57.19	56.92	56.47	56.51	57.07	56.41	57.40
TiO2	0.11	0.11	0.07	0.12	0.09	0.08	0.08	0.08	0.06	0.09	0.04	0.06	0.08	0.12	0.08	0.12	0.09
Al2O3	1.08	1.01	1.34	1.26	1.30	1.18	1.21	1.32	1.18	1.33	1.18	1.20	1.17	1.43	1.08	1.18	0.87
Cr2O3	0.26	0.21	0.50	0.36	0.45	0.37	0.34	0.46	0.42	0.39	0.44	0.44	0.41	0.50	0.44	0.41	0.16
FeO	9.29	9.54	8.85	9.02	9.12	9.24	8.99	9.64	8.87	9.10	7.62	8.52	8.69	8.11	8.39	8.26	7.67
MnO	0.21	0.21	0.21	0.19	0.20	0.19	0.21	0.18	0.21	0.22	0.18	0.17	0.19	0.21	0.18	0.17	0.19
NiO	0.08	0.08	0.09	0.09	0.09	0.09	0.05	0.12	0.04	0.07	0.06	0.05	0.06	0.06	0.10	0.05	0.07
MgO	31.78	31.11	31.19	31.33	30.90	30.63	31.48	30.18	31.70	31.59	32.22	31.60	31.53	31.44	31.62	31.76	32.75
CaO	0.63	0.79	1.22	1.07	1.44	1.44	1.24	1.35	1.26	1.21	1.06	1.07	1.10	1.57	0.97	1.45	0.82
Na2O	0.03	0.03	0.04	0.05	0.03	0.03	0.02	0.03	0.02	0.00	0.01	0.01	0.01	0.03	0.02	0.02	0.02
TOTAL	99.66	99.66	99.99	99.70	99.86	99.95	100.17	100.10	99.89	100.10	100.01	100.03	99.70	99.97	99.95	99.82	100.03
CATIONS PER 6 OXYGEN																	
Si	1.9734	1.9871	1.9756	1.9729	1.9734	1.9862	1.9750	1.9881	1.9669	1.9641	1.9853	1.9839	1.9780	1.9721	1.9889	1.9725	1.9907
Ti	0.0028	0.0028	0.0017	0.0032	0.0023	0.0021	0.0020	0.0021	0.0016	0.0023	0.0011	0.0015	0.0020	0.0032	0.0021	0.0031	0.0023
Al	0.0445	0.0418	0.0553	0.0520	0.0539	0.0489	0.0500	0.0544	0.0489	0.0547	0.0483	0.0493	0.0484	0.0586	0.0445	0.0484	0.0354
Cr	0.0078	0.0062	0.0145	0.0105	0.0132	0.0109	0.0098	0.0133	0.0122	0.0114	0.0128	0.0129	0.0121	0.0146	0.0129	0.0120	0.0047
Fe	0.2727	0.2802	0.2588	0.2648	0.2676	0.2708	0.2625	0.2824	0.2600	0.2664	0.2211	0.2482	0.2544	0.2365	0.2444	0.2414	0.2224
Mn	0.0062	0.0062	0.0063	0.0058	0.0058	0.0057	0.0061	0.0052	0.0063	0.0064	0.0053	0.0050	0.0056	0.0061	0.0052	0.0050	0.0055
Ni	0.0022	0.0023	0.0026	0.0026	0.0025	0.0025	0.0015	0.0033	0.0010	0.0018	0.0017	0.0013	0.0016	0.0017	0.0029	0.0015	0.0018
Mg	1.6635	1.6288	1.6259	1.6390	1.6165	1.5996	1.6388	1.5753	1.6560	1.6479	1.6673	1.6413	1.6459	1.6353	1.6424	1.6554	1.6929
Ca	0.0236	0.0296	0.0455	0.0402	0.0543	0.0539	0.0465	0.0507	0.0474	0.0454	0.0396	0.0398	0.0412	0.0589	0.0362	0.0543	0.0306
Na	0.0018	0.0020	0.0028	0.0033	0.0021	0.0021	0.0017	0.0022	0.0012	0.0002	0.0007	0.0008	0.0009	0.0023	0.0012	0.0015	0.0015
TOTAL	3.9985	3.9870	3.9892	3.9943	3.9918	3.9828	3.9939	3.9770	4.0016	4.0006	3.9833	3.9839	3.9902	3.9892	3.9809	3.9950	3.9878
EN #	0.8488	0.8402	0.8423	0.8431	0.8340	0.8312	0.8414	0.8254	0.8434	0.8409	0.8648	0.8507	0.8477	0.8470	0.8541	0.8484	0.8700
FS #	0.1392	0.1446	0.1341	0.1362	0.1381	0.1407	0.1348	0.1480	0.1324	0.1359	0.1147	0.1286	0.1310	0.1225	0.1271	0.1237	0.1143
WO #	0.0120	0.0153	0.0236	0.0207	0.0280	0.0280	0.0239	0.0266	0.0241	0.0232	0.0205	0.0206	0.0212	0.0305	0.0188	0.0278	0.0157
N	4	2	6	4	8	6	6	4	4	6	6	6	4	4	6	6	4

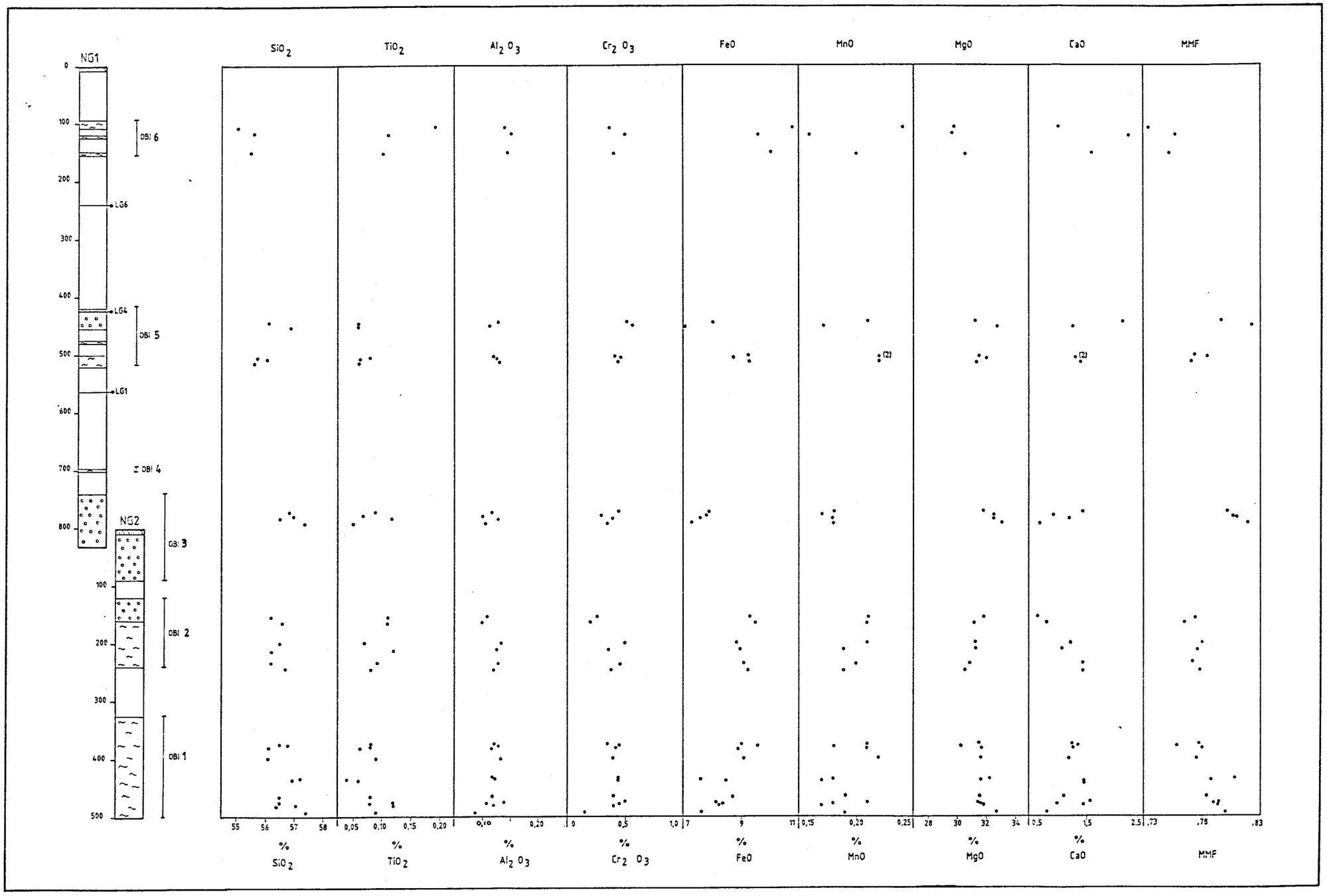

Figure 7.3: Plot of orthopyroxene compositions in the olivine-rich cumulates of the NG boreholes. Ornamentation is the same as in Figures 6.3 and 6.4.

7.3.3 The Clinopyroxenes of this study

Clinopyroxene forms only as an intercumulus phase. It falls mainly within the diopside compositional field, with two samples having an endiopside composition, and one sample having a salite composition. The average MgO content is 18.4% and the average CaO content is 20.1%. The clinopyroxene analyses determined from borehole NG1 are presented in Table 7.4. No clinopyroxenes from borehole NG2 were analysed due to their minor presence in the olivine-bearing rocks.

Table 7.4: Clinopyroxene analyses from borehole NG1.

NAME	505	783.05	783.05	783.05	783.05	783.05	783.05	783.05	818	818	830.15	830.15
SIO2	53.07	53.83	53.13	53.23	52.95	54.16	53.34	53.69	53.40	53.43	53.47	53.01
TIO2	0.25	0.32	0.24	0.19	0.27	0.13	0.25	0.45	0.24	0.15	0.14	0.26
AL2O3	2.32	2.18	2.62	2.59	2.51	2.05	2.75	1.81	2.17	2.42	2.11	2.38
CR2O3	0.97	0.93	1.12	1.11	1.00	0.93	1.09	0.65	0.91	1.04	1.02	1.08
FEO	4.4	3.66	3.36	3.7	3.46	3.99	3.25	4.07	3.59	3.35	3.59	3.24
MNO	0.15	0.08	0.15	0.13	0.10	0.10	0.10	0.09	0.10	0.12	0.14	0.09
NIO	0.01	0.04	0.02	0.05	0.06	0.05	0.00	0.07	0.05	0.01	0.04	0.04
MGO	18.37	18.95	17.93	18.42	18.10	20.05	17.04	20.05	18.68	17.74	18.20	17.34
CAO	19.74	19.5	20.61	19.87	20.47	18.08	20.95	18.93	19.89	20.76	20.49	21.56
NA2O	0.59	0.54	0.62	0.63	0.70	0.54	0.82	0.43	0.49	0.57	0.58	0.63
TOTAL	99.87	100.03	99.80	99.92	99.62	100.08	99.59	100.24	99.52	99.59	99.78	99.63

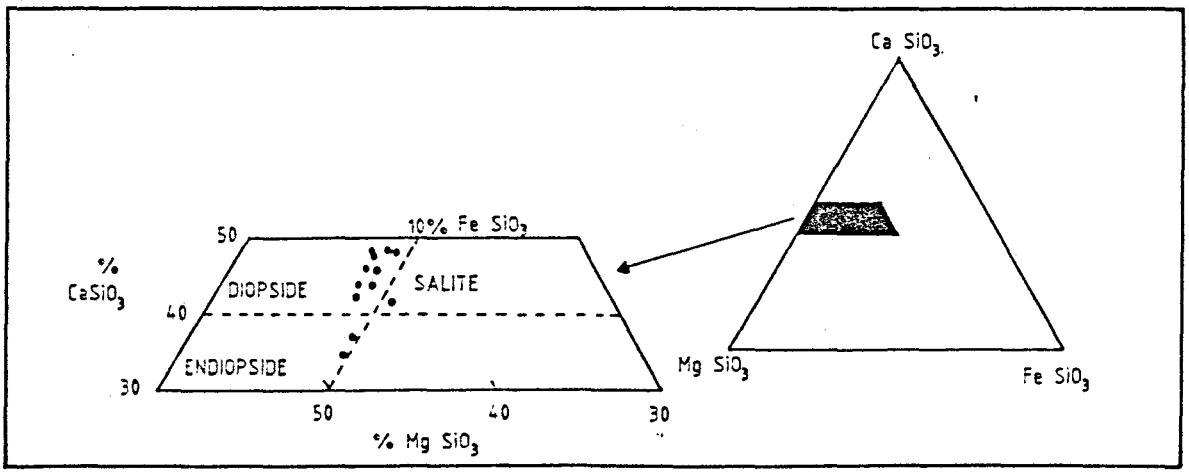

Figure 7.4: Clinopyroxene analyses plotted on a triangular composition diagram.

7.4 CHROMITE

7.4.1 A brief review of chromite

Chromite is one of the end-members of the spinel group. The word spinel refers to oxide minerals with a face-centred cubic unit cell. The unit cell contains 32 oxygen anions arranged in a cubic close-packed framework which is very flexible, in that it can accept 30 different elements, with valencies ranging from 1+ to 6+, as cations in the structure.

The general formula for ideal spinels is as follows:

$$XY_2O_4$$

where X represents the tetrahedral sites (8 per 32 oxygen),
and Y represents the octahedral sites (16 per 32 oxygen).

In the case of ferrochromite X = Fe^{2+} and Y = Cr_2^{3+}
such that the formula for chromite is:

$$FeCr_2O_4$$

The mineral chromite is part of a solid solution series with the end members $FeCr_2O_4$ and $MgCr_2O_4$, and usually contains a number of other elements in lesser amounts (Al, Ti, Fe^{3+}, Mn, V, Ni and Zn).

The general formula for spinels belies the complexity of their make-up and the numerous parameters which control their composition. Some of the most important factors influencing composition are:

- magma or host rock composition
- temperature of crystallisation or equilibration
- late stage reaction with residual liquids
- sub-solidus equilibration with olivine or pyroxene
- oxygen fugacity

- existence of a solvus between aluminium spinel and magnetite
- alteration during serpentinisation (Eales and Marsh, 1983)

The composition of chromite cannot be attributed to one factor alone, but to a number of the above. Of particular relevance is the subsolidus equilibration of chromite with olivine and/or pyroxene. Eales and Marsh (1983) investigated the partitioning of Al and Cr between coexisting spinels and pyroxenes and found that Al/Cr ratios of spinels , orthopyroxene and clinopyroxene vary in sympathy on a broad scale.

In his work on the Great Dyke of Zimbabwe, Wilson (1982) found a distinctive difference in the $Fe^{2+}/(Mg+Fe^{2+})$ ratio of chrome-spinels from olivine cumulates, orthopyroxene cumulates and chromitites. Chromite in olivine was consistently highest in Fe^{2+}, that in chromitites highest in Mg, and that in orthopyroxenites in the middle of the range. The trivalent cations, however, remained constant for chromite grains enclosed in different minerals in single samples.

Accessory chromite in the upper Critical Zone of the Bushveld Complex has also been found to be chemically different from that in massive chromitite layers. Eales and Reynolds (1986) found that reaction with residual liquids and sub-solidus reactions between oxides and silicates had an important role to play in the differing chemistry of the two. The variance in the chemical composition of chromite from massive ore is markedly less than that in accessory grains. The argument that the homogeneity found in this case is a function of post-depositional equilibration was rejected by Eales and Reynolds (1986) because they found rare, large chromite grains with a different chemistry from the vast majority of chromite grains.

The result of the exchange of ions between chromite and ferromagnesian silicates is an enrichment of Fe in chromite, with the degree of enrichment being inversely proportional to the amount of chromite present (Hatton and von Gruenewaldt, 1987). Ion exchange continues as the crystalline pile cools down to temperatures of

about 700-800°C (Hatton and von Gruenewaldt, 1987); exchange continues at lower temperatures for olivine-chromite systems than for orthopyroxene-chromite systems (Wilson, 1982; Hatton and von Gruenewaldt, 1985). Fe enrichment of chromite is commonly accompanied by an increase in Cr. Where the inverse occurs disequilibrium between chromite and the silicates is assumed (Hatton and von Gruenewaldt, 1985).

In summary, the final composition of chromite depends on the conditions of initial crystallisation, the nature of any interstitial liquid during sintering, and the degree of re-equilibration attained while cooling to approximately 700°C.

7.4.2 The chromites of this study

Chromite occurs as a ubiquitous accessory phase in all the olivine-bearing rocks. Average chromite values are presented in Table 7.5, and plots of element variations with stratigraphic height in Figure 7.5. Core and rim analyses revealed no evidence of zoning in the grains. Some general trends can be discerned in Figure 7.5, namely: the increase in Al_2O_3 with stratigraphic height in OBI3, the general decrease of total FeO with height within most intervals, mirrored by the general increase in MgO with stratigraphic height in each interval.

Chromite data from the Great Dyke (Wilson, 1982), chromitite layers in the Critical Zone (Eales and Reynolds, 1986) and from this study are plotted in Figure 7.6. These data is included here to illustrate some of the points made with respect to chromite composition in the previous section, and to compare chromite compositions from other settings with that from the olivine bearing rocks of the NG boreholes. The data have been recalculated such that the sum of the cations Cr^{3+}, Al^{3+}, Fe^{3+} and (Fe^{2+} + Ti^{4+}) is equal to 16 (Eales and Reynolds, 1986). The Bushveld datum points have a similar pattern of distribution, but the samples from lower in the stratigraphy have a slightly wider range of variability. The samples from the Great Dyke are concentrated more in the high chromium, low ferric iron and low titanium field. There is a "dog-leg" in the plot of the cations from

Table 7.5: Averaged chromite compositions (microprobe analyses) from borehole NG1.

SAMPLE	122.8	155	420.75	430.55	445.45	452	480.6	505	508	512	515	697	753.09	770	773.74
TiO2	1.64	0.99	0.55	0.46	0.30	0.58	0.77	0.85	0.88	0.33	1.02	1.28	0.47	0.30	0.32
Al2O3	15.31	17.73	17.59	15.05	16.42	16.10	16.27	13.96	16.44	15.53	11.41	16.92	16.24	18.00	16.56
Cr2O3	35.03	37.79	36.22	47.76	44.59	44.51	38.67	40.79	42.15	41.25	40.63	35.43	44.62	46.71	37.47
Fe2O3	15.05	12.15	14.72	7.42	8.26	8.64	13.60	13.08	8.90	11.30	15.28	15.21	7.55	4.45	14.23
FeO	26.72	23.06	22.36	18.60	21.41	20.82	22.59	24.37	23.23	25.58	25.34	22.41	22.71	21.07	23.26
MnO	0.36	0.25	0.32	0.33	0.33	0.33	0.36	0.35	0.37	0.38	0.35	0.32	0.38	0.29	0.41
MgO	5.50	7.94	8.03	10.28	8.46	9.02	7.95	6.56	7.52	5.65	5.70	8.35	7.64	8.89	7.07
NiO	0.19	0.15	0.15	0.10	0.10	0.09	0.14	0.11	0.10	0.08	0.12	0.20	0.07	0.10	0.09
TOTAL	99.80	100.06	99.95	100.00	99.85	100.08	100.35	100.07	99.58	100.10	99.84	100.12	99.69	99.81	99.42
CATIONS PER 32 OXYGEN															
Ti	0.3315	0.1940	0.1091	0.0896	0.0591	0.1125	0.1524	0.1717	0.1747	0.0663	0.2081	0.2506	0.0938	0.0583	0.0642
Al	4.8495	5.4445	5.4110	4.5950	5.0498	4.9332	5.0162	4.3988	5.1052	4.8879	3.6683	5.2038	5.0356	5.4796	5.1760
Cr	7.4436	7.7848	7.4784	9.7789	9.2093	9.1501	8.0012	8.6267	8.7799	8.7096	8.7750	7.3091	9.2831	9.5390	7.8553
Fe3+	3.0438	2.3822	2.8925	1.4469	1.6228	1.6914	2.6779	2.6312	1.7654	2.2708	3.1405	2.9855	1.4936	0.8649	2.8403
Fe2+	6.0056	5.0247	4.8831	4.0276	4.6748	4.5273	4.9428	5.4520	5.1180	5.7129	5.7889	4.8900	4.9971	4.5513	5.1594
Mn	0.0820	0.0552	0.0703	0.0730	0.0719	0.0721	0.0789	0.0792	0.0829	0.0860	0.0803	0.0700	0.0857	0.0634	0.0914
Mg	2.2032	3.0835	3.1233	3.9678	3.2924	3.4950	3.1020	2.6158	2.9536	2.2490	2.3134	3.2486	2.9964	3.4226	2.7939
Ni	0.0411	0.0314	0.0324	0.0212	0.0200	0.0183	0.0287	0.0246	0.0203	0.0172	0.0255	0.0427	0.0147	0.0208	0.0195
MMF	0.2684	0.3803	0.3901	0.4963	0.4132	0.4357	0.3856	0.3242	0.3659	0.2825	0.2855	0.3992	0.3749	0.4292	0.3513
N	1	1	8	2	2	4	4	4	4	1	3	3	5	1	5

SAMPLE	779	784.64	793.8	803.41	809.42	816.1	818.1	830.15
TiO2	1.25	0.75	0.40	0.91	0.33	1.12	0.56	0.74
Al2O3	17.08	16.03	16.14	16.82	15.57	16.39	16.90	16.55
Cr2O3	40.94	42.25	43.11	41.22	43.72	41.05	42.21	41.67
Fe2O3	10.70	10.27	9.25	9.20	9.34	10.45	9.39	9.84
FeO	19.19	21.73	22.47	22.70	22.78	21.62	22.32	23.07
MnO	0.30	0.36	0.39	0.34	0.36	0.36	0.35	0.38
MgO	10.53	8.44	7.66	7.81	7.41	8.71	8.07	7.60
NiO	0.20	0.12	0.13	0.15	0.10	0.16	0.04	0.13
TOTAL	100.19	99.94	99.53	99.15	99.60	99.87	99.83	99.96
CATIONS PER 32 OXYGEN								
Ti	0.2409	0.1483	0.0787	0.1796	0.0662	0.2204	0.1096	0.1465
Al	5.1589	4.9387	5.0159	5.2231	4.8544	5.0397	5.2070	5.1171
Cr	8.2954	8.7415	8.9915	8.5934	9.1525	8.4676	8.7255	8.6463
Fe3+	2.0635	2.0230	1.8353	1.8242	1.8608	2.0520	1.8476	1.9430
Fe2+	4.1129	4.7592	4.9560	5.0065	5.0444	4.7198	4.8812	5.0646
Mn	0.0651	0.0800	0.0865	0.0761	0.0803	0.0795	0.0781	0.0834
Mg	4.0223	3.2848	3.0096	3.0645	2.9208	3.3874	3.1435	2.9731
Ni	0.0412	0.0245	0.0265	0.0325	0.0207	0.0337	0.0079	0.0264
MMF	0.4944	0.4084	0.3778	0.3797	0.3667	0.4178	0.3917	0.3699
N	1	22	5	2	5	3	4	2

N : number of analyses averaged

Formula recalculated from microprobe data on assumption of stoichiometry.

Table 7.5 (cont): Averaged chromite compositions (microprobe analyses) from borehole NG2.

SAMPLE	39.35	42.55	50.20	65.25	73.60	83.75	123.40	127.15	153.35	158.60	165.62	200.50	213.30	238.90	326.86
TiO2	0.50	0.67	0.51	0.48	0.85	1.39	0.27	0.65	0.91	0.59	0.43	0.59	0.44	0.75	0.93
Al2O3	15.69	17.17	17.19	15.74	14.93	13.34	15.68	15.60	13.87	14.06	14.34	16.31	16.94	15.55	15.41
Cr2O3	38.06	44.03	35.41	37.76	38.53	38.27	34.53	39.71	37.74	47.06	35.16	41.20	39.17	43.75	39.72
Fe2O3	14.52	7.37	14.97	14.13	13.98	15.52	17.65	12.69	14.98	9.27	17.96	10.54	11.98	8.47	12.38
FeO	23.39	20.31	24.21	24.42	23.54	24.42	24.70	23.07	26.05	18.40	26.98	22.84	23.82	23.82	23.24
MnO	0.42	0.32	0.39	0.41	0.37	0.38	0.38	0.38	0.37	0.33	0.37	0.39	0.33	0.36	0.32
MgO	7.05	9.38	6.59	6.28	7.01	6.73	5.93	7.30	5.26	10.36	4.54	7.52	6.92	6.99	7.36
NiO	0.10	0.07	0.18	0.14	0.14	0.19	0.15	0.18	0.19	0.18	0.12	0.14	0.14	0.15	0.22
TOTAL	99.73	99.33	99.44	99.38	99.34	100.24	99.29	99.59	99.37	100.25	99.90	99.51	99.75	99.79	99.58
CATIONS PER 32 OXYGEN															
Ti	0.1071	0.1422	0.1097	0.0971	0.1707	0.2987	0.0584	0.1397	0.1873	0.1148	0.0879	0.1168	0.0917	0.1487	0.1868
Al	5.2518	5.7297	5.7060	4.9732	4.7089	4.4863	5.2681	5.2107	4.4464	4.3090	4.5805	5.0808	5.5841	4.8595	4.8281
Cr	8.5444	9.8526	7.8866	7.9978	8.1510	8.6282	7.7820	8.8982	8.1303	9.6672	7.5781	8.6055	8.6571	9.1694	8.3455
Fe3+	3.4486	1.7456	3.5263	2.8504	2.8140	3.7020	4.2059	3.0066	3.0699	1.8132	3.6792	2.0951	2.8008	1.6898	2.4762
Fe2+	4.9984	4.3268	5.1308	5.4737	5.2676	5.2389	5.2972	4.9202	5.9373	3.9999	6.1425	5.0467	5.0103	5.2843	5.1661
Mn	0.1016	0.0776	0.0928	0.0940	0.0847	0.0915	0.0914	0.0924	0.0861	0.0731	0.0864	0.0862	0.0791	0.0816	0.0712
Mg	1.6100	2.1363	1.4925	2.5060	2.7956	1.5452	1.3600	1.6641	2.1323	4.0134	1.8386	2.9613	1.5564	2.7586	2.9145
Ni	0.0437	0.0288	0.0765	0.0307	0.0299	0.0792	0.0650	0.0779	0.0418	0.0374	0.0267	0.0295	0.0596	0.0319	0.0460
MMF	0.2436	0.3305	0.2253	0.3140	0.3467	0.2278	0.2043	0.2527	0.2642	0.5008	0.2304	0.3698	0.2370	0.3430	0.3607
N	1	1	5	5	3	6	6	5	3	5	6	2	2	7	4

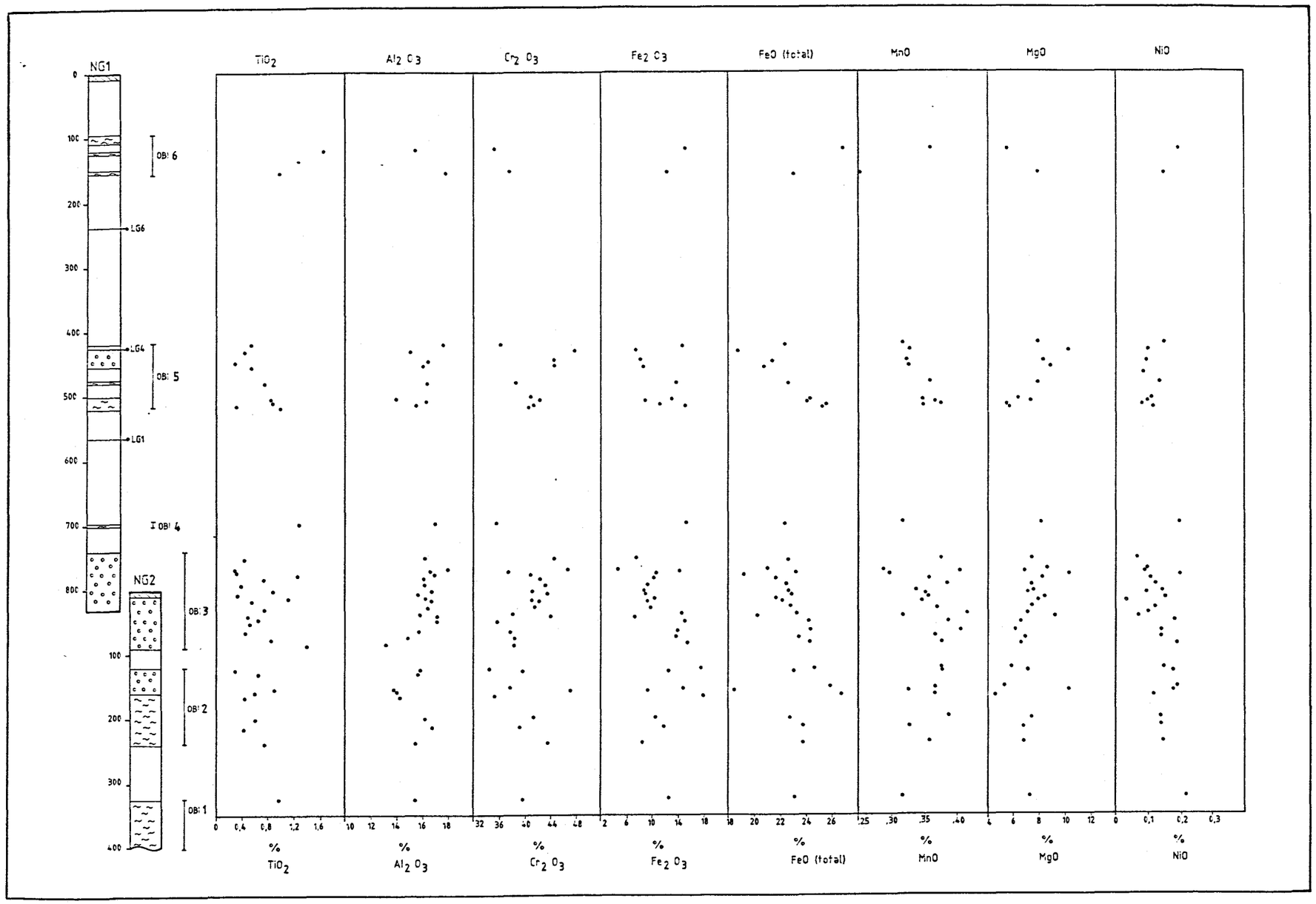

Figure 7.5: Plot of chromite compositions in the olivine-rich cumulates of the NG boreholes. Ornamentation is the same as in Figures 6.3 and 6.4.

the Great Dyke, tending towards a higher concentration of iron and titanium, which broadly overlaps with the Bushveld plots.

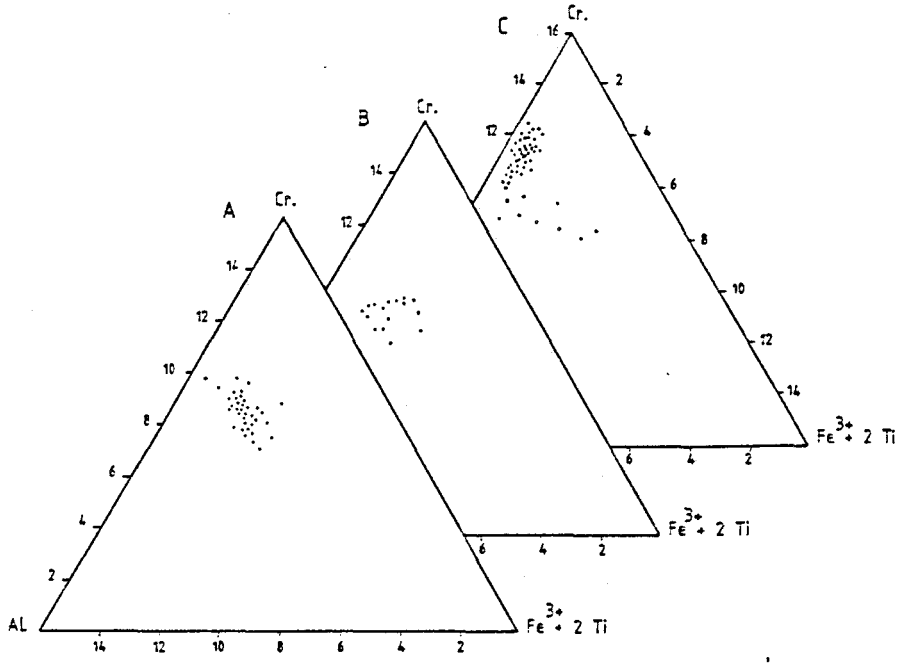

Figure 7.6: Plot of some chromite compositions from the Great Dyke of Zimbabwe and the Bushveld Complex. A - this study, B - Critical Zone (Eales and Reynolds, 1986) and C - Great Dyke (Wilson,1982).

7.5 FELDSPAR

7.5.1 A brief review of the feldspars

The feldspars are framework silicates, the majority of which fall within the ternary system $NaAlSi_3O_8$-$KAlSi_3O_8$-$CaAl_2Si_2O_8$. Those members of the series between the sodium and potassium end members are known as alkali feldspars, and those between the sodium-rich and the calcium-rich members are the plagioclase feldspars. The feldspars belong to three crystal systems. The pure calcium feldspar, anorthite, is triclinic. The pure potassium end-member can occur as monoclinic crystals, either having crystallised at high temperatures, whereupon it is called sanidine, or at lower temperatures, when it is called orthoclase. K-feldspars crystallised at the lowest temperatures are called microcline, and have a triclinic structure. The pure Na-feldspars occur as high-, low- or intermediate albite according to their temperature of crystallisation and resulting crystal structure. They are commonly triclinic, but with strong heating there may be a transition to monoclinic symmetry. The high temperature series of albite-anorthite is one of complete solid solution in terms of composition, whereas the low temperature series is more complex and shows evidence of exsolution (e.g., peristerites and Huttenlocher intergrowths).

7.5.2 The feldspars of this study

All the plagioclase occurring in the dunites and harzburgites is intercumulus. The grains are generally extremely small. Average feldspar analyses are presented in Table 7.6, and plots of the main chemical components against stratigraphic height are presented in Figure 7.7.

The amount of potassium in the minerals is trivial, with a maximum of 0,04% in NG1 809,73. The majority of grains analysed are labradorite (An_{50-70}), with five samples being bytownite (An_{70-90}) and three being andesine (An_{30-50}), an unusually wide range of composition. A sympathetic relationship exists between SiO_2 and Na2O, and between Al2O3 and CaO. An antipathetic relationship exists

Table 7.6: Averaged plagioclase compositions (microprobe analyses) from borehole NG1.

SAMPLE	420.15	430.75	505	506	515	697	773.74	784.64	803.41	809.73	816	818
SiO2	55.23	54.63	58.90	55.45	53.11	50.13	51.05	56.09	51.08	59.89	51.44	52.60
Al2O3	28.58	29.10	25.61	28.04	29.62	31.20	31.52	27.80	30.98	25.10	30.94	30.02
FeO	0.07	0.17	0.16	0.07	0.09	0.16	0.18	0.11	0.13	0.16	0.15	0.10
CaO	10.64	10.94	8.06	10.73	12.48	14.70	13.50	10.34	13.51	6.58	13.32	12.84
Na2O	5.70	5.52	7.25	5.65	4.65	3.36	3.86	5.58	3.99	8.12	4.14	4.22
K2O	0.01	0.01	0.01	0.01	0.02	0.00	0.01	0.02	0.00	0.04	0.01	0.01
TOTAL	100.24	100.38	99.99	99.95	99.96	99.56	100.10	99.95	99.71	99.88	99.99	99.79
CATIONS PER 52 OXYGEN												
Si	9.9293	9.8240	10.5359	9.9946	9.6242	9.1881	9.2716	10.0840	9.3173	10.6917	9.3520	9.5513
Al	6.0567	6.1692	5.4007	5.9593	6.3298	6.7416	6.7488	5.8966	6.6644	5.2833	6.6325	6.4265
Fe	0.0108	0.0263	0.0239	0.0110	0.0144	0.0250	0.0270	0.0170	0.0201	0.0232	0.0228	0.0152
Ca	2.0505	2.1082	1.5448	2.0718	2.4245	2.8879	2.6270	1.9954	2.6429	1.2596	2.5945	2.4983
Na	1.9874	1.9254	2.5145	1.9747	1.6315	1.1959	1.3577	1.9454	1.4108	2.8096	1.4584	1.4858
K	0.0026	0.0020	0.0023	0.0033	0.0044	0.0010	0.0015	0.0040	0.0007	0.0080	0.0014	0.0023
TOTAL	20.0373	20.0551	20.0222	20.0147	20.0289	20.0395	20.0336	19.9424	20.0563	20.0754	20.0616	19.9794
N	5	3	1	8	5	5	8	15	5	5	8	1
AN #	0.5075	0.5224	0.3803	0.5115	0.5970	0.7070	0.6591	0.5047	0.6519	0.3090	0.6400	0.6267

AN# : Ca/(Ca+Na+K)

N : number of analyses averaged

Table 7.6 (cont): Average plagioclase compositions (microprobe analyses) from borehole NG2.

SAMPLE	39.35	42.55	43.35	50.2	55.5	65.25	73.6	80.35	83.75	127.55	134.4	153.35	157.5	158.6	165.62	200.5
SiO2	50.14	51.35	51.74	51.34	52.57	54.51	56.08	48.68	51.48	51.78	54.46	53.47	52.14	53.58	51.76	49.69
Al2O3	32.26	31.40	30.60	31.02	30.36	29.14	28.05	32.68	31.36	30.87	28.97	29.64	30.90	29.96	30.99	32.28
FeO	0.13	0.13	0.19	0.14	0.14	0.11	0.15	0.14	0.13	0.16	0.08	0.15	0.08	0.20	0.14	0.09
CaO	14.47	13.54	13.07	13.32	12.47	10.94	9.78	15.40	13.35	13.05	10.79	11.78	12.89	11.71	13.19	14.76
Na2O	3.10	3.72	4.17	3.91	4.48	5.35	5.97	2.93	3.84	4.00	5.45	4.89	4.18	4.55	3.96	3.24
K2O	0.02	0.01	0.01	0.01	0.01	0.01	0.01	0.00	0.01	0.02	0.01	0.01	0.01	0.02	0.01	0.01
TOTAL	100.11	100.15	99.78	99.75	100.03	100.07	100.05	99.83	100.17	99.87	99.75	99.94	100.20	100.01	100.06	100.08
CATIONS PER 52 OXYGEN																
Si	9.1191	9.3120	9.4159	9.3486	9.5226	9.8239	10.0725	8.9211	9.3310	9.4064	9.8408	9.6730	9.4339	9.6720	9.3880	9.0589
Al	6.9163	6.7130	6.5688	6.6601	6.4833	6.1901	5.9398	7.0605	6.7005	6.6107	6.1740	6.3240	6.5916	6.3755	6.6271	6.9403
Fe	0.0193	0.0196	0.0288	0.0214	0.0213	0.0172	0.0220	0.0208	0.0190	0.0243	0.0127	0.0228	0.0115	0.0303	0.0218	0.0143
Ca	2.8202	2.6312	2.5508	2.5996	2.4205	2.1128	1.8815	3.0249	2.5918	2.5407	2.0905	2.2862	2.4997	2.2643	2.5643	2.8851
Na	1.0914	1.3082	1.4695	1.3806	1.5739	1.8707	2.0802	1.0419	1.3508	1.4086	1.9068	1.7150	1.4655	1.5925	1.3921	1.1436
K	0.0043	0.0032	0.0015	0.0029	0.0024	0.0030	0.0032	0.0006	0.0022	0.0040	0.0014	0.0028	0.0016	0.0038	0.0023	0.0012
TOTAL	19.9706	19.9872	20.0352	20.0132	20.0239	20.0179	19.9992	20.0699	19.9953	19.9946	20.0263	20.0238	20.0038	19.9384	19.9956	20.0434
N	3	3	10	3	10	8	7	3	5	5	5	7	3	3	8	8
AN #	0.7203	0.6674	0.6342	0.6526	0.6059	0.5300	0.4746	0.7437	0.6572	0.6426	0.5227	0.5717	0.6302	0.5864	0.6477	0.7159

SAMPLE	206.3	212.2	213.3	372	382	438	474	478	493
SiO2	54.50	52.91	50.24	50.52	51.14	49.77	49.31	50.79	52.11
Al2O3	29.23	30.28	31.96	31.38	30.43	31.62	32.15	31.45	30.42
FeO	0.13	0.10	0.12	0.14	0.27	0.20	0.13	0.17	0.10
CaO	11.12	12.64	14.58	13.87	13.68	14.70	15.12	14.10	13.09
Na2O	5.12	4.50	3.30	3.91	3.97	3.41	3.05	3.62	4.34
K2O	0.02	0.00	0.01	0.06	0.15	0.04	0.04	0.06	0.10
TOTAL	100.13	100.43	100.21	99.89	99.65	99.74	99.82	100.18	100.16
CATIONS PER 52 OXYGEN									
Si	9.8148	9.5456	9.1375	9.2197	9.3550	9.1163	9.0273	9.2355	9.4527
Al	6.2053	6.4422	6.8545	6.7519	6.5639	6.8273	6.9404	6.7409	6.5066
Fe	0.0203	0.0152	0.0179	0.0216	0.0418	0.0305	0.0206	0.0253	0.0159
Ca	2.1464	2.4439	2.8420	2.7129	2.6812	2.8855	2.9674	2.7469	2.5445
Na	1.7863	1.5724	1.1643	1.3835	1.4067	1.2106	1.0833	1.2771	1.5259
K	0.0052	0.0003	0.0025	0.0129	0.0356	0.0101	0.0102	0.0137	0.0225
TOTAL	19.9783	20.0196	20.0186	20.1026	20.0842	20.0803	20.0493	20.0394	20.0681
N	2	3	8	1	3	5	5	5	5
AN #	0.5451	0.6079	0.7085	0.6602	0.6504	0.7027	0.7309	0.6804	0.6220

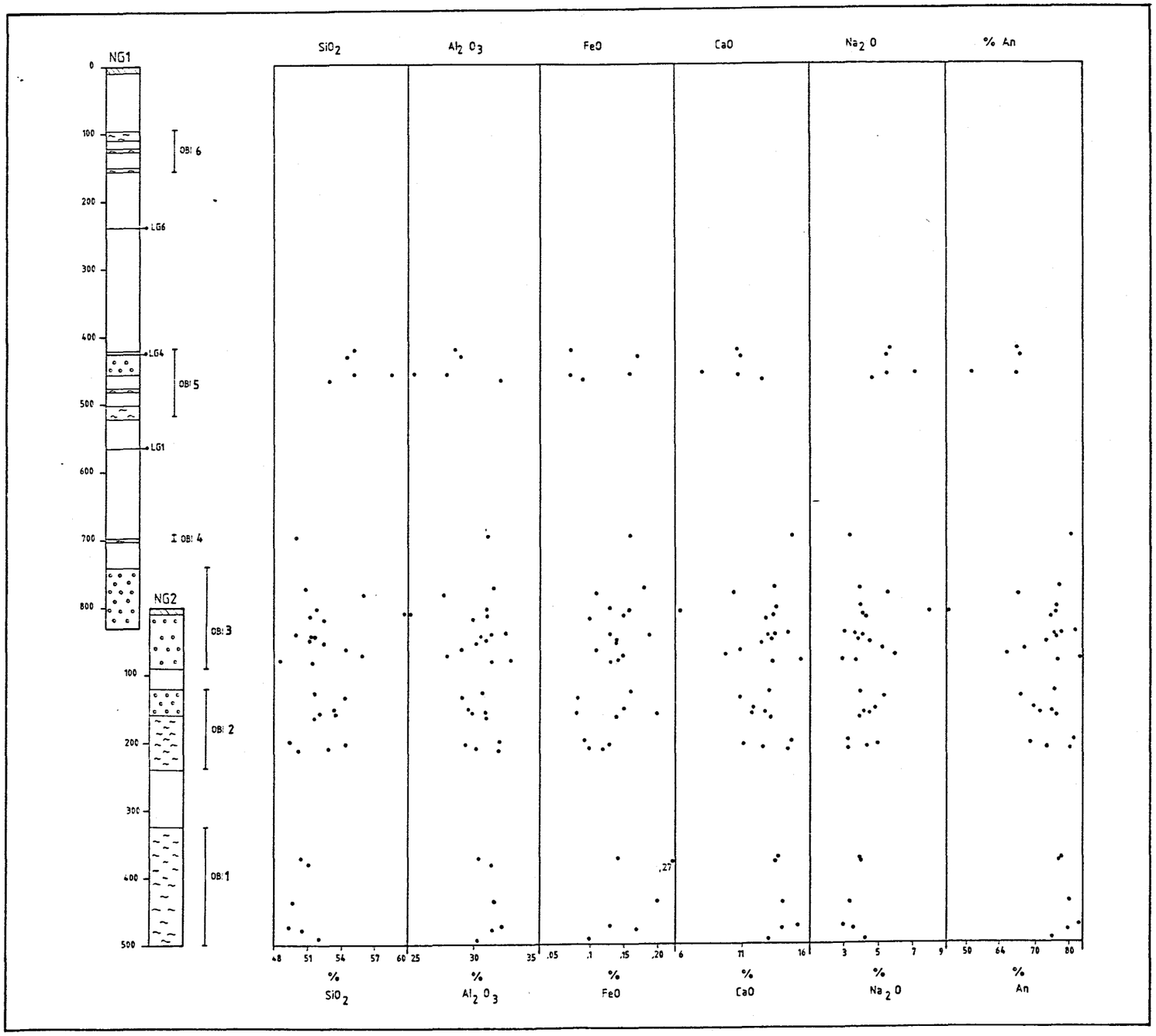

Figure 7.7: Plot of plagioclase compositions in the olivine-rich cumulates of the NG boreholes. Ornamentation is the same as in Figures 6.3 and 6.4.

between the two pairs, as would be expected.

At the base of OBI4 a distinct reversal in the normal fractionation trend is obvious. The plagioclase becomes enriched in calcium and depleted in sodium with an increase in stratigraphic height. In OBI2 there seems to be a suggestion of a normal fractionation pattern of increasing Na and decreasing Ca with increasing stratigraphic height. Within OBI1 there is a change in the fractionation trend from reversed to normal; in all the other units the pattern seems random. Reichhardt and Hatton (1991) found a correlation between the An content of plagioclase and the modal proportion of plagioclase whereby rocks with a high proportion of intercumulus An-rich plagioclase generally have a higher proportion of intercumulus minerals than do rocks with more Na-rich intercumulus plagioclase.

7.6 DISCUSSION

Early work by Bowen and Schairer (1935) showed that in most parts of the system MgO-FeO-SiO_2, olivine has a higher Mg content and a lower Fe content than the co-existing melt; relationships are shown in the olivine phase diagram (Figure 7.8).

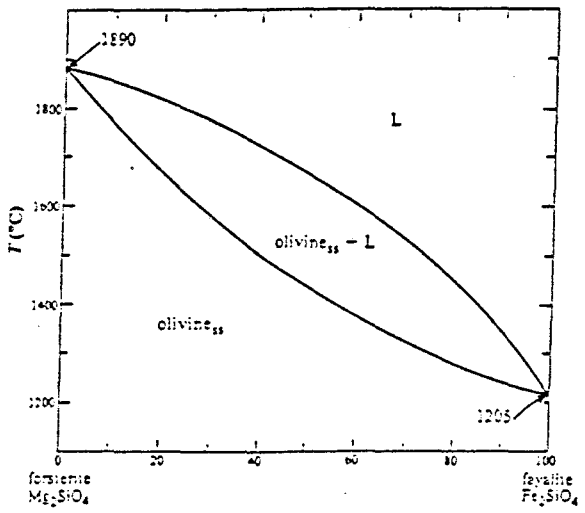

Figure 7.8: The olivine phase diagram (after Bowen and Schairer, 1935, from Cox, Bell and Pankhurst, 1979).

Although the phenomenon of reversals in the fractionation trend shown in the interval under study is not unique, some process or

processes must have been at work, either to alter the chemistry of the system, or alter the physical conditions under which the system crystallised. The following three mechanisms seem viable:

a) A sulphide phase became immiscible and being siderophile, drew Fe from the melt, making it relatively more Mg-rich;
b) There could have been periodic tapping of a primitive magma, replenishing the crystallising magma, hence making it progressively more Mg-rich;
c) Decreasing pressure in the magma chamber during fractional crystallisation could cause a reversal in the normal fractionation trend, resulting in the olivines being more Mg-rich (Osborn, 1980).

The segregation of a separate sulphide phase would be expected not only to deplete the magma in Fe, but also in Ni, a strongly chalcophile element. In the Insizwa and Tabankulu Complexes of Transkei, Lightfoot et al. (1984) found that the olivine is strongly depleted in Ni. The Ni content in olivine ranges between about 200 ppm and 1900 ppm. This is an area of known sulphide mineralisation. The olivine occurring in the NG boreholes contains a relatively high proportion of nickel, in the range 2100 - 4500 ppm. It would, therefore, appear unlikely that a separate sulphide phase is the cause of the reversal in the fractionation trend.

The possibility of a change in pressure causing a reversal in the fractionation trend was discussed by Cameron (1977 and 1980), but the magnitude of the change required to result in a reversal of the normal fractionation trend would be too great to be realistic, and as such is not a viable mechanism (Hatton, 1984).

The possibility of a periodic tapping of primitive magma causing replenishment of the chamber would account for the Mg-enrichment in olivine and the rock as a whole, the maintenance of the level of nickel in the rock, and the intercalation of dunite and harzburgite layers. This is supported by Hatton (1984) in his investigation of the effect of pressure, temperature and composition on the distribution of Fe and Mg between olivine, orthopyroxene and liquid.

He invoked "the emplacement of fresh pulses of magma" (Hatton, 1984) as the main mechanism for the reversal in fractionation trend in orthopyroxene (becoming more enstatite-rich with stratigraphic height) and for changes in phase boundaries, allowing for the crystallisation of olivine higher in the sequence than would be expected from fractional crystallisation of a single magma under pristine conditions.

8. WHOLE-ROCK CHEMISTRY

8.1 INTRODUCTION

In this chapter the whole rock chemical analyses of 36 samples drawn from NG1 (19 samples) and NG2 (17 samples) are presented and discussed. The chemistry is dealt with in three sections: major elements, trace elements and inter-element ratios.

8.2 MAJOR-ELEMENT CHEMISTRY

The original whole-rock data are presented in Appendix 2. The original data with an assumed $FeO:Fe_2O_3$ ratio of 10 (LOI- and H_2O-free) recalculated to 100%, are presented in Table 8.1. Variations in major element compositions in the olivine-bearing rocks in NG1 and NG2 are illustrated by means of plots of the oxides against stratigraphic height (Figure 8.1), and by means of binary diagrams where MgO is used as the abscissa (Figure 8.2). K_2O and P_2O_5 occur in extremely small quantities in the rocks analysed, and being of little significance, are not discussed here.

8.2.1 SiO_2

The SiO_2 content of the olivine-pyroxenites, harzburgites and dunites ranges between 39.08 and 50.98 wt.%. The ad- and mesocumulate harzburgites have SiO_2 contents which spread throughout the range. Mesocumulate dunites and poikilitic harzburgites, however, do not have SiO_2 above 45.50 wt.% (Figure 8.2). The variation in SiO_2 content with stratigraphic height (Figure 8.1) shows no general trend through the boreholes; however, within the unit correlated with the Groenfontein Harzburgite, called here the olivine-bearing intervals 4, 5 and 6 (OBI3, OBI2 and OBI1) there is a general trend of SiO_2 depletion with height.

8.2.2 TiO_2

TiO_2 partitions into orthopyroxene, clinopyroxene, chromite and biotite (ilmenite and titanomagnetite do not occur at this level of

Table 8.1: Whole rock geochemical analyses from borehole NG1, recalculated LOI- and H_2O^--free and normalised to 100 %. A ratio of FeO/ Fe_2O_3=10 is assumed.

SAMPLE	95.5	108.33	122.80	129.75	130.55	145.45	180.60	506.05	509.86	698.00	699.45	753.09	773.71	781.61	793.80	803.11	809.31	816.10	830.15
SiO2	43.651	45.146	44.758	47.882	39.082	44.546	50.975	47.072	41.846	47.069	40.609	39.631	39.709	42.130	40.386	40.580	41.976	40.648	42.001
TiO2	0.065	0.172	0.047	0.258	0.113	0.051	0.095	0.100	0.058	0.111	0.043	0.011	0.004	0.065	0.016	0.018	0.050	0.024	0.048
Al2O3	1.397	2.598	3.277	2.569	3.758	1.598	2.628	2.616	1.868	2.245	1.371	0.403	0.118	1.248	0.476	0.530	1.101	1.467	1.243
Fe2O3	1.246	1.329	1.189	1.075	1.169	1.107	0.961	1.083	1.269	1.180	1.361	1.177	1.098	1.060	1.068	1.084	1.076	1.123	1.140
FeO	12.459	13.287	11.897	10.752	11.693	11.072	9.616	10.828	12.691	11.794	13.612	11.761	10.979	10.607	10.679	10.836	10.765	11.235	11.399
MnO	0.120	0.187	0.159	0.145	0.192	0.163	0.168	0.193	0.191	0.195	0.189	0.168	0.189	0.192	0.183	0.214	0.202	0.197	0.226
MgO	35.095	34.510	36.203	33.778	38.159	39.348	32.506	34.218	39.668	34.469	41.080	45.823	47.170	41.906	45.704	45.478	42.822	43.630	41.543
CaO	2.081	1.703	1.851	1.343	1.480	1.217	1.833	1.784	1.155	1.358	0.981	0.285	0.155	1.771	0.379	0.591	0.802	0.845	1.382
Na2O	0.132	0.110	0.105	0.136	0.545	0.284	0.178	0.278	0.301	0.131	0.283	0.031	0.032	0.291	0.047	0.098	0.315	0.271	0.227
K2O	0.000	0.000	0.000	0.361	0.000	0.000	0.000	0.000	0.000	0.000	0.000	0.000	0.000	0.062	0.000	0.000	0.010	0.000	0.000
P2O5	0.000	0.000	0.000	0.000	0.000	0.000	0.000	0.000	0.000	0.000	0.000	0.000	0.000	0.000	0.000	0.011	0.026	0.005	0.012
Cr2O3	0.556	0.784	0.286	1.567	3.627	0.454	0.941	1.713	0.771	1.318	0.276	0.498	0.267	0.409	0.741	0.269	0.585	0.288	0.527
NiO	0.189	0.174	0.227	0.134	0.183	0.160	0.098	0.114	0.181	0.130	0.196	0.212	0.280	0.259	0.321	0.292	0.270	0.265	0.253
LOI	0.000	0.000	0.000	0.000	0.000	0.000	0.000	0.000	0.000	0.000	0.000	0.000	0.000	0.000	0.000	0.000	0.000	0.000	0.000
H2O-	0.000	0.000	0.000	0.000	0.000	0.000	0.000	0.000	0.000	0.000	0.000	0.000	0.000	0.000	0.000	0.000	0.000	0.000	0.000
TOTAL	100.000	100.000	100.000	100.000	100.000	100.000	100.000	100.000	100.000	100.000	100.000	100.000	100.000	100.000	100.000	100.000	100.000	100.000	100.000
Rb	0.00	0.00	0.00	17.33	0.00	0.00	0.00	0.00	0.00	0.00	0.00	0.00	0.00	6.48	0.00	0.00	3.37	1344.26	0.00
Sr	48.64	20.04	43.76	9.06	39.14	19.39	20.35	26.04	23.81	18.61	25.45	5.68	3.00	19.92	4.35	8.41	16.88	6.81	19.03
Y	3.99	5.38	3.75	4.51	3.64	0.00	3.59	5.41	0.00	2.59	0.00	0.00	0.00	3.00	0.00	0.00	2.96	0.00	2.63
Zr	3.07	12.58	5.35	22.39	3.06	3.34	5.03	3.43	3.09	5.63	3.72	0.00	0.00	11.34	0.00	2.35	11.04	0.00	6.15
Nb	0.00	0.00	0.00	0.00	0.00	0.00	0.00	0.00	0.00	0.00	0.00	0.00	0.00	0.00	0.00	0.00	0.00	0.00	0.00
Zn	74.76	136.04	73.84	73.45	83.19	66.54	50.24	77.77	82.51	80.76	87.38	68.63	69.38	59.80	67.07	57.00	63.30	64.07	73.34
Cu	7.23	44.45	11.70	17.23	20.22	13.18	17.98	21.28	15.98	14.44	14.48	10.31	6.28	14.63	10.75	11.54	14.89	15.30	15.91
Co	112.19	175.44	155.76	129.25	127.00	142.26	110.64	117.71	158.19	127.02	172.29	160.71	162.33	151.21	151.09	158.84	153.80	156.22	144.80
V	50.21	100.60	2.89	118.16	176.54	57.92	82.39	108.02	63.66	113.84	31.98	21.36	17.55	40.08	34.14	21.00	34.54	21.82	41.00

Note: Averages are given to 3 decimal places merely for the purpose of establishing the best value of the second decimal. Major elements are in percentages; trace elements in ppm.

Table 8.1 (cont): Whole rock geochemical analyses from borehole NG2, recalculated LOI- and H_2O^--free and normalised to 100 %. A ratio of FeO/ Fe_2O_3=10 is assumed.

SAMPLE	39.35	42.55	50.20	65.25	80.35	83.75	122.30	134.10	143.35	152.30	200.50	212.20	219.90	228.75	236.86	238.90	326.86
SiO2	40.742	42.561	41.323	48.970	43.780	41.240	44.156	40.713	43.451	40.490	49.963	50.212	55.729	44.540	46.872	41.444	44.078
TiO2	0.081	0.038	0.064	0.061	0.055	0.040	0.094	0.049	0.060	0.035	0.087	0.089	0.133	0.084	0.071	0.098	0.102
Al2O3	1.846	2.300	2.318	1.514	2.035	2.303	1.850	2.589	2.022	2.087	2.412	2.575	2.652	2.928	3.774	2.446	2.250
Fe2O3	1.119	1.051	1.119	0.959	1.135	1.191	1.066	1.150	1.119	1.303	0.974	0.986	0.832	1.118	1.066	1.240	1.177
FeO	11.188	10.513	11.199	9.589	11.349	11.908	10.659	11.504	11.185	13.032	9.743	9.861	8.324	11.182	10.664	12.404	11.764
MnO	0.220	0.214	0.196	0.209	0.210	0.210	0.209	0.195	0.207	0.226	0.207	0.209	0.202	0.225	0.204	0.240	0.246
MgO	41.858	40.795	40.949	36.086	39.002	40.399	38.935	41.154	39.516	40.758	34.053	33.101	28.853	36.720	33.625	39.246	37.765
CaO	1.428	1.503	1.588	1.647	1.561	1.792	1.473	1.580	1.352	1.220	1.697	1.886	2.124	1.478	2.106	1.032	1.072
Na2O	0.246	0.364	0.313	0.125	0.221	0.316	0.224	0.478	0.360	0.163	0.305	0.432	0.494	0.301	0.492	0.084	0.060
K2O	0.128	0.000	0.000	0.000	0.000	0.000	0.072	0.000	0.000	0.038	0.000	0.000	0.132	0.000	0.000	0.102	0.000
P2O5	0.004	0.000	0.013	0.000	0.007	0.000	0.012	0.003	0.000	0.000	0.003	0.000	0.000	0.002	0.000	0.030	0.017
Cr2O3	0.915	0.444	0.687	0.673	0.423	0.355	0.739	0.315	0.455	0.367	0.385	0.430	0.432	1.197	0.925	1.319	1.204
NiO	0.226	0.217	0.231	0.166	0.221	0.245	0.211	0.269	0.273	0.280	0.171	0.220	0.093	0.226	0.200	0.316	0.267
LOI	0.000	0.000	0.000	0.000	0.000	0.000	0.000	0.000	0.000	0.000	0.000	0.000	0.000	0.000	0.000	0.000	0.000
H2O-	0.000	0.000	0.000	0.000	0.000	0.000	0.000	0.000	0.000	0.000	0.000	0.000	0.000	0.000	0.000	0.000	0.000
TOTAL	100.000	100.000	100.000	100.000	100.000	100.000	100.000	100.000	100.000	100.000	100.000	100.000	100.000	100.000	100.000	100.000	100.000
Rb	7.64	2.76	2.38	0.00	4.70	0.00	5.88	0.00	0.00	4.01	4.12	0.00	9.32	0.00	0.00	5.41	4.08
Sr	28.87	42.22	38.03	16.27	43.46	45.25	27.41	47.76	31.30	46.07	33.53	37.01	29.00	55.57	51.02	29.90	14.32
Y	3.17	0.00	0.00	0.00	2.55	2.50	2.45	2.99	2.48	0.00	2.30	3.30	4.95	0.00	0.00	3.13	2.51
Zr	18.12	2.93	5.13	0.00	6.62	4.04	7.88	0.00	3.01	3.07	5.47	4.44	13.85	3.72	2.98	14.05	6.77
Nb	0.00	0.00	0.00	0.00	0.00	0.00	0.00	0.00	0.00	0.00	0.00	0.00	0.00	0.00	0.00	0.00	0.00
Zn	65.56	66.12	64.62	76.19	73.05	68.35	68.65	90.49	68.03	74.77	62.35	65.01	61.24	72.85	61.64	69.96	64.41
Cu	19.40	10.43	21.71	11.22	15.60	16.04	32.51	26.53	20.10	14.25	22.86	28.76	17.62	15.88	32.04	38.07	12.97
Co	153.50	137.83	145.69	118.38	136.28	151.43	133.65	155.87	150.06	161.63	125.48	118.21	90.33	145.32	0.00	137.64	140.41
U	53.41	35.58	47.62	66.77	43.51	37.40	70.31	35.72	41.03	31.47	70.66	74.77	90.11	65.70	0.00	97.45	81.31

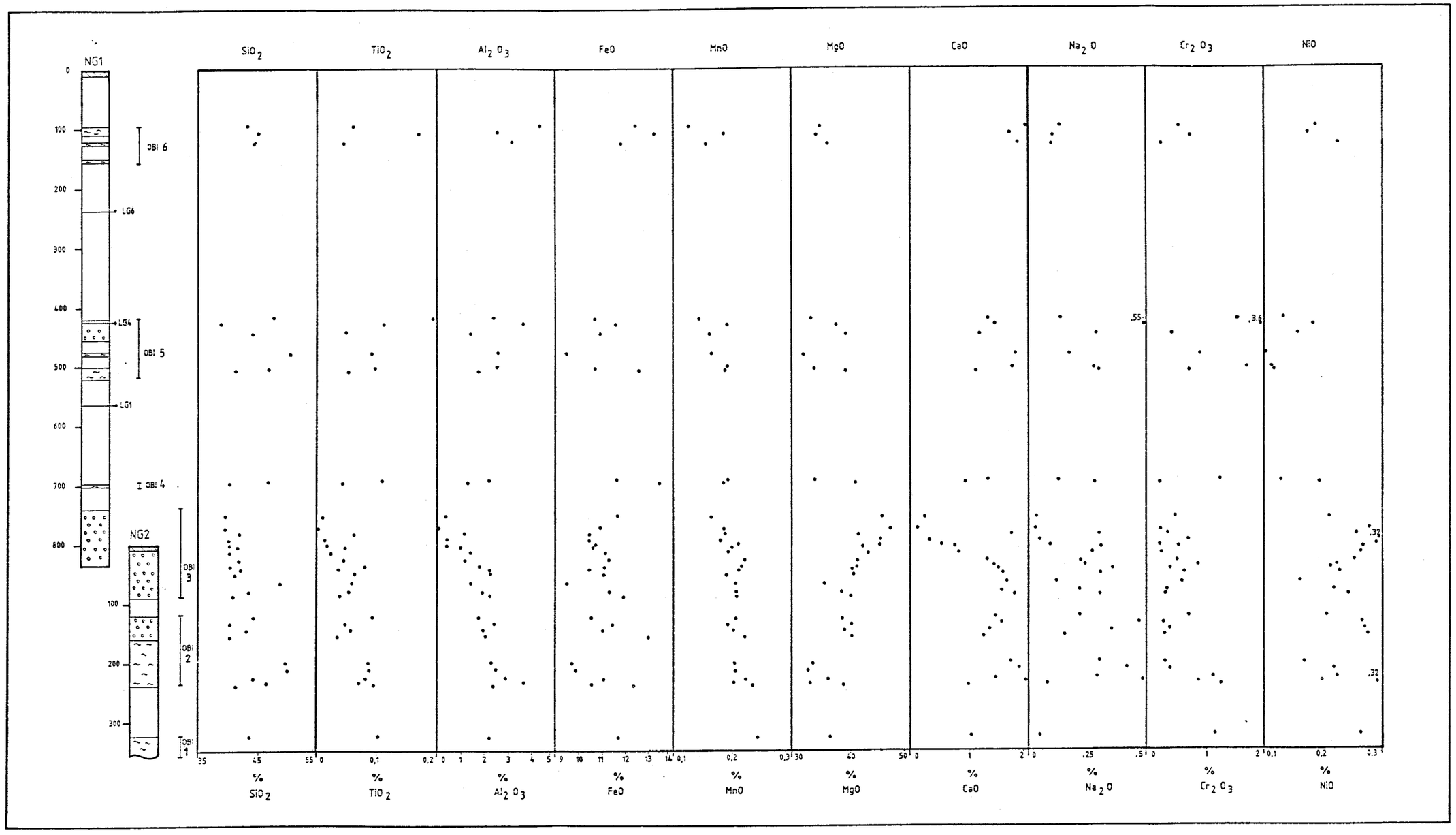

Figure 8.1: Plot of whole rock major element oxides in the olivine-rich cumulates of the NG boreholes. Ornamentation is the same as in Figures 6.3 and 6.4.

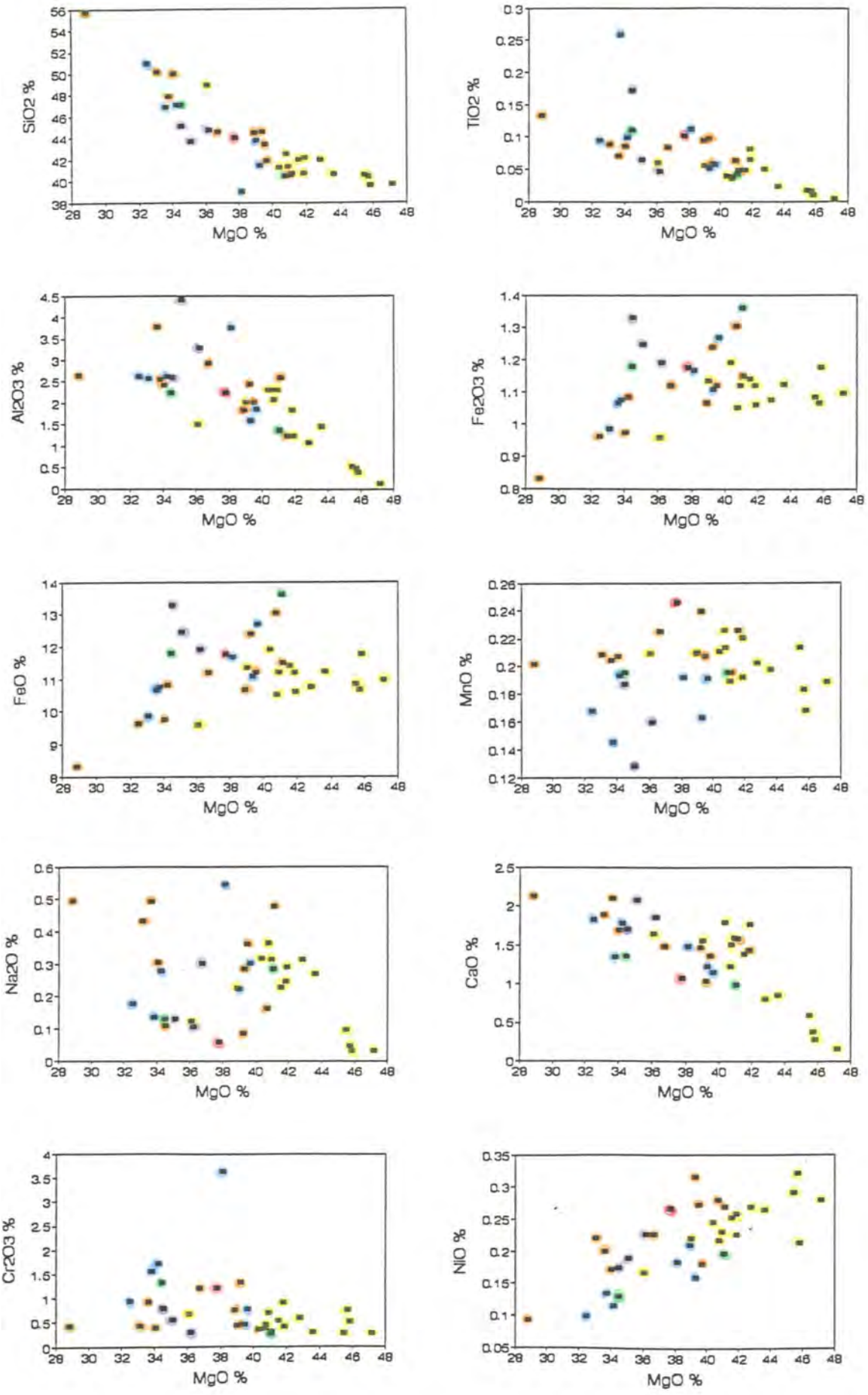

Figure 8.2: Plots of major element oxides against MgO. Purple = OBI6, blue = OBI5, green = OBI4, yellow = OBI3, orange = OBI2, red = OBI1.

the complex) . The weight percent of TiO_2 in the average compositions of these minerals is given in Table 8.2. The low concentration of TiO_2 in the first three minerals and the low volume of biotite in the rocks accounts for the low concentration of TiO_2 in the whole-rock analyses. In OBI3, OBI2 and OBI1 there is a steady decrease in TiO_2 with height (Figure 8.1), from a maximum of 0.102 wt% (NG2 326.86) to a minimum of 0.004 wt% (NG1 773.74).

Table 8.2: Weight percent of TiO_2 in the averaged analyses of chromite, clinopyroxene and orthopyroxene.

Mineral	Wt.%
Chromite	0.77
Clinopyroxene	0.26
Orthopyroxene	0.09
Biotite*	3.31

* Data from Teigler (1991)

There are reversals within this trend, however, with a distinct TiO_2 enrichment from the bottom to the top of OBI2, and in the lower part of OBI3 (at the top of NG2). This trend is not so obvious in other parts of the borehole, possibly because the units are too thin to reflect chemical changes. The variation of TiO_2 and MgO (Figure 8.2) follows a rough trend of increasing TiO_2 with decreasing MgO. There are two samples with unusually high TiO_2 values, NG1 108.33 and NG1 420.55; both contain a considerable amount of biotite (3.0 and 3.9 modal % respectively), which could account for their high TiO_2 values. The adcumulate harzburgite in OBI3 has the lowest TiO_2 concentration, because it has negligible quantities of clinopyroxene and biotite, and very fine, disseminated chromite.

8.2.3 Al_2O_3

The bulk of the Al_2O_3 present in the rock is attributable to plagioclase and chromite, with smaller proportions in clinopyroxene and orthopyroxene (Table 8.3).

Table 8.3: Weight percent of Al_2O_3 in the averaged analyses of plagioclase, chromite, clinopyroxene and orthopyroxene.

Mineral	Wt.%
Plagioclase	28.44
Chromite	15.85
Clinopyroxene	2.33
Orthopyroxene	1.29

There is a decrease in Al_2O_3 with stratigraphic height within OBI3 - OBI1 from a maximum of 3.77 wt.% (NG2 236.86) to a minimum of 0.12 wt.% (NG1 773.74) (Figure 8.1). Above these units, however, there seems to be an overall trend of Al_2O_3 enrichment with stratigraphic height, not reflected in individual units, but from unit to unit in NG1. The highest value of Al_2O_3 (4.40 wt.%) is from the sample highest in the sequence (NG1 95.5), a serpentinised mesocumulate dunite. There is a rough antipathetic correlation between Al_2O_3 and MgO, exhibiting increasing Al_2O_3 with decreasing MgO (Figure 8.2). In Figure 8.2 it can be seen that there is a decrease in Al_2O_3 from OBI6 to OBI5 (and OBI4) to part way down OBI3, where there begins an enrichment trend to the lower part of OBI3 and OBI2, then enrichment to OBI1. This is reflected in the distribution of other elements, such as SiO_2 and TiO_2, and the opposite trend is shown by MgO, and hence by the MMF ratio.

8.2.4 FeO

FeO is a major component of olivine, orthopyroxene, clinopyroxene and chromite; the amount of FeO in the averaged analyses of these minerals is given in Table 8.4.

Table 8.4: Weight percent of FeO in the averaged analyses of chromite, olivine, orthopyroxene and clinopyroxene.

Mineral	Wt.%
Chromite	22.45
Olivine	13.62
Orthopyroxene	9.11
Clinopyroxene	3.64

There is no overall pattern of FeO depletion or enrichment from the bottom to the top of the boreholes (Figure 8.1); the FeO content ranges between 9.59 wt.% (NG2 65.25) and 13.61 wt.% (NG1 699.45). There are, however, indications of cyclicity, but these are shown by trends of FeO depletion, which would not be expected from a normal fractionation event. Normally, during fractional crystallisation, the Mg-rich minerals are the first to form. This causes an increase in the Fe/Mg ratio in the residual liquid and results in relatively more Fe-enriched minerals crystallising at increasing stratigraphic height.

8.2.5 MnO

From the stratigraphically lowest sample (NG2 326.86) which has a MnO content of 0.25 wt.%, to the stratigraphically highest sample (NG1 95.5), which has 0.13 wt.% MnO, there is a steady overall decrease in MnO content. Within the olivine-bearing units there is a general trend of MnO depletion, this is well illustrated in the 8 samples at the base of NG1 (Figure 8.1) but there are also frequent reversals of MnO-enrichment. The binary diagram of MnO against MgO (Figure 8.2) shows a random scatter, from which no trends can be picked out, though the units seem to form their own distinct groups. This grouping is more on the basis of their MgO content, which separates OBI3 and OBI2 from OBI1, than on their MnO content.

8.2.6 MgO

The weight percentages of MgO in the averaged analyses of its four main host minerals in the dunites and harzburgites of NG1 and NG2 are presented in Table 8.5.

Table 8.5: Weight percent of MgO in the averaged analyses of olivine, orthopyroxene, clinopyroxene and chromite.

Mineral	Wt.%
Olivine	46.09
Orthopyroxene	31.53
Clinopyroxene	18.41
Chromite	8.02

The MgO content of the dunites and harzburgites ranges from 32.51 wt.% (NG1 480.60) to 47.17 wt.% (NG1 773.74), the highest MgO contents being in the more dunitic rocks. Plots of MgO against stratigraphic height (Figure 8.1) show trends of MgO depletion, within intervals rather than over the whole section, as well as frequent reversals.

8.2.7 CaO

CaO partitions into plagioclase, clinopyroxene and orthopyroxene. The level of CaO in olivine is trivial. Table 8.6 shows the CaO content of the averaged analyses of these minerals from NG1 and NG2.

Although the proportion of CaO in clinopyroxene and plagioclase is high, the absolute levels in the whole rock analyses are low, because these two minerals constitute a very minor part of the rock, only occurring as late-stage interstitial phases or oikocrysts.

Table 8.6: Weight percent of CaO in the averaged analyses of clinopyroxene, plagioclase, orthopyroxene and olivine.

Mineral	Wt.%
Clinopyroxene	20.07
Plagioclase	11.20
Orthopyroxene	1.22
Olivine	0.01

The CaO content in the olivine-bearing rocks shows fluctuating patterns of both CaO-enrichment and depletion with height (Figure 8.1). Sample NG1 773.74 has the lowest CaO content (0.16 wt.%) and NG2 238.86 the highest CaO content (2.11 wt.%). The lowest CaO contents occur in adcumulate dunites, where there is little intercumulus material. The variation of CaO with MgO (Figure 8.2) shows an approximately linear pattern, CaO increasing as MgO decreases. This pattern is also discernible within some of the individual units, namely OBI5 (and OBI4), OBI3, and to a lesser extent OBI1. OBI2 seems to indicate an opposing trend of increasing CaO with increasing MgO. From Figure 8.1 it is clear that CaO and Al_2O_3 do not vary in sympathy in all cases, and thus the control is

not entirely that exerted by intercumulus plagioclase.

8.2.8 Na_2O

Almost all the Na_2O in the rock is contained in plagioclase, with trace quantities in clinopyroxene and orthopyroxene. Na_2O values range from 0.03 wt.% (NG1 753.09) to 0.55 wt.% (NG1 430.55). The pattern of distribution of Na_2O with stratigraphic height (Figure 8.1) is erratic, though there is an overall decrease from OBI1 to OBI6. Similarly the plot of Na_2O against MgO (Figure 8.2) shows no trend.

8.2.9 Cr_2O_3

The amount of Cr_2O_3 in the rocks is attributable largely to the proportion of chromite present, but Cr_2O_3 occurs also in clinopyroxene and orthopyroxene (Table 8.7).

Table 8.7: Weight percent of Cr_2O_3 in the averaged analyses of chromite, clinopyroxene and orthopyroxene.

Mineral	Wt.%
Chromite	41.97
Clinopyroxene	0.99
Orthopyroxene	0.38

The lowest whole-rock Cr_2O_3 value is 0.27 wt.% (NG1 773.74), and the highest is 3.63 wt.% (NG1 430.55). The distribution of Cr_2O_3 appears to be entirely independent of the MgO content, because low values of Cr_2O_3 (> 0.5 wt.%) occur right across the spectrum of MgO values (Figure 8.2).

8.2.10 NiO

NiO is a minor component in the rock, comprising less than 0.4 wt.%; it partitions mainly into olivine, and to a lesser extent into chromite, orthopyroxene and clinopyroxene. There is a tendency towards depletion of NiO with height within the units (Figure 8.1),

except in the middle of OBI3, where there is a steady increase in NiO content. In the plot of NiO against MgO (Figure 8.2) the units are largely discrete, with a minor amount of overlap. Within each interval the higher NiO values correspond with the higher MgO values. The lowest NiO values occur in OBI5 and OBI4, particularly in the mesocumulate harzburgites.

8.2.11 Discussion of Major Element Chemistry

Due to the nature of the successions encountered in boreholes NG1 and NG2, sample spacing is uneven; it is spread out in NG1, and closely spaced in NG2. For ease of description and discussion, the rocks of this study have been grouped within six intervals, on the basis of their stratigraphic position. One of the units (OBI4) is very thin, and comprises only 2 samples. It has therefore been included in the unit above it (OBI5) in discussion, as the two units have a similar chemistry, although OBI4 is closer, stratigraphically, to OBI3.

A number of features have become evident from plots of the major element oxides:

Firstly, chemical trends both within individual intervals and between the intervals show signs of cyclicity, and indications of where new magma was mixed with the older residues. Secondly, when plotted against stratigraphic height, the samples from OBI2 appear to represent a separate cyclic unit, but when plotted on binary diagrams, their chemistry falls within the area demarcated by the OBI3 samples. Thirdly, an interesting feature, which shows up well in Figure 8.1, is the peaking of MgO and NiO values in the upper part of OBI3, with a decrease in values from this point towards the top and the bottom of the study section. This feature is also reflected by the SiO_2 and TiO_2 contents, and by the MMF ratio.

A comparison of the NiO and MgO contents of the whole rocks in the Critical and Lower Zones is illustrated in Figure 8.3. The samples from the lower Critical and Lower Zones have a higher MgO content, and a wider range of NiO content than do those from the upper

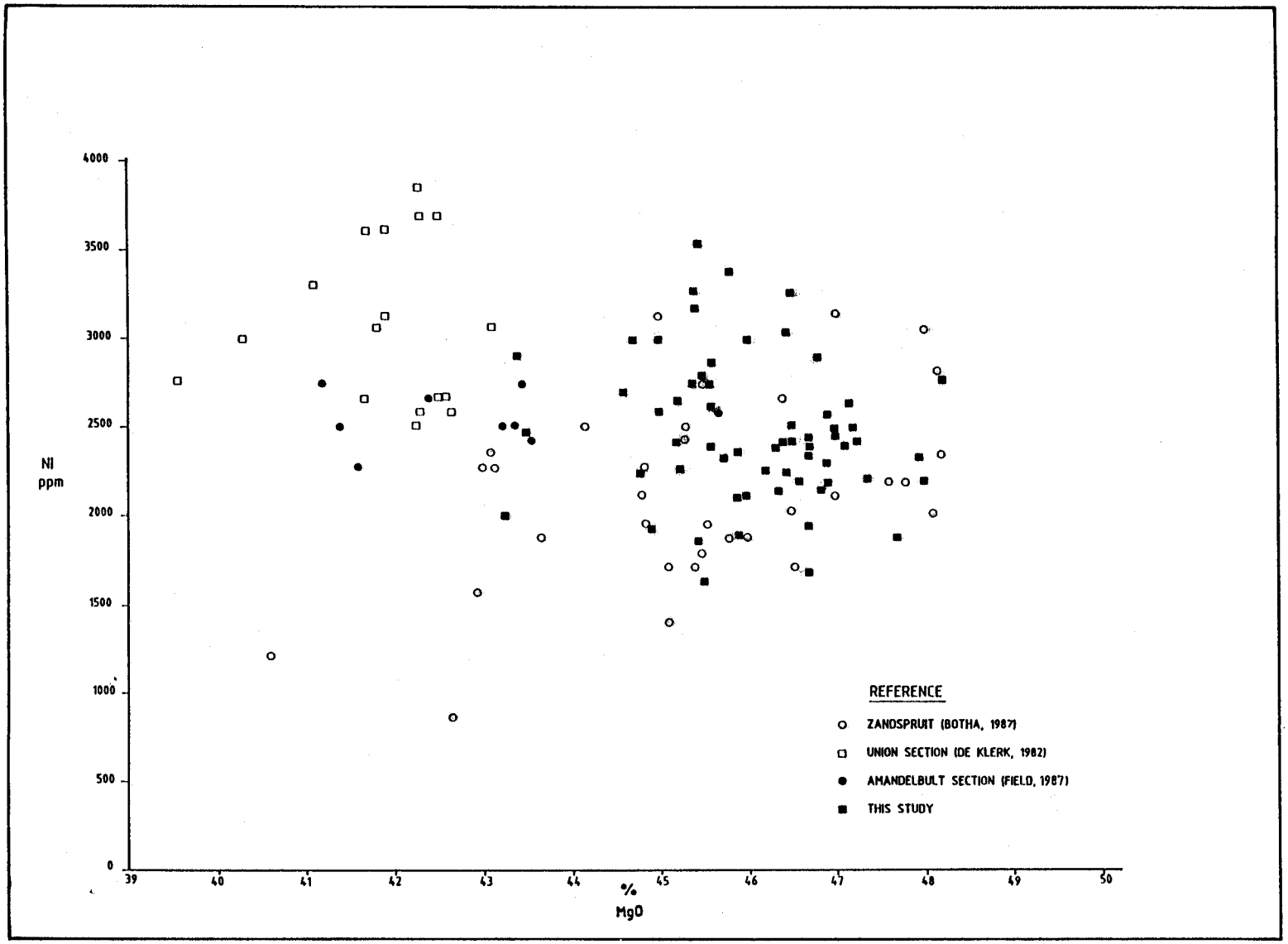

Figure 8.3: Plot of NiO against MgO (whole rock) in the Critical and Lower Zones in the Western Bushveld Complex. Yellow = upper Critical Zone and blue = lower Critical and Lower Zones.

Critical Zone.

8.3 TRACE ELEMENT CHEMISTRY

Normalised trace element data (modified by the factor used to calculate the major elements LOI and H_2O- free) are presented in Table 8.1, and the original data in Appendix 1. The data are presented graphically in Figure 8.4 (plots of the trace element concentrations against stratigraphic height) and in Figure 8.5 (binary diagrams of trace element concentrations against MgO content). Nb was analysed for, but all concentrations fell below the lower levels of determination, so Nb is not included in the data presentation.

8.3.1 Rubidium

Rubidium occurs in very low concentrations in the dunites and harzburgites, and in most the concentrations are below the lower levels of determination (detection limit); it is felt that the number of samples is too few for plots to be meaningful, so none is included here. Some samples, however, have relatively high values, e.g. NG1 420.75, which has a rubidium concentration of 17.3 ppm, the highest amongst the samples analysed. Rb occurs in trace amounts in plagioclase, orthopyroxene, clinopyroxene, olivine and mica. In the work of Griffin and Murthy (1969) the partition coefficient of Rb in plagioclase is given as 0.05, and that for olivine in the order of 0.026. Being an incompatible element, Rb concentrates in the residual liquid, and is usually taken in by late-crystallising plagioclase. Biotite also hosts a high proportion of Rb; the high Rb content in some of the rocks is attributed to the presence of late-stage biotite.

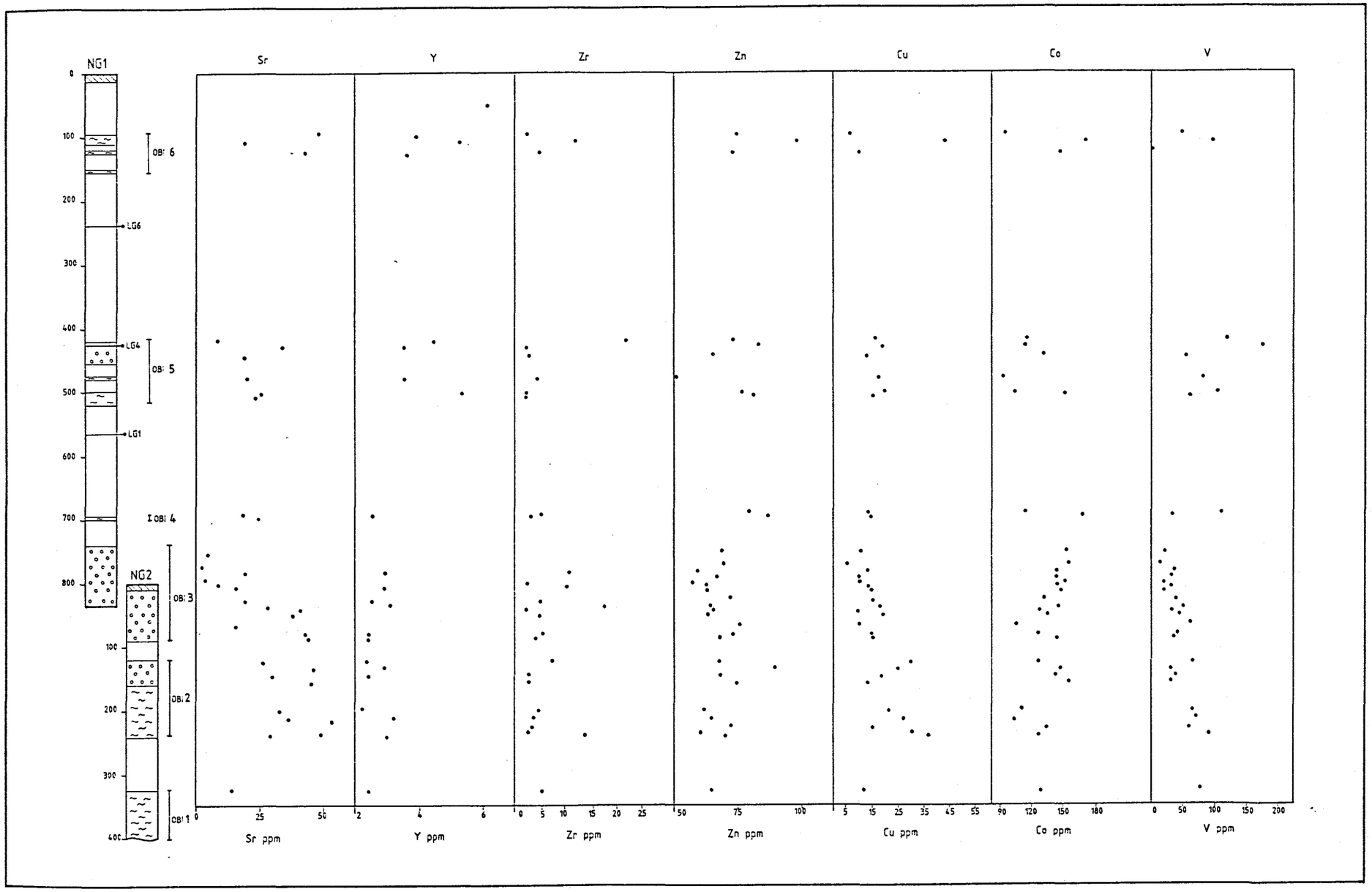

Figure 8.4: Plot of whole rock trace elements in the olivine-rich cumulates of the NG boreholes. Ornamentation is the same as in Figures 6.3 and 6.4.

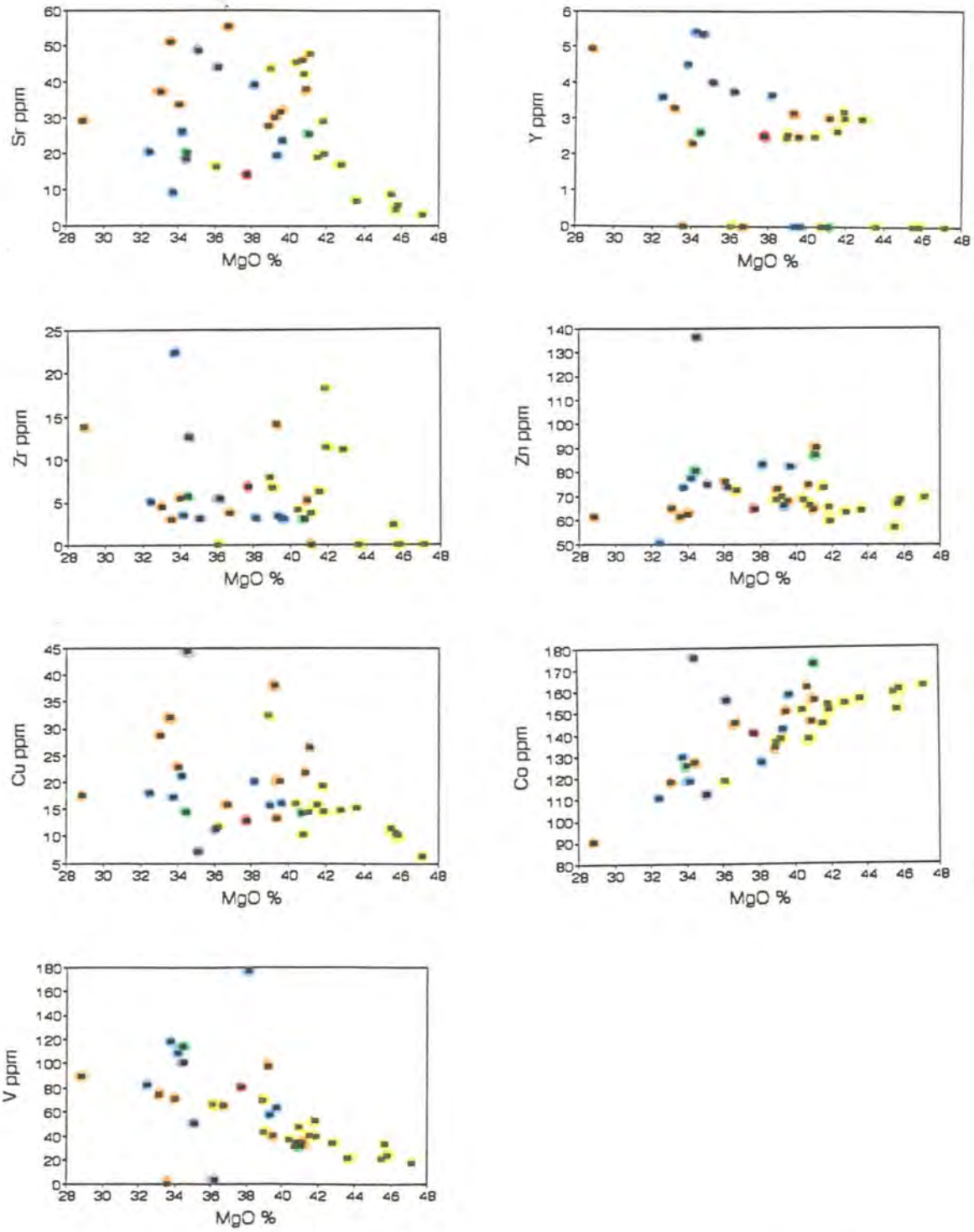

Figure 8.5: Plots of trace elements against MgO. Purple = OBI6, blue = OBI5, green = OBI4, yellow = OBI3, orange = OBI2, red = OBI1.

8.3.2 Strontium

Sr partitions primarily into plagioclase, and variations in whole-rock Sr content can be related to changes in modal plagioclase. The partition coefficient for Sr in Bushveld plagioclase has been found to be greater than unity (Mitchell, 1986), and that for clinopyroxene, orthopyroxene and olivine in general, to be lower by one, two and three orders of magnitude respectively (Griffin and Murthy, 1969). In Figure 8.4 the variation of Sr against stratigraphic height shows sporadic increases and decreases in Sr content. In the binary plot of Sr versus MgO (Figure 8.5), there is a linear trend in the samples from OBI3, Sr increasing with decreasing MgO. One sample (NG2 65.25), however, is an exception, it has a low Sr content and a low MgO content. This trend does not show up as well in other units; in OBI2 (4 samples) there seems to be a reverse trend of increasing Sr with increasing MgO, in the other units there is too much scatter to see a trend.

8.3.3 Yttrium

Thirteen of the samples analysed for Y showed concentrations below the detection limit (approximately 2 ppm). The sample analyses presented fall between 2 and 6 ppm. The partition coefficient of Y in clinopyroxene is 0.2 (Frey et al., 1978), in plagioclase less than 0.1 (Mitchell, 1986), and in orthopyroxene and olivine, 0.009 and 0.002 respectively (Frey et al., 1978). The implication of these partition coefficients is that with the exception of clinopyroxene, negligible amounts of Y occur in the minerals. Clinopyroxene occurs exclusively as an intercumulus mineral in the harzburgites and dunites, therefore the Y becomes concentrated in the residual liquid before being incorporated in the late-crystallising clinopyroxene phase. The variation of yttrium with stratigraphic height (Figure 8.4) shows a slight increase with increasing stratigraphic height. There is no systematic variation of Y with MgO (Figure 8.5). In OBI3, OBI2 and OBI1 the concentration of Y falls below 3.5 ppm, whereas in the upper two units (OBI6 and OBI5) values range between 3.5 and 5.5 ppm.

8.3.4 Zirconium

The partition coefficient of Zr in olivine and plagioclase was calculated by Pearce and Norry (1979) to be 0.01, that in orthopyroxene to be 0.03 and that in clinopyroxene to be 0.1. This indicates a similar pattern of incompatible behaviour to that of Y. Zirconium would concentrate in the residual liquid, and then partition into the late-crystallising clinopyroxene phase. Five of the samples analysed had Zr concentrations below the lower levels of determination (approximately 2 ppm); four of these samples are from OBI3 and one from OBI2. The majority of the samples have Zr values between 2 and 8 ppm, except for six samples which have values ranging between 10 and 23 ppm. There are no distinct trends discernible in the plot of Zr against stratigraphic height (Figure 8.4), neither do there seem to be any trends in Figure 8.5, in the variation of Zr with MgO.

8.3.5 Zinc

Partition coefficients of Zn in plagioclase, olivine and pyroxene (combined orthopyroxene and clinopyroxene) are given by Paster et al. (1974) to be 0.13, 1.8 and 0.49 respectively. This indicates a preference of Zn for olivine. The data do not, however, indicate any relationship between Zn and MgO. Zinc concentrations range between values of 50 and 90 ppm with a single sample (NG1 108.33) displaying an anomalously high Zn value of 140 ppm. There are indications of Zn depletion within individual cyclic units; this is well illustrated in the upper part of OBI3, OBI2 and OBI1 (Figure 8.4). The sampling interval in OBI6 and OBI5 results in no clear trend being apparent.

8.3.6 Copper

Paster et al. (1974) used Cu partition coefficients of 0.004 for plagioclase, 0.023 for olivine and 0.071 for the pyroxenes. These values indicate that Cu is incompatible with the silicate phases present. The work of Campbell (1977) implies that where Cu concentrations are greater than 10 ppm, sulphides must be present. Copper values in the author's sample suite range between 5 and 45

ppm, but no sulphide mineralisation has been recognised. There are enrichment and depletion trends throughout the study section. In OBI2 there is a regular trend of Cu enrichment and near the top of OBI3 there is a distinctive Cu depletion trend (Figure 8.4). The binary diagram (Figure 8.5) shows no general trend of variation, but concentrations from OBI2, OBI4 and OBI3 are restricted between 5 and 22 ppm, and those from OBI1 between 15 and 40 ppm, indicating a Cu depletion with increasing stratigraphic height. An exception is sample NG1 108.33 which contains nearly 45 ppm Cu.

8.3.7 Cobalt

A number of different values for partition coefficients for Co in silicate phases are available in the literature, but all have approximately the same value. Allegre et al. (1977) recommended values of 3.8 for olivine, 3.2 for orthopyroxene, 1.5 for clinopyroxene and 0.1 for plagioclase. Frey et al. (1978) preferred 6.5 - 1.3 for olivine, 2.0 for orthopyroxene and 1.2 for clinopyroxene. Paster et al. (1974) used 3.1 for olivine, 1.2 for the combined pyroxenes and 0.026 for plagioclase. Whichever values are used, there is a clear affinity of Co for olivine and orthopyroxene, which accounts for the high levels of this trace element in the rocks analysed. Cobalt concentrations vary between 110 and 180 ppm. Co plotted against stratigraphic height (Figure 8.4) indicates Co-enrichment at the top of OBI3, but Co-depletion in the lower part of OBI3, and in OBI2 and OBI1. The binary plot (Figure 8.5) shows a relationship of increasing Co with increasing MgO, hence reinforcing the statement regarding the preference of Co for olivine and orthopyroxene. An exception to the general trend is sample NG1 108.33, which has a very high Co value (176 ppm) for a fairly low MgO value (34.5 wt.%).

8.3.8 Vanadium

Partition coefficients for V are given by Frey et al. (op. cit.) as follows: 1.5 in clinopyroxene, 0.3 in orthopyroxene and 0.09 in olivine. All these coefficients are most certainly too low for the proportions of the minerals in these rocks to account for their high

V contents. Vanadium must, therefore, have a high partition coefficient in chromite, wherein most of the V must reside . This is borne out by sample NG1 430.55, which has a high modal percentage of chromite in the sample (13.5%), and the highest V content (177 ppm) of all the samples analysed. Measured vanadium concentrations range between 0 and 177 ppm. These two extreme values are anomalous, and fall to either side of the general field between 15 and 120 ppm. Variations with stratigraphic height (Figure 8.4) are erratic and show opposing trends of depletion and enrichment, as do most of the other elements. There is a depletion trend from the base of OBI1 to the top of OBI3, above which the concentrations increase and decrease irregularly. There is a trend of increasing V with depletion of MgO, which, when the highest and lowest V values are ignored, form a roughly linear field (Figure 8.4).

8.3.9 Discussion of Trace Element Chemistry

Chromium and nickel, which are usually treated as trace elements, have been included with the major elements, due to their compatibility with the main cumulate phases of the rocks of this study, in particular chromite and olivine. Other trace elements which show an affinity for the cumulus phases are Co, Zn and V. The plot of Co vs. MgO in Figure 8.4 clearly shows a positive relationship, reflecting the high partition coefficient for Co in olivine, but the same does not apply to the plot of Zn against MgO (Figure 8.5), where no trend is seen at all. The plot of V vs. MgO (Figure 8.5) shows a definite negative relationship, indicating the incompatibility of V with the dominant mafic silicates present, but its affinity for chromite, and, perhaps, intercumulus clinopyroxene.

The incompatible elements display a random relationship with MgO. These elements include Rb, Cu, Y and Zr. Sr behaves incompatibly with respect to the ferromagnesian silicates, but compatibly with respect to intercumulus plagioclase. The incompatible elements tend to be concentrated in the residual liquid, and then are taken up by late crystallising phases such as plagioclase (Rb, Sr, Y), clinopyroxene (Y, Zr), biotite (Rb,Y) or sulphides (Cu). The proportion of incompatible elements can therefore be directly

related to the amount of intercumulus minerals present, and hence the trace element data are strongly controlled by rock textures.

8.4 INTER-ELEMENT RATIOS

8.4.1 Introduction

Inter-element ratios largely eliminate the effects of modal variations, which, as mentioned in the previous section, have a strong influence on the absolute levels of elements present. The inter-element ratios discussed below are: Ni/Mg, Sr/Al_2O_3, Ni/Co and the MMF ratio (Mg/[Mg+Fe]). The ratios plotted against stratigraphic height are presented in Figure 8.6.

8.4.2 Ni/Mg

Nickel and magnesium both partition into olivine, orthopyroxene and to a lesser extent, clinopyroxene. In all three minerals Mg is a major component, and Ni a trace component which partitions preferentially into the minerals in the order given above. Ni is a compatible trace element with respect to Fe-Mg phases and will therefore tend to be more enriched in the early- formed minerals, rather than in the later ones. Hence the Ni/Mg ratio would be expected to decrease as olivine and then orthopyroxene crystallisation takes place. It should be borne in mind however that this ratio could be effected by other phases crystallising at the same time, and by small quantities of sulphides. The pattern of decreasing Ni/Mg with fractional crystallisation can be seen (Figure 8.6) in the lower olivine-bearing units (OBI2 and OBI1), and in the bottom three, and top four samples of OBI3; in the middle of the latter unit there is an increase in the Ni/Mg ratio. The units above show no discernible trend. The Ni/Mg ratios range between 0.0016 and 0.0043.

8.4.3 Sr/Al_2O_3

Most of the strontium in the rock is incorporated in plagioclase, with lesser amounts in clinopyroxene. Aluminum is distributed

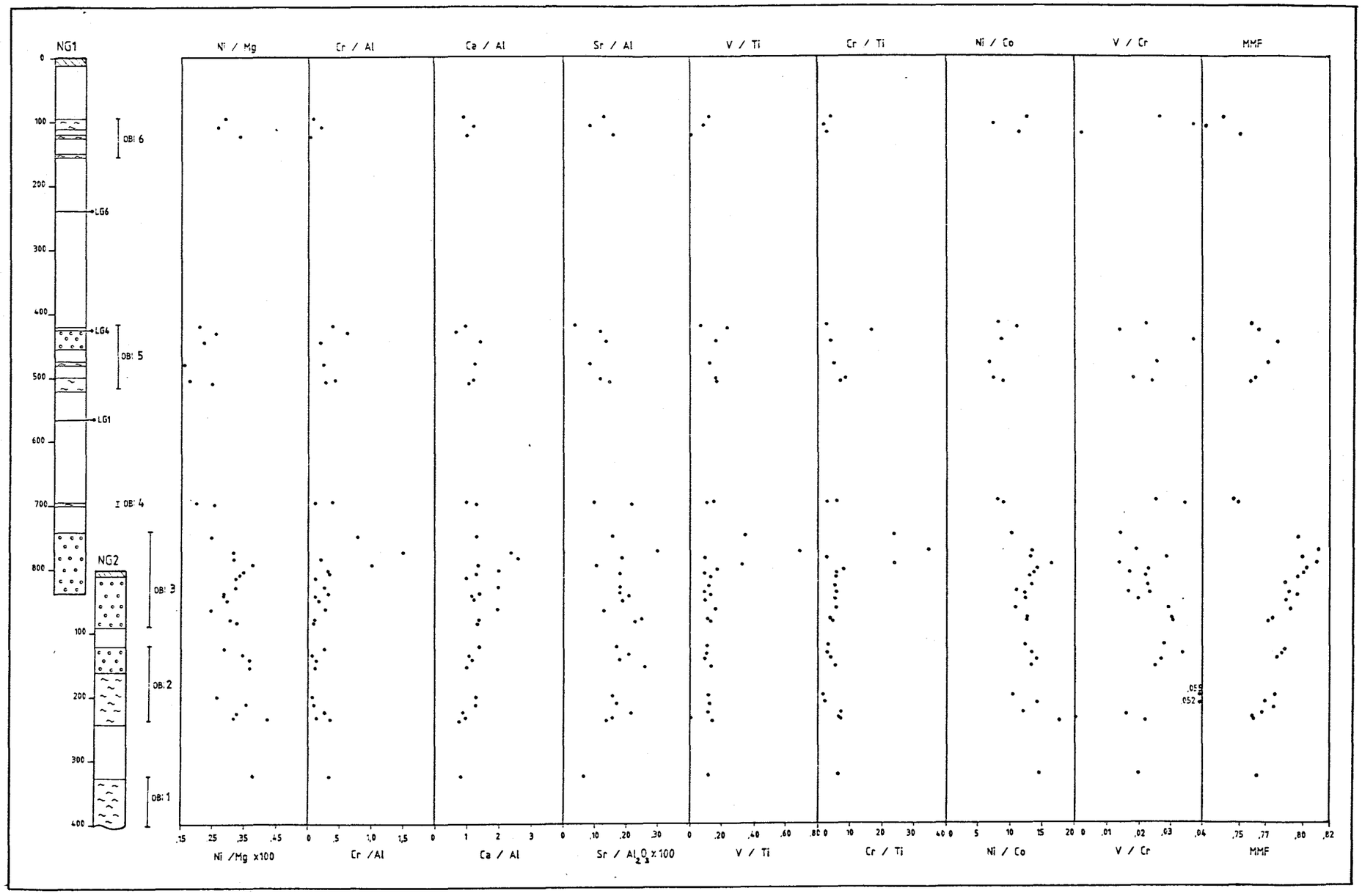

Figure 8.6: Plot of whole rock inter-element ratios in the olivine-rich cumulates of the NG boreholes. Ornamentation is the same as in Figures 6.3 and 6.4.

between intercumulus plagioclase and pyroxenes, and therefore Sr/Al_2O_3 ratios are of most value in rocks with high levels of feldspar. Where feldspar is a minor phase, ratios are erratic unless a correction is applied for Al in the pyroxenes (Eales, et al., 1986). The Sr/Al_2O_3 ratio, which is most useful in rocks where plagioclase is a cumulus phase, does not seem to be meaningful in the writer's suite of rocks where plagioclase is a minor intercumulus phase. The plot of Sr/Al against stratigraphic height (Figure 8.6) shows a fairly erratic distribution, with hints at cyclicity in OBI5 and OBI2. The scatter of points is attributed to the high proportion of Al_2O_3 in the orthopyroxenes, for which no correction factor has been applied here.

8.4.4 Ni/Co

The Ni/Co ratio plotted against stratigraphic height (Figure 8.6) seems to be a good indicator of cyclicity. Both Ni and Co partition into olivine, but Ni seems to be taken up in preference to Co, therefore, within a cyclic unit the ratio of Ni/Co should decrease towards the top of the unit. This can clearly be seen in the lower part of OBI5, the upper and lower parts of OBI3 (excluding the middle samples), and in OBI2 and OBI1.

8.4.5 Mg/(Mg+Fe)

The Mg/(Mg+Fe) (MMF) ratio is useful as a process indicator, because both Mg and Fe are major elements, along with SiO_2, in the mafic minerals which are the first to crystallise from a magma. As the Mg-rich end-members are normally earliest in the paragenesis, it is to be expected that the MMF ratio would decrease with increasing stratigraphic height as the residual liquid becomes progressively more Mg-poor. However, the MMF ratio plotted against stratigraphic height (Figure 8.6) shows clear trends of Fe-depletion (and hence Mg-enrichment) in all the olivine-bearing units. At the top of OBI4 and OBI3 there is an indication of Fe-enrichment (Mg-depletion); similarly, in the OBI5 the upper three samples (NG1 420.75, NG1 430.55 and NG1 445.45) show an Fe-enrichment trend. From the bottom to the top of NG1 there is an overall trend of Fe-enrichment.

8.4.6 Discussion of Inter-element Ratios

The inter-element ratios presented above have varying degrees of usefulness, in helping to understand the evolution of the sequence. One of the most striking features to emerge from the inter-element ratios is the discontinuity between the mineralogically and the chemically most primitive parts of the sequence as indicated by the MMF ratios. It is suggested by Eales et al. (1990) that the olivine-rich layers are not representative of sharp changes in the whole rock chemistry, but rather are the ultimate result of chemical changes which commenced while underlying pyroxenites were still crystallising. It seems that the Sr/Al_2O_3 ratio is of use only where plagioclase is a cumulus mineral; in the samples here it does not yield much information. Both Ni/Mg and Ni/Co indicate a certain amount of cyclicity in their behaviour, which is reflected with more clarity by the MMF ratio.

9. SUMMARY OF OBSERVATIONS

In this chapter features discussed in chapters 6, 7 and 8 are summarised.

9.1 TEXTURES

The textures of the dunites in the NG core range from adcumulate to mesocumulate, whereas the harzburgites and olivine-pyroxenites vary from adcumulate to mesocumulate to poikilitic (the term 'cumulate' is used in the descriptive sense only, and has no implied genetic connotation). Zoning was not detected in any of the cumulate phases; and no "way-up" textures in the rocks were found, such as might indicate settling processes.

The adcumulate dunites comprise olivine with ubiquitous cumulus chromite and minor intercumulus phases. Extreme adcumulate textures are, however, not pervasive. Mesocumulate dunites comprise cumulus olivine and chromite, with intercumulus orthopyroxene, plagioclase and, to a lesser extent, clinopyroxene and biotite.

The adcumulate harzburgites (harzburgites including olivine-pyroxenites) comprise cumulus olivine, orthopyroxene and chromite. The silicates display a classic foam texture. Intercumulus minerals include orthopyroxene, clinopyroxene and biotite, but are extremely rare. The mesocumulate harzburgites comprise the same minerals as the adcumulate harzburgites but include significant plagioclase as an intercumulus mineral as well. The intercumulus minerals occur in considerably larger proportions. Poikilitic harzburgites have the same mineralogy as the above, but are dominated by large orthopyroxene oikocrysts.

9.2 TRENDS WITHIN INDIVIDUAL MINERALS

9.2.1 Olivine

Olivine falls in the forsterite-fayalite solid solution series, having compositions of between $Fo_{80,9}$ and $Fo_{88,4}$. Some of the olivine

has been altered. Recognised alteration minerals are serpentinite, iddingsite, bowlingite and magnetite. The NiO content of olivine varies between 2100 and 4900 ppm, and shows an overall decrease with stratigraphic height; MnO (400 to 1900 ppm) displays a high degree of scatter, and no discernible trend with stratigraphic height.

9.2.2 Pyroxenes

Orthopyroxene is restricted to bronzitic compositions. Trends are not discernible in all intervals, but, an increase in Al_2O_3, Cr_2O_3, and FeO towards the top of OBI1 is accompanied by a concomitant decrease in SiO_2, TiO_2, and MgO. Clinopyroxene occurs as an intercumulus phase only, and is largely restricted to diopside compositions.

9.2.3 Chromite

Chromite compositions are comparable with those from the rest of the Critical Zone, and overlap to a small degree with chromite compositions from the Great Dyke. As in the case of orthopyroxene, chemical trends are not clear in all the intervals, but, there appears to be a general decrease in FeO content of chromite with stratigraphic height, mirrored by an increase in MgO. In OBI3 there is an increase in Al_2O_3 with stratigraphic height.

9.2.4 Plagioclase

Plagioclase occurs as a minor intercumulus mineral, but displays an unusually wide range of compositions. Most of the grains analysed fall within the labradorite field, but five are in the bytownite field and three in the andesine field. There is a reversal in the normal fractionation trend at the base of OBI4, where plagioclase becomes enriched in calcium and depleted in sodium with increasing height, whereas in OBI2 the normal fractionation trend is obvious.

9.3 WHOLE ROCK CHEMICAL TRENDS

The chemical trends indicated by whole rock chemical analyses show distinct cyclicity, which is clearer in some intervals than others. When plotted against stratigraphic height the samples from OBI2 are distinct from those of OBI3, but on the binary plots there is some overlap of data indicating a repetition of chemical trends.

A reversal in the chemical trend occurs at the top of OBI3 (close to the Lower Zone/lower Critical Zone boundary, this is best illustrated by MgO, NiO, SiO_2, TiO_2 and the MMF ratio. The plot of MMF ratios against stratigraphic height indicates that chemical changes were initiated at stratigraphically lower levels in the sequence than is indicated by changes in the lithology. The inter-element ratios Ni/Mg and Ni/Co both indicate cyclicity, reinforcing the MMF trend, but offer no new information. The Sr/Al_2O_3 ratio, which is of particular use where plagioclase is a cumulus mineral, which is not the case here, reflects some of the cyclicity illustrated by MMF and other ratios. This is illustrated in summarised form in Figure 9.1. There is no universal agreement between all the ratios presented in Figure 9.1 as to exactly where a reverse fractionation trend changes to a normal trend, and vice versa. This is regarded as being the result of the complexity of a system which does not behave in an ideal manner.

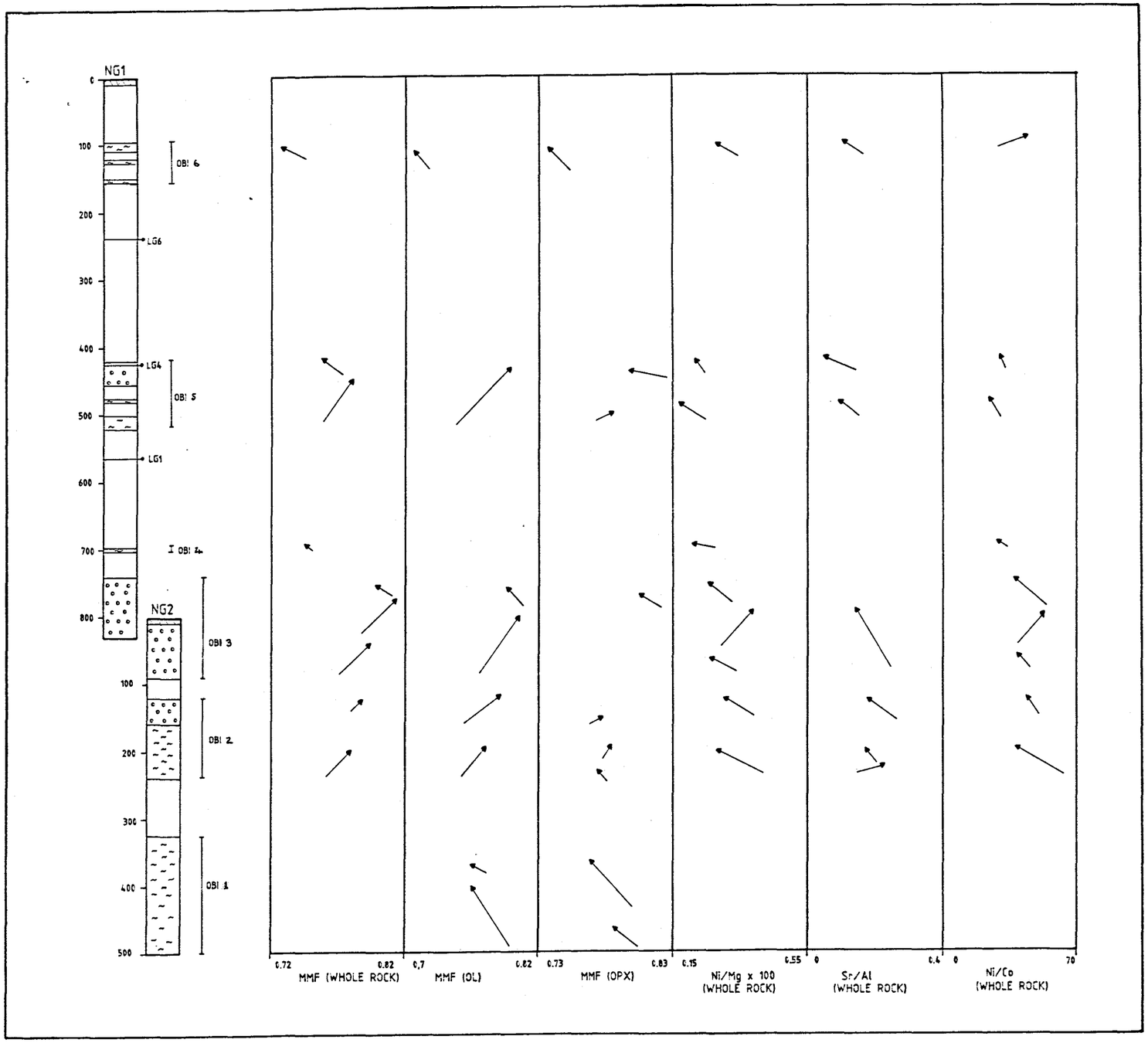

Figure 9.1: Summary diagram of trends of normal and reversed fractionation.
↖ normal; ↗ reversed.

10. CONCLUSIONS

The olivine-bearing rocks of the lower Critical and Lower Zones of the Bushveld Complex as intersected from NG1 and NG2 are dunites, harzburgites and olivine pyroxenites. They comprise cumulus olivine, and orthopyroxene with minor chromite, and intercumulus orthopyroxene, clinopyroxene and plagioclase. The NG rocks form part of a sequence of pyroxenites and harzburgites named the Ruighoek Pyroxenite, Tweelaagte Bronzitite and Groenfontein Harzburgite (SACS, 1980), and, as such, may be correlated with other intersections from both the eastern and western Bushveld Complex.

The textures of the rocks can be described as adcumulate, mesocumulate and poikilitic, bearing in mind that the terms are used in a descriptive sense and in no way imply acceptance of the cumulus theory of Wager and Brown (1968). The adcumulate and mesocumulate textures appear to be of primary origin, whereas some, but not all of the poikilitic textures seem to be of secondary origin. Frequently, indications of the original texture of the rock are preserved.

Whole rock and mineral chemical analyses have indicated cyclicity in the rock and mineral compositions. The fractionation patterns indicated by the MMF ratio is not always in agreement with that of the trace elements (Figure 9.1). In OBI1 the fractionation trend as indicated by the MMF ratios appears to be normal. That in OBI2 is mainly reversed. In OBI3 the trend is reversed throughout most of the interval, becoming normal towards the top section; OBI4 appears normally fractionated, but with so little data available for this interval, no great significance should attached to this finding. The fractionation trend of the MMF ratios in OBI5 is reversed at the base becoming normal towards the top, and that of OBI6 is normal.

The data collected in the course of this study is not enough on its own to provide the basis for a model for the crystallisation of this portion of the Bushveld Complex. It is enough, however, to provide the following constraints to which a model must adhere:

- the Lower Zone is dominated by olivine cumulates, with lesser pyroxenite cumulates,

- the lower Critical Zone is dominated by pyroxene cumulates, with lesser olivine cumulates, and chromitite layers,

- the textures of the olivine-bearing rocks are predominantly ad- and mesocumulate,

- there are indications of cyclicity within and between the olivine-bearing intervals (OBI's),

- whole rock MMF ratios generally increase through the Lower Zone, reaching a peak near the upper contact with the Critical Zone,

- in some intervals there is a reversed fractionation trend through most of the interval, then an abrupt change to a normal fractionation trend near the top,

- the mineralogically and chemically most primitive parts of the sequence do not always coincide.

Numerous models have been proposed to account for the formation of the Bushveld Complex. Comparisons between the Bushveld Complex and the Skaergaard and Kiglapait Complexes have been unfruitful, as the latter two show no evidence of repeated influxes of magma as is indicated by variations in the Sr_i from Bushveld cumulates (Eales el al., 1990). The theory that the cumulate pile crystallised from a single magma, has now been completely discounted; this then leads logically to the conclusion that numerous pulses of magma were required to form the Complex.

Cameron (1978) suggested that the Lower Zone was formed by a single magma, with pressure changes within the magma chamber causing the different fractionation trends, but this model has been questioned on the basis that the changes in pressure required would be too great to be generated under the conditions prevailing in the magma chamber. The idea that repeated influxes of magma occurred during

the formation of the lower Critical and Lower Zones was rejected by Cameron (1978, 1980) as he felt that this would require cumulates from each pulse to be of the same composition as the previous ones. He also expected that the bronzite would immediately form with higher enstatite values. As the data from this study and the more extensive data of Eales et al. (1990) show, the reversals are gradual rather than sharp, and can extend over hundreds of metres, which would suggest gradual mixing of the new and residual magmas, rather than the replacement of the old by the new as implied by Cameron (Eales et al., 1990).

The idea of double diffusive convection, whereby the magma chamber is "...density stratified into discrete layers. Exchange of both heat and chemical constituents will take place by diffusion across boundaries between layers, and layers will convect in response to differential buoyancy effects induced by this diffusion" (Naldrett et al., 1987) has been applied to the Bushveld Complex (Irvine et al., 1983). According to Irvine's model the layered sequence is formed by crystallisation from discrete layers of magma. Convection within the layers of magma maintains homogeneity, and as magma fractionates and the residual liquid becomes less dense, the residual magma could rise up and mix with the magma in the layer above it. According to this model the individual layers of magma will crystallise in an inwards direction. The direction should thus be recorded in the composition of the cumulates, and in their changing composition in the direction of their growth. The extent of the cumulate layer's variation in composition inwards and with stratigraphic height will depend on the degree of slope upon which it is crystallising. The steeper the slope, the greater the degree of change in the inward direction. Naldrett et al. (1987) point out that "any particular igneous facies within a given layer will have a limited development laterally in the direction towards the centre of the intrusion. This is to say that any particular layer... will not extend right across the intrusion, but will undergo a facies change to a different mineralogical composition." There is, however, a large degree of lateral continuity, over hundreds of kilometres across the Bushveld Complex, which casts the ideas of Irvine et al. (1983) into doubt.

Tait and Kerr (1987) reported on some experiments carried out on crystallisation and compositional convection in a porous medium, and on convection of interstitial liquid caused by magma chamber replenishment. They found that dense melt emplaced above a porous cumulus pile can sink into the pore spaces and replace the less dense residual magma. Convective exchange occurs in the form of fingers of the denser liquid penetrating the lighter one. The experimental results suggest that "exchange may proceed at rates of metres to tens of metres per year in mafic to ultramafic magma chambers" (Tait and Kerr, 1987). This conclusion is more dependent on cumulus pile porosity than on magma velocity. The porosity of the crystalline pile appears to be of primary importance because if the pore spaces are small and/or restricted, a crystalline cap can form at the top of the crystalline pile (as occurred in one of Tait and Kerr's experiments) effectively blocking exchange of fluids above the crystalline pile with interstitial fluids. The latter event is likely to give rise to orthocumulates; a system where free exchange of fluids is possible will be likely to result in adcumulates being formed.

Following a study of the chromitite layers, it was proposed by Campbell and Turner (1986) that the portion below the LG6, and in particular the chromitite layers, were formed by repeated mixing of U-type magmas with residual liquids derived from previous magmas, and the LG6 and the portion above it, particularly the chromitite layers, were formed by mixing A-type magmas with residual liquids. But Teigler (1990) in his study of the whole NG sequence and other along strike sections showed that the cumulates of the NG sequence were derived from U-type magmas and their derivatives only.

This then leaves the question of the manner in which the new magma entered the chamber. Three different forms for the magma entering the chamber have been suggested:

- as a plume (Barnes and Naldrett, 1986)
- as a fountain (Campbell and Turner, 1989)
- as a basal layer between the supernatant liquid and the crystal mush (Huppert and Sparks, 1980, Huppert and Turner, 1981)

The densities, temperatures and velocities of the residual and new magmas and the velocity at which the new magma enters the chamber will all have an influence on the form of the influx. The density of the residual liquid is largely dependent on the phases and volumes thereof which have crystallised from it. Generally for U-type magmas this means that the residual liquid will be less dense (mafic phases having crystallised, leaving the residue relatively more felsic), cooler and more evolved than a new pulse of magma would be. This effectively rules out the plume model of Barnes and Naldrett (1986), because pluming of the new magma would require it to be less dense than the residual magma. The basal flow as opposed to fountain model is more difficult to resolve, as it is likely that the basal flow is the final stage of a fountaining influx after it has lost its momentum and has gained its density equilibrium within the chamber. The writer is in agreement with Teigler (1990) who stated that "it seems unlikely that the filling of a magma chamber, especially one as large as the BIC, was wholly achieved by the rather passive style of basal flows."

The model proposed by Teigler (1990) for the lower Critical and Lower Zones was based on the replenishment of the crystallising magma chamber by fountains of new magma which subsequently developed into basal flows. His model was developed as follows:

After the development of the Marginal Zone, once stable physical and chemical conditions had been established, repeated influxes of U-type magmas into the chamber gave rise to the olivine-dominated sequences at the base of the NG section. Cyclic units formed comprising successive thin packages of dunite, poikilitic harzburgite, granular harzburgite, olivine pyroxenite and minor pyroxenite. The bulk composition of the magma became progressively more primitive in Teigler's segment 1 (Figure 10.1). He suggested that this was caused by progressive melting of the mantle source. There was a short period where the rate of replenishment ceased, and normal fractionation was the dominant trend (segment 2, Figure 10.1). The episode terminated with the formation of pyroxenites at a depth of 1570 m in the NG sequence. New pulses of magma then caused the bulk composition to move to more primitive values

(segment 3), and formed cyclic units similar to those in segment 1. At a depth of about 1550 m the rejuvenation ceased and normal fractionation became dominant again. The fractionation trend moved the bulk composition of the magma into the orthopyroxene field; as a result the main rock type to crystallise was pyroxenite. Fractionation continued to the extent that orthopyroxene in this segment (segment 4) attained the lowest MMF value in the Lower Zone. As a result of the extensive fractional crystallisation, the residual liquid became progressively more enriched in the plagioclase component which resulted in the formation of a leuconorite at about 1340 m. Teigler (1990) emphasised that this cumulus feldspar package overlies the thickest sequence of pyroxenites in the Lower Zone.

The disappearance of cumulus feldspar at the top of the leuconorite coincides with a reversal in the fractionation trend caused by further tapping of the primitive magma (Teigler, 1990) (segment 5). At the beginning the reversal did not cause major crystallisation of olivine. This occurred only at a depth of 1280m. The dunites that formed at the top of this cycle are the most primitive of the cumulate silicates in the NG sequence (top of OBI3, of this study). In segment 5 two pyroxenite packages with normal fractionation trends are associated with periods of reduced magmatic activity. The nature of the replenishing magma changed slightly during the formation of segment 5. It remained a U-type magma, but was relatively more enriched in Cr than the previous magmas had been. This magma gave rise to the formation of a minor chromitite layer at about 1200 m in the NG sequence, and to higher modal proportions of chromite in the olivine-bearing lithologies. As the magmatic activity waned fractional crystallisation again took place (segment 6), and orthopyroxene came back onto the liquidus, forming a monotonous sequence of pyroxenites. The continued orthopyroxene crystallisation enriched the residual liquid in plagioclase components.

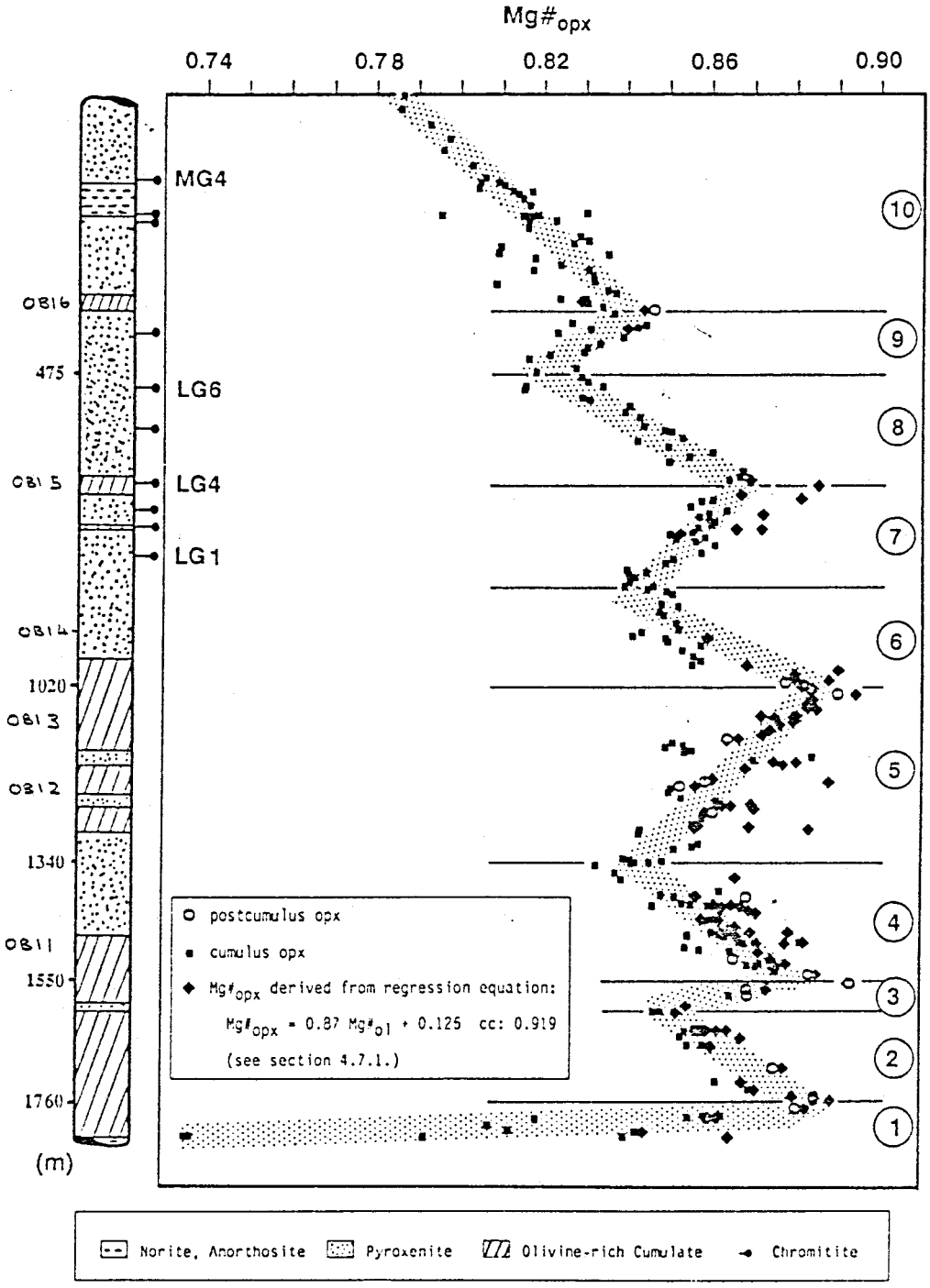

Figure 10.1: Variations of $Mg\#_{opx}$ (MMF of orthopyroxene) through the NG sequence, showing the segments referred to in the model of Teigler (1990). After Teigler (1990).

The evolution of the cumulate pile changed at the Lower Zone-lower Critical Zone boundary. In the Lower Zone the major process was the rejuvenation of the crystallising liquid by new inputs of primitive magma. This led to a generally reversed fractionation trend, where normal fractional crystallisation occurred for limited periods when magmatic activity slowed down and/or ceased. The Critical Zone, however, was dominated by fractional crystallisation, with only two episodes of rejuvenation (segments 7 and 9).

Just below the LG1 Chromitite Layer, at the top of segment 6, new magma entered the chamber, causing the fourth major reversal of the NG sequence and the first major reversal of the lower Critical Zone. When replenishment stopped the pyroxenites of segment 8 formed. Due to the limited degree of rejuvenation in the segment below, the fractional crystallisation process soon changed the composition of the crystallising liquid to a composition more evolved than that prior to the previous reversal event. At 475m the final major reversal occurred as a result of influxes of primitive magma. Again, olivine did not begin to crystallise immediately. Pyroxenes with progressively increasing MMF ratios formed until the composition of the crystallising fluid intersected the primary olivine field. The period of magma influxes was short, and fractional crystallisation again took over, continuing to the lower Critical Zone-upper Critical Zone boundary.

Teigler (1990) termed the major reversals in the lower Critical Zone megacyclic units, and pointed out that minor reversals occurred within them. The minor reversals are thought to be responsible for most of the massive chromitite layers, whereby the Cr-rich primitive magma mixed with residual liquid. The bulk composition fell within the chromite stability field and chromitite layers formed. The exceptions are the LG2, LG3 and LG4 Chromitite Layers which show the most primitive compositions.

Eales et al. (1988) proposed a model whereby primitive cumulates represent proximal facies to a feeder zone from which primitive liquids periodically enter the crystallising magma. Their study was carried out on upper Critical Zone rocks at Union Section, and they

concluded that this was very close to or at the feeder. Teigler (1990) supported this model for the lower Critical Zone as well, noting that the supply of fresh magma would be greatest near the feeder zone, and with distance from the feeder the volume of primitive liquid would decrease.

Some of the olivine-bearing intervals (OBIs) of this study do not coincide with the general trend of either normal or reversed fractionation of Teigler's megacyclic units. Rather, they represent minor reversals (small cycles) within the megacyclic units as noted by Teigler (1990), which in this case is illustrated by changes in olivine compositions over a relatively small distance.

Teigler's (1990) model for the formation of the lower Critical and Lower Zones of the eastern Bushveld Complex, as intersected in the NG boreholes meets all the requirements of the constraints imposed by this study.

REFERENCES

Allegre, C.L., Treuil, M., Minster, J-F., Minster, B. and Albarede, F. (1977) Systematic use of trace element in igneous process. Part I: Fractional crystallisation processes in volcanic suites. Contributions to Mineralogy and Petrology, **60**, 57-57.

Barnes, S.J. and Naldrett, A.J. (1985) Geochemistry of the J-M (Howland) Reef of the Stillwater Complex, Minneapolis Adit area. I: Sulphide chemistry and sulphide-olivine equilibrium. Economic Geology, **80**, 627-645.

Barnes, S.J. and Naldrett, A.J. (1986) Geochemistry of the J-M (Howland) Reef of the Stillwater Complex, Minneapolis Adit area. II: Silicate mineral chemistry and petrogenesis. Journal of Petrology, **27**, 791-825.

Barrett, D.M., Jacobsen, J.B.E., McCarthy, T.S. and Cawthorn, R.G. (1978). The structure of the Bushveld Complex south of Potgietersrus as revealed by a gravity survey. Geological Society of South Africa Transactions, **81**, 271-276.

Botha, M.J. (1987). Petrology and geochemistry of the lower group chromitites and host rocks on the farm Zandspruit 168 JP, western Bushveld Complex. MSc. Thesis, Rhodes University (unpubl.), 216pp.

Bowen, N.L. and Shairer, J.F. (1935). The system MgO-FeO-SiO_2. American Journal of Science, **37**, 487-500.

Buchanan, D.L. (1975). The petrography of the Bushveld Complex intersected by boreholes in the Bethal area. Transactions of the Geological Society of South Africa, **78**, 335-348.

Cameron, E.N. (1970). Composition of certain co-existing phases in the eastern part of the Bushveld Complex. Geological Society of South Africa, **Special Publication No. 1**, 46-58.

Cameron, E.N. (1977). Chromite in the central sector of the eastern Bushveld Complex, South Africa. American Mineralogist, **62**, 1082-1096.

Cameron, E.N. (1978). The Lower Zone of the eastern Bushveld Complex in the Olifants River Trough. Journal of Petrology, **19**, 437-462.

Cameron, E.N. (1980). Evolution of the lower Critical Zone, central sector, eastern Bushveld Complex and its chromite deposits. Economic Geology, **75**, 845-871.

Cameron, E.N. and Desborough, G.A. (1969). Occurrence and characteristics of chromite deposits, eastern Bushveld Complex. Economic Geology Monograph 4, 23-40.

Cameron, M. and Papike, J.J. (1980). Crystal chemistry of silicate pyroxenes : In: Prewitt C.T. (ed.) Reviews in Mineralogy Volume 7: Pyroxenes, Mineralogical Society of America, 5-87.

Campbell, I.H. (1977). A study of Macro-Rhythmic layering and cumulative processes in the Jimberlana Intrusion, Western Australia. Part I: the Upper Layered Series. Journal of Petrology, **18**, 183-215.

Campbell, I.H. and Turner, J.S. (1986). The role of convection in the formation of platinum and chromitite deposits in layered intrusions. In: Scarfe, C.M. (ed.) Silicate Melts: their Properties and Structure Applied to Problems in Geochemistry, Petrology, Economic Geology and Planetary Geology. Short Course Handbook, Mineralogical Association of Canada, Edmonton, 236-278.

Campbell. I.H. and Turner, J.S. (1989). Fountains in magma chambers. Journal of Petrology, **30**, 825-923.

Clubley-Armstrong, A.R. (1977). The geology of the Selousriver area, north of Middelburg, Transvaal, with special reference to the structure of the regions of the Dennilton Dome. Msc. Thesis, University of Pretoria, (unpubl.).

Coertze, F.J. (1962). The Rustenburg fault as a controlling factor of ore deposition south-west of Pilanesberg. Geological Society of South Africa Transactions, **65**, 253-257.

Coertze, F.J. (1974). The geology of the basic portion of the western Bushveld Igneous Complex. South African Geological Survey Bulletin, **38**, 48pp.

Coleman, R.G. (1977). Ophiolites. Springer-Verlag, Berlin, Germany,

Cox, K.G., Bell, J.D. and Pankhurst, R.J. (1979). The Interpretation of Igneous Rocks. George Allen and Unwin Ltd, London, 450 pp.

Daly, R.A. (1928). The Bushveld Igneous Complex of the Transvaal. Bulletin of the Geological Society of America, **39**, 703-768.

Davies, G. and Tredoux, M. (1985). The platinum-group element and gold contents of the Marginal rocks and sills of the Bushveld Complex. Economic Geology, **80**, 838-848.

De Bruiyn, H. and Rhodes, R.C. (1975). A new variety of Bushveld Granite in the Dennilton area, Transvaal. Geological Society of South Africa Transactions, **78**, 89-95.

Deer, W.A., Howie, R.A. and Zussman, J. (1966). An introduction to the rock forming minerals. Longman Group Limited, England, (thirteenth impression, 1982), 528 pp.

Deer, W.A., Howie, R.A. and Zussman, J. (1982). Rock forming minerals, Volume 1A, Orthosilicates. Longman Group Limited, Essex England., Second Edition, 3-336.

De Klerk, W.J. (1982). The geology, geochemistry and silicate mineralogy of the upper Critical Zone of the north western Bushveld Complex, at Rustenburg Platinum Mines, Union Section. MSc. Thesis, Rhodes University (unpubl.), 210pp.

De Villiers, J.S. (1970). The structure and petrology of the mafic rocks of the Bushveld Complex south of Potgietersrust. Geological Society of South Africa Special Publication, **No. 1**, 23-25.

De Waal, S.A. (1972). The Bushveld granites in the Zaaiplaats area. Geological Society of South Africa Transactions, **75**, 135-147.

Dunham, A.C. and Wadsworth, W.J. (1978). Cryptic variation in the Rhum layered intrusion. Mineralogical Magasine, **42**, 347-356.

Eales, H.V., de Klerk, W.J. and Teigler, B. (1990). Evidence for magma mixing processes within the Critical and Lower Zones of the northwestern Bushveld Complex, South Africa. Chemical Geology, **88**, 261-278.

Eales, H.V., Field, M., de Klerk, W.J. and Scoon, R.N. (1988). Chemical variation and thermal erosion in the upper Critical Zone, western Bushveld Complex. Mineralogical Magasine, **52**, 63-79.

Eales, H.V. and Marsh, J.S. (1983). Al/Cr ratios of coexisting pyroxenes and spinellids in some ultramafic rocks. Chemical Geology, **38**, 57-74.

Eales, H.V., Marsh, J.S., Mitchell, A.A., De Klerk, W.J., Kruger, F.J. and Field, M. (1986). Some geochemical constraints upon models for the crystallisation of the upper Critical Zone-Main Zone interval, northwestern Bushveld Complex. Mineralogical Magasine, **50**, 567-582.

Eales, H.V. and Reynolds, I.M. (1986). Cryptic variations within chromites of the upper Critical Zone, northwestern Bushveld Complex. Economic Geology, **81**, 1056-1066.

Faithfull, J.W. (1985). The lower Eastern Layered Series of Rhum. Geological Magasine, **122**, 459-468.

Field, M. (1987). The petrology and geochemistry of the upper Critical Zone of the Bushveld Complex at Amandelbult Section of Rustenburg Platinum Mines Limited, northwestern Transvaal, South Africa : MSc. Thesis , Rhodes University (unpubl.), 129 pp.

Frick, C. (1973). The 'Sill Phase' and the 'Chill Zone' of the Bushveld Igneous Complex. Geological Society of South Africa Transactions, **76**, 7-14.

Frey, F.A., Green, D.H. and Roy, S.D. (1978). Integrated models of basalt petrogenesis: a study of quartz tholeiites to olivine melilites from south eastern Australia using geochemical and experimental data. Journal of Petrology, **19**, 463-513.

Friedman, G.M. (1958). Determination of sieve-size distribution from thin section data for sedimentary petrological studies. Journal of Geology, **66**, 394-416.

Gain, S.B. (1980). The geology and PGE distribution in the upper chromite layers at Maandagshoek 254KT, eastern Bushveld Complex. University of Pretoria Institute for geological Research on the Bushveld Complex, **Research Report**, 22-24.

Griffin, W.L. and Murthy, V.R. (1969). Distribution of K, Rb, Sr and Ba in some minerals relevent to basalt genesis.Geochimica et Cosmochimica Acta, **33**, 1389-1414.

Hall, A.L. (1932). The Bushveld Igneous Complex of the central Transvaal. Geological Survey of South Africa Memoirs, **28**, 560pp.

Hamer, R.E. and Sharpe, M.R. (1985). Field relations and strontium isotope systematics of the Marginal rocks of the eastern Bushveld Complex. Economic Geology, **80**, 813-837.

Hattingh, P.J. (1986). The palaeomagnetism of the Main Zone of the Bushveld Complex. Tectonophysics, **124**, 271-295.

Hatton, C.J. (1984). The effect of pressure, temperature and composition on the distribution of Fe and Mg between olivine, orthopyroxene and liquid; an appraisal of the reversal in the normal fractionation trend in the Bushveld Complex. Contributions to Mineralogy and Petrology, **86**, 45-53.

Hatton, C.J. and von Gruenewaldt, G. (1985). Chromite from the Zwartkop Chrome mine - an estimate of the effects of subsolidus re-equilibration. Economic Geology, **80**, 911-924.

Hatton, C.J. and Von Gruenewaldt, G. (1987). The geological setting and petrogenesis of the Bushveld chromitite layers. In: Stowe, C.W. (ed) Evolution of the Chromium Ore Fields. Von Nostrand Reinhold Co., 109-143.

Hess, H.H. (1960). Stillwater Igneous Complex, Montana: A quantitative mineralogical study. Geological Society of America, **Memoir 8**,148 pp.

Himmelberg, G.R. and Loney, R.A. (1980). Petrology of ultramafic and gabbroic rocks of the Canyon Mountain Ophiolite, Oregon. American Journal of Science, **280-A**, 232-368.

Hulbert, L.J. (1983). A petrological investigation of the Rustenburg Layered Suite and associated mineralisation south of Potgietersrus. DSc. Thesis, University of Pretoria (unpubl.), 511pp.

Hulbert, L.J. and Von Gruenewaldt, G. (1986). The structure and petrology of the upper and lower chromitite layers on the farms Grasvally and Zoetveld, south of Potgietersrus. In: Anhausser C.R. and Maske S. (eds.) Mineral Deposits of Southern Africa, Volume II; Geological Society of South Africa Johannesburg, 1237-1240.

Huntington, H.D. (1979). Kiglapait Mineralogy I: Apatite, biotite and volatiles. Journal of Petrology, **20**, 625-652.

Huppert, H.E. and Sparks, R.S.J. (1980). The fluid dynamics of a basaltic magma chamber replenished by influx of hot,dense ultrabasic magma. Contributions to Mineralogy and Petrology, **75**, 279-289.

Huppert, H.E. and Turner, J.S. (1981). A laboratory model of a replenished magma chamber. Earth and Planetary Science Letters, **54**, 144-152.

Ianello, P. (1976). The Bushveld granites around Rooiberg, Transvaal, South Africa. Geologische Rundschau, **60**, 630-655.

Irvine, T.N. (1963). Origin of the ultramafic complex at Duke Island, south eastern Alaska. Mineralogical Society of America Special Paper, **1**, 36-45.

Irvine, T.N. (1967). The Duke Island Ultramafic Complex, southeastern Alaska. In. Wyllie P.J. (ed.) Ultramafic and Related rocks, John Wiley and Sons New York, 84-97.

Irvine, T.N. (1980a). Magmatic infiltration metasomatism, double-diffusive fractional crystallisation, and adcumulus growth in the Muskox Intrusion and other layered intrusions. In: Hargraves R.B. (ed.). Physics of Magmatic Processes. Princeton University Press. Princeton, Ch. 8, 325-383.

Irvine, T.N. (1980b). Magmatic density currents and cumulus processes. American Journal of Science, **280-A**, 1-58.

Irvine, T.N. (1982). Terminology for layered intrusions. Journal of Petrology, **23**, 127-162.

Irvine, T.N. Keith, D.W. and Todd, S.G. (1983). The J-M platinum-palladium Reef of the Stillwater Complex, Montana: II. Origin by double-diffusive convective magma mixing and implications for the Bushveld Complex. Economic Geology, **78**, 1287-1334.

Jackson, E.D. (1967). Ultramafic cumulates in the Stillwater, Great Dyke and Bushveld intrusions. In: Wyllie P.J. (ed.) Ultramafic and Related Rocks, John Wiley and Sons, New York, 20-38.

Jackson, E. D. (1970). The cyclic unit in layered intrusions - a comparison of repetitive stratigraphy in the ultramafic parts of the Stillwater, Muskox, Great Dyke and Bushveld Complexes. Geological Society of South Africa, **Special Publication No. 1**, 391-424.

Kruger, F.J. (1983). The petrology of the Merensky cyclic unit and associated rocks, and their significance in the evolution of the western Bushveld Complex. PhD. Thesis, Rhodes University (unpubl.), 123pp.

Kuschke, O.H. (1950). Granitic rocks of the Bushveld, northwest of Brits. MSc. Thesis (unpubl.), University of Pretoria.

Lee, C.A. and Sharpe, M.R. (1986). The structural setting of the Bushveld Complex - an assessment aided by Landsat imagery. In: Anhausser C.R. and Maske S. (eds.) Mineral Deposits of Southern Africa, Volume II; Geological Society of South Africa Johannesburg, 1031-1038.

Le Maitre, R.W. (Ed.), Bateman, P., Dudek, A., Keller, J., Lameyre, J., Le Bas, M.J., Sabine, P.A., Schmid, R., Sorensen, H., Streckeinsen, A., Woolley, A.R. and Zanettin, B. (1989). A Classification of Igneous Rocks and Glossary of Terms: Recommendations of the International union of Geological Sciences Subcommission on the Systematics of Igneous Rocks. Blackwell Scientific Publications, Oxford, 193 pp.

Lenthall, D.H. (1973). A proposed nomenclature system for the granophyres associated with the Bushveld Complex. Geological Society of South Africa Transactions, **76**, 75-76.

Lenthall, D.H. and Hunter, D.R. (1977). The geochemistry of the Bushveld granites in the Potgietersrus tin-field. Precambrian Research, **5**, 359-400.

Lightfoot, P.C., Naldrett, A.J. and Hawkesworth, C.J. (1984). The geology and geochemistry of the Waterfall Gorge section of the Insizwa Complex with particular reference to the origin of the nickel sulphide deposits. Economic Geology, **79**, 1857-1879.

McCallum, I.S., Raedeke, L.D. and Mathez, E.A. (1980). Investigations of the Stillwater Complex: Part I. Stratigraphy and structure of the Banded Zone. American Journal of Science, **280-A**, 59-87.

McDonald, J.A. (1967). Evolution of part of the lower Critical Zone, Farm Ruighoek, western Bushveld. Journal of Petrology, **8**, 165-209.

Mitchell, A.A. (1986). The petrology, mineralogy and geochemistry of the Main Zone of the Bushveld Complex at Rustenburg Platinum Mines, Union Section. PhD. Thesis , Rhodes University (unpubl.), 104 pp.

Morse, S.A. (1979). Kiglapait Geochemistry II: Petrography. Journal of Petrology, **20**, 591-624.

Morse, S.A. (1980). Basalts and phase diagrams. Springer-Verlag, 493 pp.

Morse, S.A. (1986). Convection in aid of adcumulus growth. Journal of Petrology, **27**, 1183-1214.

Naldrett, A.J., Cameron, G., von Gruenewaldt, G. and Sharpe, M.R. (1987). The formation of stratiform PGE deposits in layered intrusions. In: Parsons, I. (ed.), Origins of Igneous Layering. D. Reidel Publishing Company, 313-397.

Nel, H.J. (1940). The basal rocks of the Bushveld Igneous Complex north of Pretoria. Geological Society of South Africa Transactions, **43**, 37-68.

Nicholson, S.W. and Lipin, B.R. (1984) Guide to the Gish Mine area. In: Czamanske G.K. and Zientek M.L. (eds.), The Stillwater Complex Montana: geology and guide. Montana Bureau of Mines and Geology Special Publication, **92**, 358-367.

Osborn, E.F. (1980). On the cause of the reversal of the normal fractionation trend - an addendum to the paper by E.N.Cameron "Evolution of the lower Critical Zone, central sector, eastern Bushveld Complex and its chromite deposits.". Economic Geology, **75**, 872-875.

Page, N.J., Shimek, R. and Huffman, C. (1972). Grain size variations within an olivine cumulate, Stillwater Complex, Montana. United States Geological Survey Professional Paper, **800-C**, C29-C37.

Paster, T.P., Schauwecker, D.S. and Haskin, L.A. (1974). The behaviour of some trace elements during solidification of the Skaergaard layered series. Geochimica et Cosmochimica Acta, **38**, 1549-1577.

Pearce, J.A. and Norry, M.J. (1979). Petrogenetic implications of Ti, Zr, Y and Nb variations in volcanic rocks. Contributions to Mineralogy and Petrology, **69**, 33-47.

Prendergast, M.D. (1987). The chromite ore field of the Great Dyke, Zimbabwe. In: Stowe, C.W. (Ed.), Evolution of Chromium Ore Fields, Von Nostrand Reinhold Company Inc., 89-108.

Ragan, D.M. (1967). The Twin Sisters Dunite, Washington. In: Wyllie P.J. (ed.) Ultramafic and Related Rocks, John Wiley and Sons New York.

Reichhardt, F.J. and Hatton, C.J. (1991). Post-cumulus processes in the lower Critical Zone, eastern Bushveld Complex, South Africa. Institute for Geological Research on the Bushveld Complex , Research report **93** , 19pp.

Reynolds, I.M. (1985). The nature and origin of titaniferous magnetite rich layers in the Upper Zone of the Bushveld Complex: a review and synthesis. Economic Geology, **80**, 1089-1108.

Rhodes, R.C. (1975). Bushveld granophyre in the Stavoren tin district, Transvaal. Geological Society of South Africa Transactions, **78**, 71-74.

Rhodes, R.C. and Du Plessis, M.D. (1976). Notes on some stratigraphic relations in the Rooiberg Felsite. Geological Society of South Africa Transactions, **79**, 183-185.

Schwellnus, J.S.I., Engelbrecht, L.N.J., Coertze, F.J., Russell, M.D., Malherbe, S.J., van Rooyen, D.P. and Cooke, R. (1962). The geology of the Olifants River area, Transvaal; explanation sheets 2429B (Chuniespoort) and 2430A (Wolkberg). Geological Survey of South Africa, 87 pp.

Scoon, R.N. (1985). Discordant bodies of post-cumulus, ultramafic rock in the upper Critical Zone of the Bushveld Complex: iron rich ultramafic pegmatite bodies at Amandelbult and the Driekop platiniferous ultramafic pipe. PhD Thesis, Rhodes University (unpubl.), 265pp.

Scoon, R.N. and de Klerk, W.J. (1987). The relationship of olivine cumulates and mineralisation to cyclic units in part of the upper Critical Zone of the western Bushveld Complex. Canadian Mineralogist, **25**, 51-77.

Sharpe, M.R. (1986). Bushveld Complex - Excursion Guide book, Geocongress '86. Geological Society of South Africa, Marshalltown, 143 pp.

Sharpe, M. and Chadwick, B. (1982). Structures in the Transvaal Sequence rocks within and adjacent to the eastern Bushveld Complex. Transactions of the. Geological Society of South Africa, **85**, 29-41.

South African Committee for Stratigraphy (SACS) (1980). Stratigraphy of South Africa. Part 1 (Comp. L.E.Kent) Lithostratigraphy of the Republic of South Africa, South West Africa/Namibia and the republics of Bophuthatswana, Transkei and Venda. Handbook of the Geological Survey of South Africa, **No. 8.**

Sparks, R.S.J., Huppert, H.E, Kerr, R.C., McKenzie, D.P. and Tait, S.R. (1985) Postcumulus processes in layered intrusions. Geological Magasine, **122**, 555-568.

Strauss, C.A. and Truter, F.C. (1944). The Bushveld granites in the Zaaiplaats tin mining area. Transactions of the Geological Society of South Africa, **47**, 47-77.

Tait, S.R., Huppert, H.E. and Sparks, R.S.J. (1984). The role of compositional convection in the formation of adcumulate rocks. Lithos, **17**, 139-146.

Tait, S.R. and Kerr, R.C. (1987). Experimental modelling of interstitial melt convection in cumulus piles. In: Parsons, I. (ed.) Origins of Igneous Layering. D. Reidel Publishing Company, 569-587.

Tankard, A.J., Jackson, M.P.A., Eriksson, K.A., Hobday, D.K., Hunter, D.R. and Minter, W.E.L. (1982). Crustal Evolution of South Africa - 3.8 billion years of earth history. Springer-Verlag, New York, 175-199.

Teigler, B. (1990). Platinum Group Element distribution in the Lower and Middle Group chromitites in the western Bushveld Complex. Mineralogy and Petrology, **42**, 165-179.

Teigler, B. (1991). Mineralogy, petrology and geochemistry of the Lower and lower Critical Zones, northwestern Bushveld Complex. PhD Thesis , Rhodes University (unpubl.), 247 pp.

Textoris, D.A. (1971). Grain-size measurement in thin section. In: Carver R.E. (ed.), Procedures in Sedimentary Petrology. John Wiley and Sons. USA, Ch. 5, 95-107.

Van Der Merwe, M.J. (1976). The layered sequence of the Potgietersrus limb of the Bushveld Complex. Economic Geology, **71**, 1337-1351.

Vermaak, C.F. (1976). The Merensky Reef - thoughts on its enviroment and genesis. Economic Geology, **71**, 1270-1298.

Viljoen, M.J. and Scoon, R.N. (1985). The distribution and main geologic features of discordant bodies of iron-rich ultramafic pegmatite in the Bushveld Complex : Economic Geology, **80**, 1109-1128.

Von Gruenewaldt, G. (1968). The Rooiberg Felsite north of Middelburg, and its relation to the layered sequence of the Bushveld Complex. Geological Society of South Africa Transactions, **71**, 153-172.

Von Gruenewaldt, G. (1973). The Main and Upper Zones of the Bushveld Complex in the Roossenekal area, eastern Transvaal. Geological Society of South Africa Transactions, **76**, 207-227.

Von Gruenewaldt, G. and Worst, B.G. (1986). Chromite deposits at Zwartklip Chrome Mine, western Bushveld Complex. In: Anhaeusser, C.R. and Maske, S. (eds), Mineral Deposits of South Africa, Volume II. Geological Society of South Africa, 1217-1227.

Wager, L.R. and Brown, G.M. (1968). Layered Igneous Rocks. Oliver and Boyd, London, 588p.

Wager, L.R., Brown, G.M. and Wadsworth, W.J. (1960). Types of igneous cumulates. Journal of Petrology, **1**, 73-85.

Walraven, F. (1976). Notes on the late stage history of the western Bushveld Complex. Geological Society of South Africa Transactions, **79**, 13-21.

Walraven, F. and Darracott, B.W. (1976). Quantitative interpretation of a gravity profile across the western Bushveld Complex. Transactions of the Geological Society of South Africa, **79**, 22-26.

Willemse, J. (1959). The "floor" of the Bushveld Igneous Complex and its relationships, with special reference to the eastern Transvaal. Geological Society of South Africa Transactions and Proceedings, **62**, xxi-lxxx.

Wilson, A.H. (1982). The geology of the Great 'Dyke', Zimbabwe: the ultramafic rocks. Journal of Petrology, **23**, 240-292.

Wilson, A.H. and Tredoux, M. (1990). Lateral and vertical distribution of the platinum-group elements in the P1 pyroxenite layer of the Darwendale Subchamber of the Great Dyke of Zimbabwe, and petrogenetic controls on the sulphide mineralisation. Economic Geology, **85**, 556-584.

Zientek, M.L., Czamanske, G.K. and Irvine, T.N. (1985). Stratigraphy and nomenclature for the Stillwater Complex. In: Czamanske G.K. and Zientek M.L. (eds.), The Stillwater Complex Montana: geology and guide. Montana Bureau of Mines and Geology Special Publication, **92**, 21-32.

APPENDIX I

Descriptive Logs of boreholes NG1 and NG2

LOG OF NG1

Logged By : H V Eales
W J de Klerk
R N Scoon
B Teigler
S Haikney

Depth in metres	Petrographic Description
0,00 - 2,00	Overburden : black turf soil.
2,00 - 3,50	Fragmented and weathered pyroxenite.
3,50 - 6,15	Fresher pyroxenite, finer grained; pyroxenite with disseminated chromite stringers (5,20 - 5,90); probably some core loss.
6,15 - 6,50	Chromitite layer (ca. 40% dissemination); more massive towards the base.
6,50 - 7,00	Caliche (weathering mainly magnesite with sporadic, pyroxenitic sandy layers.
8,05 - 16,10	Medium grained pyroxenite, partially weathered; chromite disseminations (9,40 - 9,50; wispy stringers); numerous small fractures with associated alteration.
16,10 - 55,90	Fresh medium to fine grained pyroxenite; thin chromitite lenses at 20,90, 29,80, 40,15 and 46,20; igneous lamination occurs from 54,80 - 55,90; pyroxenite is more medium grained and feldspathic towards the base.
55,90 - 65,19	Medium to coarse grained pyroxenite with large intercumulus plagioclase crystals (up to 3cm in diameter); no igneous lamination; much more feldspathic than the pyroxenite above. Isolated chromitite lenses at 56,55, 56,70, 56,85, 57,12, 57,35 and 58,30; sporadic occurrence of large clinopyroxene oikocrysts; from 61,71 onwards pyroxenite is finer grained.
65,19 - 89,95	Medium to fine grained pyroxenite; thin chromitite blebs occur at 71,46 and 78,50; at 82,10 - 82,75 and 84,85 - 85,20 chromite disseminations (10-20%).
89,95 - 90,30	Pyroxenite with layers of heavy dissemination of chromite.
90,30 - 90,70	Medium to coarse grained pyroxenite.
90,70 - 91,42	Pyroxenite with heavy dissemination of chromite in layers and a massive chromitite (3 cm) at the base; dip ca. 20°.
91,42 - 92,02	Core loss associated with a serpentinised shear zone.
92,02 - 95,00	Medium grained pyroxenite.
95,00 - 95,85	Harzburgite interlayered with pyroxenite; harzburgite layers range from only a few mm to 45 cm in thickness; sharp basal contacts.
95,85 - 100,50	Massive pyroxenite with sporadic olivine and rather abundant phlogopite; at 96,75 thin chromitite lens in somewhat coarser pyroxenite; a layer of harzburgite occurs between 99,50 and 99,76; from 100,00 the pyroxenite is finer grained.
100,50 - 100,80	Harzburgite.
100,80 - 108,26	Medium to coarse grained pyroxenite with phlogopite.
108,26 - 108,76	Harzburgite, serpentinised.
108,76 - 122,61	Coarse grained pyroxenite with sporadic olivine; thin lenses of chromitite at 114,36 (3 mm) and 118,54 (1 cm); harzburgite layer (25 cm) at 118,70.
122,61 - 122,98	Highly feldspathic harzburgite.
122,98 - 152,51	Coarse grained pyroxenite with igneous lamination.
152,51 - 152,54	Massive chromitite layer (LG7-chromitite); dipping at ca. 15°.
152,54 - 159,40	Medium to coarse grained pyroxenite with ca. 5 cm of harzburgite at 155,00; chromitite lens at 159,32.
159,40 - 160,25	Pyroxenite with 15-20% disseminated chromite at 159,85 and 160,25.
160,25 - 242,18	Medium to fine grained massive pyroxenite; chromitite lenses at 162,78, 163,27, 173,39, 174,15 and 174,95.
242,18 - 242,24	Pyroxenite with disseminated chromite layers dipping at ca. 20°.
242,24 - 242,42	Massive chromitite layer (LG6A-chromitite).
242,42 - 242,74	Pyroxenite with disseminated chromite.

242,74 - 255,46	Medium grained pyroxenite with a probable increase in grain size.
255,46 - 255,91	Pyroxenite with disseminated chromite.
255,91 - 256,95	Massive chromitite layer (LG6-chromitite); base of chromitite dips at ca25°.
256,95 - 351,16	Medium to coarse grained pyroxenite; thin chromitite lens at 301,08.
331,16 - 331,71	Massive chromitite layers (LG5-chromitite) interlayered with pyroxenite; basal part of chromitite displays abundant orthopyroxene oikocrysts.
331,71 - 332,02	Pyroxenite.
332,02 - 332,34	Massive chromitite layer with orthopyroxene oikocrysts towards the base; underlying 0.5 cm of pyroxenite is highly altered.
332,34 - 332,70	Pyroxenite, highly altered; chromitite layer (1 cm) at 332,70.
332,70 - 417,10	Medium grained pyroxenite; chromitite lens (0.5 cm) at 337,20.
417,10 - 418,20	Pyroxenite grading into a harzburgite.
418,20 - 420,82	Olivine pyroxenite grading into harzburgite at the base.
420,82 - 421,36	Pyroxenite with olivine coming in at 421,20 to harzburgite.
421,36 - 425,24	Olivine pyroxenite grading into harzburgite and dunite at 422,50.
425,24 - 425,34	Pyroxenite with a basal chromitite layer (1-2 cm).
425,34 - 429,43	Dunite with abundant large (3-5 cm) oikocrysts of orthopyroxene; at 428.00 chromitiferous dunite over 20 cm.
429,43 - 429,70	Chromitite layer with olivine (LG4-chromitite).
429,70 - 434,90	Dunite with a heavy dissemination of chromite; gradation into chromitite at base.
434,90 - 452,06	Dunite with minor disseminations of chromite; chromite stringer at 435,75.
452,06 - 452,52	Pyroxenite, partly feldspathic.
452,52 - 452,63	Massive chromitite layer.
452,63 - 475,02	Medium grained pyroxenite; chromitite lamina (2 mm) at 474,40.
475,02 - 475,51	Massive chromitite with abundant orthopyroxene oikocrysts and pyroxenite partings (LG3-chromitite).
475,51 - 481,25	Medium to coarse grained pyroxenite with disseminated chromite; olivine-rich lamina (ca. 5 mm thick) occur from 480.45-480.70.
481,25 - 481,32	Chromitite layer.
481,32 - 496,35	Medium to coarse grained pyroxenite with a chromite dissemination; chromitiferous pyroxenite at the base (25 cm).
496,35 - 496,43	Massive chromitite layer; dip ca. 25°.
496,43 - 505,64	Medium to coarse grained pyroxenite; thin layers of dunite (1-2 mm) at 498,10 - 498,25.
505,64 - 506,50	Dunite with disseminated chromite.
506,50 - 506,70	Chromitite layer (LG2B-chromitite); very friable with abundant orthopyroxene oikocrysts.
506,70 - 512,72	Dunite and harzburgite layers with thin pyroxenite interlayers.
512,72 - 513,20	Medium to coarse grained pyroxenite.
513,20 - 515,00	Harzburgite and dunite.
515,00 - 523,98	Harzburgite and dunite layers (1 cm thick) alternating with pyroxenite; thin chromitite layer at 517,25; dipping at 20°.
523,98 - 524,18	Massive chromitite layer (LG2A-chromitite).
524,18 - 559,92	Coarse to medium grained pyroxenite; chromitite lenses occur at 525,96, 526,41 and 535,91; pyroxenite is chromitiferous between 533,00 to 534,50; chromitite layer (1,5 cm) at 546,90; basal part with heavy chromite dissemination.
559,92 - 560,28	Massive chromitite layer (LG1-chromitite).
560,28 - 597,65	Pyroxenite with sporadic green clinopyroxene; chromitite lens at 595,05 (0,8 x 1,5 cm).
597,65 - 597,70	Chromitiferous pyroxenite grades into chromitite layer at the base.
597,70 - 609,57	Pyroxenite.
609,57 - 609,63	Massive chromitite layer with sharp upper and lower contacts; dip of ca. 25°.
609,63 - 643,10	Pyroxenite, fine grained.
643,10 - 644,26	Chromitiferous pyroxenite with some chromitite laminae.
644,26 - 697,80	Pyroxenite.
697,80 - 699,73	Dunite, sharp contact.
699,73 - 700,37	Pyroxenite.

700,37 - 701,10	Chromitiferous dunite to 700,70 undelain by dunite.
701,10 - 744,80	Medium grained pyroxenite.
744,80 - 745,10	Medium grained pyroxenite with sporadic olivine; gradation into harzburgite at 745,10.
745,10 - 745,20	Harzburgite.
745,20 - 762,60	Coarse to medium grained chromitiferous dunite.
762,60 - 773,67	Poikilitic harzburgite (mottled dunite).
773,67 - 774,44	Medium grained dunite.
774,44 - 793,72	Very coarse grained dunite with some poikilitic orthopyroxene and sporadic dissemination of chromite.
793,72 - 803,52	Poikilitic harzburgite (mottled dunite).
803,52 - 831,06	Coarse grained dunite with some poikilitic orthopyroxene; sporadic dissemination of chromite.

End of Hole at 831,06m.

LOG OF NG2

Logged By : W J de Klerk
R N Scoon
B Teigler
W Maier
S Haikney

Depth in metres	Petrographic Description
0,00 - 3,00	Overburden : Black turf soil.
3,00 - 12,50	Highly weathered material with some magnesite.
12,50 - 38,00	Medium grained dunite, but heavily weathered.
38,00 - 51,60	Medium grained dunite with some poikilitic orthopyroxene.
51,60 - 52,50	Medium to coarse grained pyroxenite.
52,50 - 91,00	Medium grained dunite; contact is sheared and serpentinised; a thin layer of medium grained pyroxenite occurs at 69,40 - 69,70; between 70,45 - 71,55 olivine pyroxenite, at about 77,00 gradation into harzburgite, which grades into dunite at ca. 83.30.
91,00 - 120,60	Medium grained pyroxenite with sporadic clinopyroxene oikocrysts; harzburgite lens at 119,45.
120,60 - 123,15	Coarse grained granular harzburgite.
123,15 - 159,20	Medium to coarse grained poikilitic harzburgite; chromitite lens (15 cm) at 158,50.
159,20 - 197,30	Medium grained pyroxenite with sporadic olivine; at 161,00 harzburgite layers at 161,00 (10 cm) and 165,50 (52 cm).
197,30 - 199,65	Medium grained granular harzburgite.
199,65 - 202,00	Olivine pyroxenite with gradations into harzburgite.
202,00 - 206,45	Medium grained pyroxenite.
206,45 - 208,75	Olivine pyroxenite with gradations into harzburgite.
208,75 - 211,00	Medium grained pyroxenite.
211,00 - 212,60	Olivine pyroxenite.
212,60 - 221,43	Poikilitic harzburgite.
221,43 - 225,65	Medium grained pyroxenite.
225,65 - 228,05	Poikilitic harzburgite with gradations into dunite.
228,05 - 229,12	Granular harzburgite with conspicuous amount of phlogopite.
229,12 - 233,00	Medium grained pyroxenite.
233,00 - 234,20	Granular harzburgite.
234,20 - 234,90	Medium grained pyroxenite.
234,90 - 237,00	Granular harzburgite with inch scale layering of poikilitic harzburgite and dunite.
237,00 - 241,05	Medium grained feldspathic poikilitic harzburgite and dunite.
241,05 - 297,13	Medium grained pyroxenite.
297,13 - 300,00	Norite with sheared upper contact.
300,00 - 326,56	Medium grained pyroxenite; pegmatoidal development at 323,86 (17 cm).
326,56 - 327,73	Dunite and poikilitic harzburgite.
327,73 - 337,02	Medium grained pyroxenite.
337,02 - 337,59	Poikilitic harzburgite and dunite.
337,59 - 358,66	Medium grained feldspathic pyroxenite.
358,66 - 360,20	Harzburgite.
360,20 - 372,60	Medium grained pyroxenite.
372,60 - 374,26	Harzburgite grading downwards into dunite.
374,26 - 374,85	Pyroxenite.
374,85 - 375,68	Dunite grading into harzburgite.
375,68 - 376,10	Pyroxenite - olivine pyroxenite - harzburgite.
376,10 - 376,62	Harzburgite.
376,62 - 377,38	Olivine pyroxenite.

377,38 - 380,22	Harzburgite grading into dunite.
380,22 - 382,94	Dunite.
382,94 - 384,37	Harzburgite.
384,37 - 397,68	Pyroxenite
397,68 - 399,50	Harzburgite.
399,50 - 410,60	Pyroxenite.
410,60 - 411,74	Harzburgite with a basal dunite layer.
411,74 - 415,86	Pyroxenite.
415,86 - 418,55	Harzburgite.
418,55 - 418,95	Olivine pyroxenite.
418,95 - 420,01	Dunite.
420,01 - 421,50	Pyroxenite.
421,50 - 424,10	Harzburgite.
414,10 - 426,05	Pyroxenite.
426,05 - 436,58	Harzburgite with gradations into olivine pyroxenite and dunite at 428,00 and 430,00.
436,58 - 437,04	Pyroxenite.
437,04 - 437,50	Harzburgite.
437,50 - 438,29	Pyroxenite.
438,29 - 438,43	Harzburgite.
438,43 - 439,30	Pyroxenite.
439,30 - 439,42	Harzburgite.
439,42 - 449,45	Pyroxenite.
449,45 - 450,00	Dunite with gradational contact to underlying harzburgite.
450,00 - 450,70	Harzburgite.
450,70 - 451,71	Pyroxenite.
451,71 - 452,85	Harzburgite.
452,85 - 454,44	Dunite.
454,44 - 466,10	Pyroxenite.
466,10 - 467,65	Harzburgite.
467,85 - 478,46	Dunite.
478,46 - 479,47	Pyroxenite.
479,47 - 480,80	Harzburgite.
480,80 - 481,40	Dunite.
481,40 - 488,87	Pyroxenite.
488,87 - 489,25	Dunite, highly altered.
489,25 - 489,95	Harzburgite.
489,95 - 531,02	Dunite.

End of core available for this study.

For the complete log, see Teigler (1991).

APPENDIX II

Modal Analyses for boreholes NG1 and NG2

SAMPLE	PLAG	CPX	OPX	OL	CT	Bi/PHL	QTZ	OTHERS	TOTAL
NG1									
17.00	9.2	6.3	84.0	0.0	0.0	0.4	0.0	0.1	100.0
21.00	12.4	7.4	78.6	0.0	0.5	0.0	0.0	1.1	100.0
25.00	12.1	3.6	83.5	0.0	0.0	0.8	0.0	0.0	100.0
29.80	23.9	3.3	72.8	0.0	0.0	0.0	0.0	0.0	100.0
35.00	7.2	5.7	86.1	0.0	1.0	0.0	0.0	0.0	100.0
46.25	12.8	3.2	84.0	0.0	0.0	0.0	0.0	0.0	100.0
49.75	8.1	4.5	87.4	0.0	0.0	0.0	0.0	0.0	100.0
55.40	12.8	4.3	82.9	0.0	0.0	0.0	0.0	0.0	100.0
56.00	5.9	0.8	83.1	0.0	0.0	5.1	4.2	0.9	100.0
58.60	7.7	1.1	82.5	0.0	1.1	3.3	2.7	1.6	100.0
61.71	5.2	0.5	78.4	0.0	0.9	4.2	9.9	0.9	100.0
65.19	9.8	3.7	84.8	0.0	1.6	0.0	0.0	0.1	100.0
65.25	7.9	3.2	87.5	0.0	1.1	0.0	0.0	0.3	100.0
69.20	8.4	3.2	88.0	0.0	0.4	0.0	0.0	0.0	100.0
B71.46	7.7	1.8	90.5	0.0	0.0	0.0	0.0	0.0	100.0
74.40	9.5	4.7	85.8	0.0	0.0	0.0	0.0	0.0	100.0
79.75	5.7	3.9	89.7	0.0	0.7	0.0	0.0	0.0	100.0
82.75	11.0	0.7	68.7	0.0	19.3	0.0	0.0	0.3	100.0
84.90	3.8	1.7	73.4	0.0	21.0	0.0	0.0	0.1	100.0
85.85	5.0	3.4	87.2	0.0	0.0	2.7	1.7	0.0	100.0
89.55	6.6	3.6	88.5	0.0	1.3	0.0	0.0	0.0	100.0
A90.33	0.0	0.8	23.5	4.4	64.5	0.0	0.0	6.8	100.0
B90.33	1.5	1.5	54.6	0.0	38.7	0.6	0.0	3.1	100.0
C90.33	2.6	1.5	71.1	0.0	24.8	0.0	0.0	0.0	100.0
94.60	9.1	2.9	84.5	0.0	0.6	0.0	0.0	2.9	100.0
95.00	12.7	0.0	0.0	74.7	0.8	1.2	0.0	10.6	100.0
96.75	12.0	7.5	77.2	0.6	0.0	1.2	0.0	1.5	100.0
A100.30	6.0	1.8	91.9	0.0	0.0	0.0	0.0	0.3	100.0
B100.33	5.0	4.3	90.3	0.0	0.3	0.0	0.0	0.1	100.0
100.70	3.7	11.9	14.8	61.7	0.0	0.0	0.0	7.9	100.0
105.45	7.3	12.0	80.4	0.0	0.0	0.3	0.0	0.0	100.0
108.30	0.4	2.3	59.8	27.2	0.0	0.0	0.0	10.3	100.0
108.30	3.0	1.6	0.3	74.1	0.0	3.0	0.0	18.0	100.0
110.52	7.8	10.2	79.6	0.0	0.0	1.7	0.7	0.0	100.0
115.10	9.5	1.5	87.1	0.0	0.4	0.8	0.0	0.7	100.0
118.80	12.3	2.8	7.5	57.1	1.2	0.4	0.0	18.7	100.0
118.87	11.0	3.7	49.2	29.7	5.3	0.0	0.0	1.1	100.0
119.90	8.3	2.2	89.1	0.0	0.0	0.3	0.0	0.1	100.0
122.80	5.4	4.5	0.4	72.7	0.8	0.0	0.0	16.2	100.0
126.00	4.2	1.6	91.9	0.0	0.7	0.3	0.0	1.3	100.0
130.60	5.5	4.1	90.4	0.0	0.0	0.0	0.0	0.0	100.0
136.30	9.4	1.7	88.8	0.0	0.0	0.0	0.0	0.1	100.0
146.50	3.8	2.4	93.8	0.0	0.0	0.0	0.0	0.0	100.0
148.20	4.7	2.6	84.7	0.0	0.4	2.1	4.7	0.8	100.0
152.20	2.3	2.7	87.3	0.4	1.3	0.7	0.0	5.3	100.0
158.20	8.3	0.7	82.1	0.0	4.0	0.0	0.3	4.6	100.0
163.27	10.4	1.0	87.2	0.0	0.3	0.7	0.0	0.4	100.0
168.15	4.5	2.3	90.2	0.0	1.9	0.0	0.0	1.1	100.0
173.37	1.5	2.3	94.7	0.0	1.5	0.0	0.0	0.0	100.0
178.45	2.8	2.4	91.7	0.0	0.4	0.0	2.0	0.7	100.0
183.70	3.7	0.0	90.0	0.0	1.7	0.3	0.0	4.3	100.0

SAMPLE	PLAG	CPX	OPX	OL	CT	BI/PHL	QTZ	OTHERS	TOTAL
NG1									
191.00	2.8	2.8	89.8	0.0	0.0	0.9	0.0	3.7	100.0
197.50	1.6	2.2	93.3	0.0	1.0	0.0	0.0	1.9	100.0
204.50	15.8	0.0	84.2	0.0	0.0	0.0	0.0	0.0	100.0
210.30	16.0	0.0	82.5	0.0	0.0	0.0	0.6	0.9	100.0
218.60	12.0	0.9	85.2	0.0	0.3	0.0	0.0	1.6	100.0
225.90	10.9	0.8	87.9	0.0	0.0	0.4	0.0	0.0	100.0
233.60	1.1	1.9	89.3	0.0	0.9	4.6	2.3	0.0	100.0
237.50	10.9	0.0	87.5	0.0	1.5	0.0	0.0	0.1	100.0
242.00	2.2	3.0	86.6	0.0	8.2	0.0	0.0	0.0	100.0
A242.15	4.4	0.7	85.2	0.0	9.5	0.0	0.0	0.1	100.0
242.70	4.8	0.0	80.7	0.0	13.8	0.0	0.0	0.7	100.0
242.72	9.8	0.8	89.4	0.0	0.0	0.0	0.0	0.0	100.0
245.25	0.8	1.7	97.1	0.0	0.4	0.0	0.0	0.0	100.0
250.15	0.8	2.1	95.8	0.0	1.3	0.0	0.0	0.0	100.0
255.25	5.5	1.2	90.5	0.0	2.5	0.0	0.0	0.3	100.0
257.10	12.4	4.8	76.0	0.0	5.2	0.8	0.0	0.8	100.0
257.70	18.8	1.8	74.3	0.0	5.0	0.0	0.0	0.1	100.0
262.17	14.3	1.6	70.6	0.0	11.9	1.6	0.0	0.0	100.0
267.00	2.0	2.8	95.2	0.0	0.0	0.0	0.0	0.0	100.0
277.25	6.0	2.5	91.1	0.0	0.4	0.0	0.0	0.0	100.0
282.25	4.5	3.0	92.4	0.0	0.0	0.0	0.0	0.1	100.0
287.15	4.4	4.4	90.6	0.0	0.4	0.0	0.0	0.2	100.0
292.30	2.4	0.7	94.8	0.0	0.7	0.0	0.0	1.4	100.0
297.40	1.9	2.5	94.6	0.0	0.9	0.0	0.0	0.1	100.0
302.00	5.4	3.3	89.5	0.0	1.8	0.0	0.0	0.0	100.0
307.30	4.0	3.2	90.6	0.0	1.8	0.4	0.0	0.0	100.0
312.10	2.0	0.8	96.7	0.0	0.4	0.0	0.0	0.1	100.0
317.60	6.1	1.6	92.3	0.0	0.0	0.0	0.0	0.0	100.0
322.75	3.9	2.8	93.3	0.0	0.0	0.0	0.0	0.0	100.0
327.45	2.2	1.5	94.8	0.0	0.7	0.4	0.4	0.0	100.0
331.13	1.7	1.4	80.5	0.0	2.5	0.0	0.0	13.9	100.0
334.30	3.3	0.4	94.4	0.0	1.9	0.0	0.0	1.1	100.0
338.45	2.0	2.3	94.4	0.0	0.7	0.0	0.0	0.6	100.0
343.40	4.1	3.7	91.7	0.0	0.0	0.4	0.0	0.1	100.0
348.20	4.6	2.5	92.5	0.0	0.4	0.0	0.0	0.0	100.0
A353.40	7.0	0.6	86.9	0.0	0.0	4.9	0.5	0.0	100.0
B353.40	13.2	1.6	83.2	0.0	0.0	1.9	0.0	0.1	100.0
C353.40	9.7	2.0	88.3	0.0	0.0	0.0	0.0	0.0	100.0
358.75	10.4	0.0	88.2	0.0	0.0	0.9	0.5	0.0	100.0
364.25	6.3	5.1	87.8	0.0	0.0	0.4	0.4	0.0	100.0
374.35	8.5	2.0	87.1	0.0	0.0	0.7	1.7	0.0	100.0
380.35	3.6	1.0	91.3	0.0	0.5	0.8	2.8	0.0	100.0
385.40	8.1	2.5	85.6	0.0	0.0	1.3	2.2	0.3	100.0
B390.60	12.1	1.4	83.6	0.0	0.4	0.7	1.8	0.0	100.0
396.00	6.3	4.3	88.0	0.0	0.0	0.7	0.7	0.0	100.0
396.70	6.5	1.8	90.6	0.0	0.0	0.4	0.7	0.0	100.0
401.38	8.3	3.0	84.9	0.0	0.4	1.1	2.3	0.0	100.0
406.40	8.0	1.5	90.5	0.0	0.0	0.0	0.0	0.0	100.0
411.12	6.0	8.7	84.5	0.0	0.0	0.4	0.0	0.4	100.0
414.85	5.9	1.4	92.0	0.0	0.7	0.0	0.0	0.0	100.0
418.10	1.0	1.0	36.5	59.6	0.5	1.0	0.0	0.4	100.0

SAMPLE	PLAG	CPX	OPX	OL	CT	Bi/PHL	QTZ	OTHERS	TOTAL
NG1									
418.30	4.3	0.0	72.8	19.6	1.1	0.0	0.0	2.2	100.0
418.30	9.0	0.7	90.3	0.0	0.0	0.0	0.0	0.0	100.0
419.80	11.5	1.9	85.9	0.0	0.4	0.0	0.0	0.3	100.0
420.20	10.3	0.0	87.8	0.0	0.7	1.1	0.0	0.1	100.0
420.75	2.9	12.6	46.4	33.3	0.5	3.9	0.0	0.4	100.0
421.00	0.0	6.4	83.7	0.0	0.0	7.5	0.7	1.7	100.0
422.15	3.0	10.6	40.3	37.4	1.5	7.2	0.0	0.0	100.0
423.60	3.5	8.1	0.0	78.2	10.1	0.0	0.0	0.1	100.0
425.20	0.0	0.0	13.7	71.3	15.0	0.0	0.0	0.0	100.0
427.00	8.7	0.0	0.0	83.2	2.7	0.0	0.0	5.4	100.0
430.55	0.0	0.0	63.9	22.1	13.5	0.5	0.0	0.0	100.0
439.30	1.4	0.0	36.6	50.5	9.3	2.2	0.0	0.0	100.0
445.45	0.0	0.0	57.0	41.9	1.1	0.0	0.0	0.0	100.0
451.25	4.1	0.0	60.8	23.4	9.3	0.0	0.0	2.4	100.0
452.00	3.9	1.4	64.4	22.8	6.0	0.0	0.0	1.5	100.0
455.65	6.3	1.7	91.7	0.0	0.0	0.3	0.0	0.0	100.0
459.30	9.4	2.6	85.8	0.0	1.6	0.6	0.0	0.0	100.0
459.70	6.2	2.9	88.0	0.0	0.0	1.2	1.5	0.2	100.0
464.10	4.3	1.0	87.7	0.0	0.7	2.3	4.0	0.0	100.0
A469.40	1.8	1.0	91.7	0.0	0.8	2.3	1.3	1.1	100.0
474.45	5.0	0.0	93.1	0.0	1.9	0.0	0.0	0.0	100.0
476.40	8.0	0.6	87.2	0.0	3.8	0.0	0.0	0.4	100.0
478.90	6.6	1.4	89.0	0.0	0.3	1.2	1.4	0.1	100.0
480.60	2.3	0.5	63.4	31.4	0.8	0.0	0.0	1.6	100.0
481.90	3.3	1.7	94.7	0.0	0.3	0.0	0.0	0.0	100.0
486.55	7.2	1.5	89.8	0.0	0.6	0.9	0.0	0.0	100.0
492.15	6.6	3.3	88.9	0.0	0.3	0.6	0.3	0.0	100.0
495.90	2.9	2.9	89.3	0.0	3.9	0.0	0.0	1.0	100.0
496.43	8.7	0.3	90.7	0.0	0.3	0.0	0.0	0.0	100.0
500.50	3.2	8.2	86.1	0.0	0.4	2.1	0.0	0.0	100.0
506.05	4.3	2.6	34.8	55.7	2.2	0.0	0.0	0.4	100.0
508.01	4.4	2.8	15.8	72.2	4.8	0.0	0.0	0.0	100.0
509.86	2.2	0.0	24.5	71.6	1.3	0.2	0.0	0.2	100.0
511.35	0.0	0.0	23.8	71.5	2.6	1.3	0.0	0.8	100.0
512.60	3.3	0.0	17.1	77.6	2.0	0.0	0.0	0.0	100.0
515.35	3.2	8.8	59.7	26.9	0.9	0.5	0.0	0.0	100.0
519.26	6.7	1.0	88.9	0.0	1.5	0.5	0.3	1.1	100.0
523.90	10.3	0.7	83.7	0.0	1.8	0.7	2.8	0.0	100.0
524.35	5.1	1.0	91.1	0.0	1.5	0.6	0.6	0.0	100.0
A527.62	3.1	0.3	95.6	0.0	0.9	0.0	0.0	0.1	100.0
528.50	4.5	2.1	90.3	0.0	0.6	0.9	1.5	0.1	100.0
532.14	5.8	2.8	90.0	0.0	0.8	0.3	0.3	0.0	100.0
536.95	3.3	0.5	95.6	0.0	0.0	0.3	0.3	0.0	100.0
543.23	1.2	0.0	96.7	0.0	1.8	0.0	0.0	0.3	100.0
546.85	0.5	0.5	96.0	0.0	2.8	0.2	0.0	0.0	100.0
553.33	5.9	0.6	92.5	0.0	0.6	0.3	0.0	0.1	100.0
558.75	9.8	1.0	87.5	0.0	0.7	0.3	0.7	0.0	100.0
564.45	7.3	1.3	89.2	0.0	0.0	0.8	1.3	0.1	100.0
569.20	8.8	1.0	88.9	0.0	0.0	0.3	0.8	0.2	100.0
575.35	7.3	1.4	89.9	0.0	0.0	0.0	0.6	0.8	100.0
581.00	4.6	0.8	93.8	0.0	0.0	0.8	0.0	0.0	100.0

SAMPLE	PLAG	CPX	OPX	OL	CT	BI/PHL	QTZ	OTHERS	TOTAL
NG1									
586.00	4.7	1.1	94.1	0.0	0.0	0.0	0.0	0.1	100.0
589.60	5.2	0.9	93.0	0.0	0.0	0.0	0.9	0.0	100.0
595.05	4.3	2.6	91.8	0.0	0.5	0.5	0.3	0.0	100.0
B597.62	0.0	0.0	74.6	0.0	25.4	0.0	0.0	0.0	100.0
597.77	5.4	2.5	92.1	0.0	0.0	0.0	0.0	0.0	100.0
603.10	6.2	2.3	89.6	0.0	0.3	0.6	1.0	0.0	100.0
608.25	6.7	1.4	89.8	0.0	0.2	1.2	0.7	0.0	100.0
609.47	11.0	0.5	85.3	0.0	1.8	0.9	0.5	0.0	100.0
609.68	4.8	0.8	93.6	0.0	0.0	0.5	0.3	0.0	100.0
614.76	5.8	0.5	92.1	0.0	0.0	0.5	1.0	0.1	100.0
619.85	5.2	1.5	91.7	0.0	0.0	0.0	0.3	1.3	100.0
624.70	4.0	1.7	94.0	0.0	0.0	0.0	0.0	0.3	100.0
635.25	7.2	1.0	90.1	0.0	0.0	1.0	0.7	0.0	100.0
639.95	6.0	1.0	92.2	0.0	0.7	0.0	0.0	0.1	100.0
A644.00	2.6	1.0	90.5	0.0	5.2	0.7	0.0	0.0	100.0
645.17	6.6	0.6	88.7	0.0	1.2	1.7	1.2	0.0	100.0
649.66	6.4	2.0	91.2	0.0	0.4	0.0	0.0	0.0	100.0
A655.15	5.2	1.4	91.0	0.0	0.0	1.6	0.8	0.0	100.0
B655.20	3.0	1.4	95.3	0.0	0.0	0.0	0.3	0.0	100.0
660.40	5.6	0.4	86.3	0.0	0.0	2.2	5.2	0.3	100.0
670.10	5.8	0.6	90.0	0.0	0.0	1.6	1.6	0.4	100.0
675.25	3.1	1.5	93.9	0.0	0.0	0.5	0.5	0.5	100.0
680.17	2.9	0.7	96.4	0.0	0.0	0.0	0.0	0.0	100.0
685.40	4.6	2.2	90.2	0.0	0.3	0.8	1.9	0.0	100.0
690.30	5.7	1.5	92.5	0.0	0.0	0.3	0.0	0.0	100.0
695.50	7.0	0.9	90.4	0.0	0.0	0.6	1.1	0.0	100.0
698.00	1.7	3.8	55.1	33.1	6.3	0.0	0.0	0.0	100.0
699.45	7.1	1.0	5.2	82.8	1.3	0.3	0.0	2.3	100.0
700.65	0.0	0.0	51.0	28.6	20.4	0.0	0.0	0.0	100.0
701.75	3.5	0.5	95.7	0.0	0.3	0.0	0.0	0.0	100.0
702.75	4.2	1.2	94.3	0.0	0.0	0.3	0.0	0.0	100.0
706.90	6.6	0.6	89.5	0.0	3.0	0.0	0.3	0.0	100.0
711.60	1.5	0.6	95.5	0.0	2.4	0.0	0.0	0.0	100.0
715.35	2.1	1.2	95.9	0.0	0.6	0.0	0.0	0.2	100.0
720.15	2.8	1.4	88.5	0.0	0.0	3.9	2.8	0.6	100.0
725.35	4.5	1.4	94.1	0.0	0.0	0.0	0.0	0.0	100.0
730.35	5.1	1.0	93.8	0.0	0.0	0.0	0.0	0.1	100.0
735.10	1.4	1.1	96.9	0.0	0.6	0.0	0.0	0.0	100.0
739.80	3.1	3.3	92.4	0.0	0.0	0.7	0.5	0.0	100.0
744.70	1.8	0.9	95.1	1.5	0.6	0.0	0.0	0.1	100.0
745.45	2.2	11.4	80.3	1.3	3.9	0.9	0.0	0.0	100.0
745.65	3.9	2.1	18.2	69.3	5.0	0.4	0.0	1.1	100.0
749.30	1.2	1.6	55.3	39.1	2.4	0.4	0.0	0.0	100.0
752.40	3.7	0.9	18.7	72.9	3.3	0.5	0.0	0.0	100.0
754.54	1.6	0.0	2.6	94.3	0.8	0.0	0.0	0.7	100.0
753.09	0.5	4.5	9.0	83.0	2.5	0.0	0.0	0.5	100.0
761.95	0.0	0.0	0.0	100.0	0.0	0.0	0.0	0.0	100.0
762.75	0.0	0.0	0.0	100.0	0.0	0.0	0.0	0.0	100.0
773.74	0.0	0.0	0.0	100.0	0.0	0.0	0.0	0.0	100.0
774.25	0.0	0.0	0.0	97.0	1.5	0.0	0.0	1.5	100.0
776.10	2.4	4.1	0.0	88.9	0.6	4.1	0.0	0.0	100.0
777.43	8.0	0.0	0.0	89.2	2.4	0.4	0.0	0.0	100.0

SAMPLE	PLAG	CPX	OPX	OL	CT	Bi/PHL	QTZ	OTHERS	TOTAL
NG1									
779.59	6.0	8.8	1.2	79.5	1.6	2.8	0.0	0.1	100.0
781.37	4.7	0.0	0.0	94.7	0.6	0.0	0.0	0.0	100.0
782.05	7.7	0.4	4.7	82.1	4.3	0.4	0.0	0.4	100.0
784.06	1.6	1.2	45.4	46.8	5.0	0.0	0.0	0.0	100.0
784.64	2.4	13.4	8.7	72.4	3.1	0.0	0.0	0.0	100.0
786.60	7.1	3.2	0.0	86.5	0.0	3.2	0.0	0.0	100.0
787.00	10.0	0.0	0.4	88.7	0.4	0.4	0.0	0.1	100.0
791.35	0.4	0.0	42.8	54.9	0.8	0.8	0.0	0.3	100.0
793.60	0.0	12.8	0.0	84.9	2.3	0.0	0.0	0.0	100.0
793.80	0.0	0.9	0.0	89.6	1.8	0.0	0.0	7.7	100.0
796.04	0.0	0.5	0.0	99.0	0.5	0.0	0.0	0.0	100.0
802.23	0.0	0.0	0.8	98.0	1.2	0.0	0.0	0.0	100.0
803.41	0.4	0.0	16.6	81.7	0.4	0.0	0.0	0.9	100.0
803.69	0.5	2.0	0.0	90.2	1.0	2.9	0.0	3.4	100.0
806.80	2.4	3.6	0.0	91.9	1.2	0.8	0.0	0.1	100.0
814.00	2.2	0.0	30.5	66.1	0.0	1.1	0.0	0.1	100.0
816.10	0.0	5.7	5.7	88.6	0.0	0.0	0.0	0.0	100.0
816.20	2.6	11.9	7.7	77.8	0.0	0.0	0.0	0.0	100.0
822.44	4.1	0.0	26.1	69.8	0.0	0.0	0.0	0.0	100.0
824.23	5.7	0.9	1.9	88.7	1.4	1.4	0.0	0.0	100.0
830.15	1.5	12.4	8.6	76.9	0.3	0.3	0.0	0.0	100.0

SAMPLE	PLAG	CPX	OPX	OL	CT	Bi/PHL	QTZ	OTHERS	TOTAL
NG2									
39.35	4.4	5.5	16.5	69.1	1.8	2.6	0.0	0.1	100.0
42.55	6.6	0.0	12.4	79.5	1.1	0.4	0.0	0.0	100.0
46.40	0.4	2.3	2.0	86.0	0.4	6.6	0.0	2.3	100.0
51.50	1.9	0.5	7.8	80.5	1.2	1.9	0.0	6.3	100.0
A51.90	3.8	1.0	94.2	0.0	0.0	1.0	0.0	0.0	100.0
B51.90	5.4	1.0	87.5	0.0	0.0	2.0	0.2	3.9	100.0
53.50	0.0	3.8	19.3	74.2	1.5	0.4	0.0	0.8	100.0
55.50	2.3	3.2	54.4	39.3	0.8	0.0	0.0	0.0	100.0
59.10	0.7	1.1	26.1	70.3	0.7	0.7	0.0	0.4	100.0
63.35	4.6	4.2	47.2	40.7	0.9	0.9	0.0	1.5	100.0
69.42	3.0	4.0	45.5	47.0	0.0	0.5	0.0	0.0	100.0
71.50	0.0	6.4	66.4	26.0	1.1	0.0	0.0	0.1	100.0
73.60	2.4	4.7	53.5	38.6	0.8	0.0	0.0	0.0	100.0
77.20	7.6	5.3	29.2	56.8	1.1	0.0	0.0	0.0	100.0
80.35	3.5	0.0	28.6	67.3	0.5	0.0	0.0	0.1	100.0
83.75	6.3	1.6	18.0	72.9	0.4	0.8	0.0	0.0	100.0
86.20	1.5	1.5	31.1	64.6	0.4	0.8	0.0	0.1	100.0
89.30	0.0	0.0	29.4	70.1	0.4	0.0	0.0	0.1	100.0
89.95	0.0	9.9	22.9	64.9	1.5	0.8	0.0	0.0	100.0
91.40	2.9	1.4	94.8	0.0	0.0	0.9	0.0	0.0	100.0
98.00	4.0	9.5	85.5	0.0	0.0	0.6	0.3	0.1	100.0
A102.60	1.2	2.3	95.5	0.0	0.0	0.9	0.0	0.1	100.0
B102.60	11.1	2.2	85.5	0.0	0.0	0.7	0.4	0.1	100.0
106.60	6.3	2.6	90.6	0.0	0.0	0.3	0.0	0.2	100.0
110.80	2.0	1.3	95.3	0.0	0.0	0.7	0.7	0.0	100.0
115.25	3.1	1.0	95.8	0.0	0.0	0.0	0.0	0.1	100.0
119.10	0.0	0.0	71.1	28.9	0.0	0.0	0.0	0.0	100.0
120.40	13.8	0.9	84.6	0.0	0.0	0.6	0.0	0.1	100.0
122.30	1.9	5.7	38.7	51.8	0.0	1.9	0.0	0.0	100.0
123.40	0.0	4.2	19.1	72.5	2.3	1.9	0.0	0.0	100.0
127.15	4.4	1.6	19.9	70.5	0.4	0.5	0.0	2.7	100.0
130.20	5.3	1.6	18.3	74.4	0.4	0.0	0.0	0.0	100.0
134.40	7.8	3.1	19.1	67.9	1.0	1.0	0.0	0.1	100.0
138.80	5.7	3.4	1.5	86.7	1.1	1.5	0.0	0.1	100.0
143.30	2.5	0.0	24.7	71.7	0.5	0.4	0.0	0.2	100.0
143.35	6.3	0.0	6.8	85.6	1.3	0.0	0.0	0.0	100.0
152.35	7.9	5.8	14.5	70.5	1.2	0.0	0.0	0.1	100.0
157.30	0.0	0.0	18.3	79.9	0.6	1.2	0.0	0.0	100.0
159.35	2.7	0.4	92.4	4.5	0.0	0.0	0.0	0.0	100.0
161.65	4.1	0.0	91.0	4.1	0.8	0.0	0.0	0.0	100.0
165.40	0.0	0.0	92.3	5.3	0.0	2.4	0.0	0.0	100.0
165.62	0.4	0.0	76.7	21.1	0.8	0.8	0.0	0.2	100.0
A176.00	5.5	0.8	93.6	0.0	0.0	0.0	0.0	0.1	100.0
B176.00	3.2	0.0	96.4	0.0	0.0	0.4	0.0	0.0	100.0
180.55	4.1	1.7	92.5	0.0	0.0	1.7	0.0	0.0	100.0
185.40	5.9	1.5	92.1	0.0	0.0	0.5	0.0	0.0	100.0
189.40	5.6	1.7	91.6	0.0	0.0	1.0	0.0	0.1	100.0
194.20	5.4	0.4	94.2	0.0	0.0	0.0	0.0	0.0	100.0
197.00	1.7	0.0	92.7	5.5	0.0	0.0	0.0	0.1	100.0
197.75	0.8	1.3	61.5	35.1	0.8	0.4	0.0	0.1	100.0
198.85	1.4	0.0	41.7	56.2	0.0	0.7	0.0	0.0	100.0

SAMPLE	PLAG	CPX	OPX	OL	CT	BI/PHL	QTZ	OTHERS	TOTAL
NG2									
200.50	1.7	0.0	54.7	43.2	0.4	0.0	0.0	0.0	100.0
204.40	5.0	0.8	86.2	7.9	0.0	0.0	0.0	0.1	100.0
206.30	1.9	0.0	93.0	4.6	0.0	0.5	0.0	0.0	100.0
208.40	3.8	0.0	92.0	4.2	0.0	0.0	0.0	0.0	100.0
210.50	1.9	6.4	80.8	10.9	0.0	0.0	0.0	0.0	100.0
212.20	3.4	0.8	65.7	30.1	0.0	0.0	0.0	0.0	100.0
213.30	4.9	7.8	9.9	74.9	2.5	0.0	0.0	0.0	100.0
217.60	0.5	0.0	49.8	48.3	0.5	0.9	0.0	0.0	100.0
220.50	4.1	6.0	9.3	79.5	0.7	0.4	0.0	0.0	100.0
225.51	0.4	2.6	94.8	1.5	0.0	0.7	0.0	0.0	100.0
226.75	3.4	0.4	43.2	51.7	0.4	0.9	0.0	0.0	100.0
231.80	5.0	0.8	81.1	11.2	1.9	0.0	0.0	0.0	100.0
233.85	8.7	0.0	81.3	9.5	0.4	0.0	0.0	0.1	100.0
234.85	6.1	0.0	86.6	6.1	1.1	0.0	0.0	0.1	100.0
239.90	0.0	23.4	18.8	52.6	5.2	0.0	0.0	0.0	100.0
241.27	1.8	0.5	71.0	12.9	13.8	0.0	0.0	0.0	100.0
A241.27	4.9	1.6	68.4	9.4	15.2	0.4	0.0	0.1	100.0
A241.55	10.9	0.8	87.9	0.0	0.0	0.4	0.0	0.0	100.0
B241.55	13.1	0.7	68.8	17.0	0.0	0.4	0.0	0.0	100.0
284.66	19.3	0.0	79.8	0.0	0.0	0.9	0.0	0.0	100.0
289.00	15.3	0.6	83.4	0.0	0.0	0.6	0.0	0.1	100.0
293.60	28.3	0.0	71.7	0.0	0.0	0.0	0.0	0.0	100.0
294.12	15.7	0.0	76.6	0.0	0.0	4.2	1.5	2.0	100.0
294.30	11.1	2.1	86.8	0.0	0.0	0.0	0.0	0.0	100.0
294.65	19.1	0.7	78.1	0.0	0.0	2.1	0.0	0.0	100.0
A296.95	9.8	0.6	88.6	0.0	0.0	0.6	0.0	0.4	100.0
B296.95	13.2	0.4	85.5	0.0	0.0	0.4	0.0	0.5	100.0
A299.89	43.3	0.0	56.7	0.0	0.0	0.0	0.0	0.0	100.0
305.75	11.4	1.8	86.3	0.0	0.0	0.0	0.5	0.0	100.0
307.10	6.6	0.5	90.7	0.0	1.6	0.5	0.0	0.1	100.0
313.18	1.5	2.4	84.9	0.0	0.0	7.7	3.5	0.0	100.0
320.15	13.8	2.0	83.2	0.0	0.0	0.5	0.5	0.0	100.0
B326.28	9.7	4.3	81.6	0.0	0.3	0.3	0.0	3.8	100.0
B327.73	2.0	0.5	65.3	24.8	7.3	0.0	0.0	0.1	100.0
A332.25	5.0	0.9	89.2	0.0	1.7	0.0	2.6	0.6	100.0
B332.25	15.7	0.8	80.3	0.0	0.8	1.5	0.5	0.4	100.0
339.13	0.3	4.5	81.0	0.0	0.0	6.2	6.2	1.8	100.0
A344.39	10.2	1.8	87.4	0.0	0.3	0.3	0.0	0.0	100.0
350.48	14.8	1.0	83.8	0.0	0.2	0.0	0.0	0.2	100.0
355.70	13.4	4.3	79.8	0.0	0.3	0.0	2.0	0.2	100.0
B358.66	5.2	1.9	52.5	37.8	2.5	0.0	0.0	0.1	100.0
A360.20	1.1	0.3	80.5	14.1	3.7	0.3	0.0	0.0	100.0
B360.20	13.2	0.2	83.9	0.0	0.2	0.7	0.0	1.8	100.0
366.00	12.8	4.3	82.3	0.0	0.3	0.3	0.0	0.0	100.0
372.60	6.0	0.2	72.3	19.2	2.2	0.0	0.0	0.1	100.0
377.38	7.9	1.8	88.1	0.9	1.1	0.2	0.0	0.0	100.0
A382.65	1.3	1.1	3.5	92.0	2.1	0.0	0.0	0.0	100.0
397.58	1.8	0.0	81.8	12.6	2.5	1.3	0.0	0.0	100.0
398.65	1.2	0.0	51.9	43.3	3.3	0.2	0.0	0.1	100.0
405.00	7.0	0.2	91.3	0.0	1.0	0.5	0.0	0.0	100.0
411.10	5.0	0.4	52.6	38.4	3.3	0.2	0.0	0.1	100.0

SAMPLE	PLAG	CPX	OPX	OL	CT	BI/PHL	QTZ	OTHERS	TOTAL
NG2									
A420.00	4.0	3.3	34.7	55.6	2.4	0.0	0.0	0.0	100.0
424.44	8.6	1.9	86.4	1.7	0.7	0.7	0.0	0.0	100.0
426.60	7.4	0.7	77.4	13.8	0.5	0.2	0.0	0.0	100.0
428.15	8.0	2.9	86.9	0.0	0.2	1.2	0.0	0.8	100.0
429.47	7.5	4.2	45.0	40.2	1.9	0.2	0.0	1.0	100.0
436.58	10.3	0.8	76.5	9.6	2.3	0.5	0.0	0.0	100.0
B438.29	7.1	2.5	30.0	59.8	0.5	0.0	0.0	0.1	100.0
438.57	9.8	6.8	83.0	0.0	0.2	0.2	0.0	0.0	100.0
442.00	12.0	3.4	82.7	0.0	0.7	1.2	0.0	0.0	100.0
447.00	5.3	3.2	89.1	0.0	0.2	1.2	0.7	0.3	100.0
449.40	6.8	1.0	24.8	65.8	1.0	0.5	0.0	0.1	100.0
450.70	8.5	2.6	88.1	0.0	0.0	0.8	0.0	0.0	100.0
452.00	7.3	2.1	74.8	13.4	1.2	1.2	0.0	0.0	100.0
454.26	5.5	1.1	19.0	71.9	2.5	0.0	0.0	0.0	100.0
458.00	6.0	3.0	87.8	0.0	0.0	0.7	1.8	0.7	100.0
467.65	6.3	1.6	55.5	33.4	2.5	0.7	0.0	0.0	100.0
480.80	5.1	5.6	51.6	35.5	1.3	0.9	0.0	0.0	100.0
481.00	4.9	2.3	32.0	59.5	0.5	0.8	0.0	0.0	100.0
488.35	8.6	4.4	85.4	0.0	0.0	0.7	0.0	0.9	100.0
490.05	4.9	3.7	33.4	55.5	2.0	0.5	0.0	0.0	100.0

APPENDIX III

Original whole rock analyses from boreholes NG1 and NG2

ORIGINAL MAJOR ELEMENT ANALYSES FROM NGI

SAMPLE	95.5	108.33	122.80	420.75	430.55	445.45	480.60	506.05	509.86	698.00	699.45	753.09	773.74	784.61	793.80	803.41	809.31	816.10	830.15
SiO2	39.825	42.046	39.891	44.852	38.551	45.181	50.644	47.281	41.798	47.479	39.007	40.153	40.213	41.673	40.351	40.655	41.495	39.985	42.453
TiO2	0.059	0.160	0.042	0.242	0.111	0.052	0.094	0.100	0.058	0.112	0.041	0.011	0.004	0.064	0.016	0.018	0.049	0.024	0.049
Al2O3	4.012	2.420	2.921	2.406	3.707	1.621	2.611	2.628	1.866	2.265	1.317	0.408	0.119	1.234	0.476	0.531	1.088	1.443	1.256
Fe2O3	1.137	1.238	1.060	1.007	1.153	1.123	0.955	1.088	1.268	1.190	1.307	1.192	1.112	1.049	1.067	1.086	1.064	1.105	1.152
FeO	11.367	12.375	10.603	10.072	11.534	11.230	9.554	10.876	12.676	11.897	13.075	11.916	11.118	10.492	10.670	10.856	10.642	11.052	11.522
MnO	0.117	0.174	0.142	0.136	0.189	0.165	0.167	0.194	0.191	0.197	0.182	0.170	0.191	0.190	0.183	0.214	0.200	0.194	0.228
MgO	32.019	32.140	32.266	31.641	37.641	39.909	32.295	34.370	39.623	34.769	39.459	46.426	47.769	41.452	45.665	45.562	42.332	42.918	41.990
CaO	1.899	1.586	1.650	1.258	1.460	1.234	1.821	1.792	1.154	1.370	0.942	0.289	0.157	1.752	0.379	0.592	0.793	0.831	1.397
Na2O	0.120	0.102	0.094	0.127	0.538	0.288	0.177	0.279	0.301	0.132	0.272	0.031	0.032	0.288	0.047	0.098	0.311	0.267	0.229
K2O	0.000	0.000	0.000	0.338	0.000	0.000	0.000	0.000	0.000	0.000	0.000	0.000	0.000	0.061	0.000	0.000	0.010	0.000	0.000
P2O5	0.000	0.000	0.000	0.000	0.000	0.000	0.000	0.000	0.000	0.000	0.000	0.000	0.000	0.000	0.000	0.011	0.026	0.005	0.012
Cr2O3	0.507	0.730	0.255	1.468	3.578	0.460	0.935	1.721	0.770	1.329	0.265	0.505	0.270	0.405	0.740	0.270	0.578	0.283	0.533
NiO	0.172	0.162	0.202	0.126	0.180	0.162	0.098	0.115	0.180	0.131	0.188	0.215	0.284	0.256	0.321	0.293	0.267	0.261	0.256
LOI	10.195	8.163	10.669	6.318	0.808	0.510	2.773	0.396	0.641	0.979	4.595	0.657	0.413	0.437	0.213	0.538	0.312	0.417	1.138
H2O-	0.140	0.435	0.725	0.408	0.154	0.085	0.345	0.060	0.295	0.125	0.290	0.215	0.150	0.124	0.075	0.143	0.096	0.163	0.250
TOTAL	101.869	101.731	100.520	100.399	99.604	102.020	102.469	100.900	100.821	101.975	100.940	102.188	101.832	99.477	100.203	100.867	99.263	98.948	102.465
Rb	0.00	0.00	0.00	16.23	0.00	0.00	0.00	0.00	0.00	0.00	0.00	0.00	0.00	6.41	0.00	0.00	3.33	1322.32	0.00
Sr	44.38	18.66	39.00	8.49	38.61	19.67	20.22	26.16	23.78	18.77	24.45	5.75	3.04	19.70	4.35	8.43	16.69	6.70	19.23
Y	3.64	5.01	3.34	4.22	3.59	0.00	3.57	5.43	0.00	2.61	0.00	0.00	0.00	2.97	0.00	0.00	2.93	0.00	2.66
Zr	2.80	11.72	4.77	20.97	3.02	3.39	5.00	3.45	3.09	5.68	3.57	0.00	0.00	11.22	0.00	2.35	10.91	0.00	6.22
Nb	0.00	0.00	0.00	0.00	0.00	0.00	0.00	0.00	0.00	0.00	0.00	0.00	0.00	0.00	0.00	0.00	0.00	0.00	0.00
Zn	68.21	126.70	65.81	68.80	82.06	67.49	49.91	78.12	82.42	81.46	83.93	69.53	70.26	59.15	67.01	57.11	62.58	63.02	74.13
Cu	6.60	41.40	10.43	16.14	19.95	13.37	17.86	21.37	15.96	14.57	13.91	10.45	6.36	14.47	10.74	11.56	14.72	15.05	16.08
Co	102.36	163.39	138.82	121.07	125.28	144.29	109.92	118.23	158.01	128.13	165.49	162.82	164.39	149.57	150.96	159.14	152.12	153.67	146.36
V	45.84	93.69	2.58	110.96	174.14	58.75	81.86	108.50	63.59	114.83	30.72	24.68	17.77	39.65	34.11	21.04	34.14	21.46	41.44

ORIGINAL MAJOR ELEMENT ANALYSES FROM NG2

SAMPLE	39.35	42.55	50.20	65.25	80.35	83.75	122.30	134.40	143.35	157.30	200.50	212.20	219.90	228.75	236.86	238.90	326.86
SiO2	39.993	41.656	40.788	48.284	43.428	40.557	43.375	40.850	42.830	39.747	50.110	49.761	56.124	42.943	45.623	38.528	40.719
TiO2	0.080	0.037	0.063	0.060	0.055	0.039	0.092	0.049	0.059	0.034	0.087	0.088	0.134	0.081	0.069	0.091	0.094
Al2O3	1.812	2.251	2.288	1.493	2.019	2.265	1.805	2.598	1.993	2.049	2.419	2.552	2.671	2.823	3.673	2.274	2.079
Fe2O3	1.098	1.029	1.105	0.946	1.126	1.171	1.040	1.154	1.103	1.279	0.977	0.977	0.838	1.078	1.038	1.153	1.087
FeO	10.982	10.289	11.054	9.455	11.258	11.711	10.400	11.543	11.025	12.793	9.772	9.772	8.383	10.781	10.380	11.531	10.868
MnO	0.216	0.209	0.193	0.206	0.208	0.207	0.204	0.196	0.204	0.222	0.208	0.207	0.203	0.217	0.199	0.223	0.227
MgO	41.089	39.927	40.419	35.581	38.688	39.730	37.988	41.292	38.951	40.010	34.153	32.804	29.058	35.403	32.729	36.485	34.887
CaO	1.402	1.471	1.567	1.624	1.548	1.762	1.437	1.585	1.333	1.198	1.702	1.869	2.139	1.425	2.050	0.959	0.990
Na2O	0.241	0.356	0.309	0.123	0.219	0.311	0.219	0.480	0.355	0.160	0.306	0.428	0.498	0.290	0.479	0.078	0.055
K2O	0.126	0.000	0.000	0.000	0.000	0.000	0.070	0.000	0.000	0.037	0.000	0.000	0.133	0.000	0.000	0.095	0.000
P2O5	0.004	0.000	0.013	0.000	0.007	0.000	0.012	0.003	0.000	0.000	0.003	0.000	0.000	0.002	0.000	0.028	0.016
Cr2O3	0.898	0.435	0.678	0.664	0.420	0.349	0.721	0.316	0.448	0.360	0.386	0.426	0.435	1.154	0.900	1.226	1.112
NiO.	0.222	0.213	0.228	0.164	0.219	0.241	0.205	0.270	0.269	0.275	0.172	0.218	0.093	0.218	0.195	0.293	0.246
LOI	1.861	1.929	1.347	1.199	1.253	2.207	2.238	1.730	1.217	1.505	1.283	1.141	0.153	3.452	3.095	6.374	8.203
H2O-	0.189	0.308	0.160	0.166	0.305	0.170	0.183	0.195	0.124	0.285	0.120	0.135	0.235	0.277	0.289	0.285	0.290
TOTAL	100.213	100.110	100.212	99.965	100.753	100.720	99.989	102.261	99.911	99.954	101.698	100.378	101.097	100.144	100.719	99.623	100.873
Rb	7.50	2.70	2.35	0.00	4.66	0.00	5.74	0.00	0.00	3.94	4.13	0.00	9.39	0.00	0.00	5.03	3.77
Sr	28.34	41.32	37.54	16.04	43.11	44.50	26.74	47.92	30.85	45.22	33.63	36.68	29.21	53.58	49.66	27.80	13.23
Y	3.11	0.00	0.00	0.00	2.53	2.46	2.39	3.00	2.44	0.00	2.31	3.27	4.99	0.00	0.00	2.91	2.32
Zr	17.79	2.87	5.06	0.00	6.57	3.97	7.69	0.00	2.97	3.01	5.49	4.40	13.95	3.59	2.90	13.06	6.25
Nb	0.00	0.00	0.00	0.00	0.00	0.00	0.00	0.00	0.00	0.00	0.00	0.00	0.00	0.00	0.00	0.00	0.00
Zn	64.36	64.71	63.78	75.12	72.46	67.22	66.98	90.79	67.06	73.40	62.53	64.43	61.67	70.24	60.00	65.04	59.50
Cu	19.04	10.21	21.43	11.06	15.47	15.77	31.72	26.62	19.81	13.99	22.93	28.50	17.75	15.31	31.19	35.39	11.98
Co	150.68	134.90	143.80	116.72	135.18	148.92	130.40	156.39	147.91	158.66	125.85	117.15	90.97	140.11	0.00	127.96	129.71
U	52.43	34.82	47.00	65.84	43.16	36.78	68.60	35.84	40.44	30.89	70.87	74.10	90.75	63.34	0.00	90.59	75.11